PROJECT SPEAR

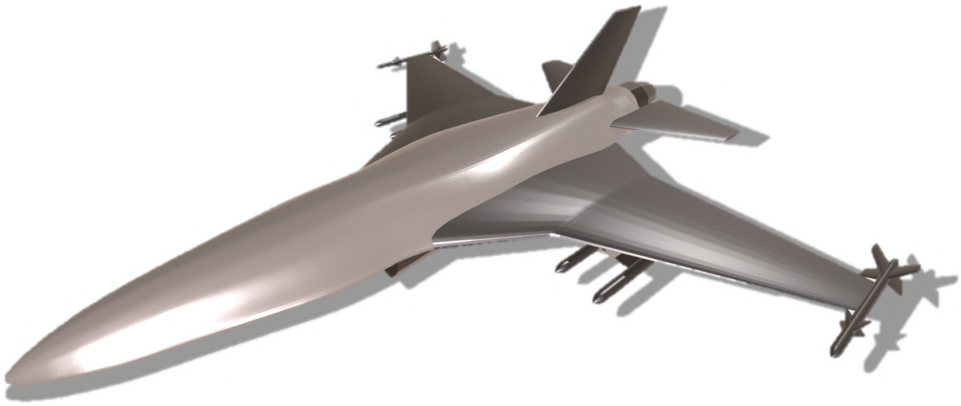

Homeland Defense Interceptor
2025 AIAA Undergraduate Design Team Competition

May 16, 2025

Alexander Bashensky, Anthony Dersahakian, Basile Fages, Joey Gould,
Seth Rosina, Nathan Shune, Calvin Siemers, Salvatore Vella

Anthony Dersahakian
Project Manager
AIAA: 1180176

KEVIN T. CROFTON DEPARTMENT OF AEROSPACE AND OCEAN ENGINEERING
VIRGINIA TECH

Nathan Shune
Chief Engineer
AIAA: 1325474

Project Spear Team

Seth Rosina
Propulsion
AIAA: 1811627

Calvin Siemers
Systems & Avionics
AIAA: 1328078

Joseph Gould
Performance | Stability & Control
AIAA: 1373073

Basile Fages
Propulsion
AIAA: 1811623

Alexander Bashensky
Structures & Materials
AIAA: 1811626

Salvatore Vella
Aerodynamics
AIAA: 1762516

Dr. Darshan Sarojini
Faculty Advisor

VIRGINIA TECH

Dr. Robert Canfield
Faculty Advisor

TABLE OF CONTENTS

Acronyms, Abbreviations, and Symbols

$\alpha_{L=0}$	Zero-Lift Angle of Attack
AIAA	American Institute of Aeronautics and Astronautics
AEP	Aircraft Estimated Price
AESA	Active Electronically Scanned Array
AFP	Automated Fiber Placement
APU	Auxiliary Power Unit
AWACS	Airborne Warning And Control System
BLOS	Beyond Line of Sight
BVR	Beyond-Visual-Range
COTS	Commercial Off The Shelf
CG	Center of Gravity
C_{L_α}	Lift Slope
$C_{L_{max}}$	Maximum 3D Lift Coefficient
DCAP	Defensive Counter Air Patrol
EMI	Electro-Magnetic Interference
ESM	Electronic Support Measures
EW	Electronic Warfare
EIS	Entry-into-Service
FOD	Foreign Object Debris
FEA	Finite Element Analysis
GNC	Guidance, Navigation, and Control
HARV	High Alpha Research Vehicle
HDI	Homeland Defense Interceptor
HF	High Frequency
HoQ	House of Quality
ILS	Instrument Landing Conditions
IMC	Instrument Meteorological Conditions
IRSTS	Infrared Search and Track System with Laser Ranging
IFF	Identification Friend or Foe
IFDL	Intraflight Data Link
JPALS	Joint Precision Approach and Landing Systems
MoM	Measure of Merit
GPS	Global Positioning System
KLOC	Kilo-Lines of Code
LOS	Line of Sight
LAAS	Local-Area Augmentation Systems
LEX	Leading-Edge Extension
LIDAR	Light Detection and Ranging
MTOW	Maximum Takeoff Weight
MAC	Mean Aerodynamic Chord
MoM	Measure of Merit
M1	Mission 1
M2	Mission 2
M3	Mission 3
NATO	North Atlantic Treaty Organization
OBIGGS	On-Board Inert Gas Generation System
PSC	Preferred System Concept
PDI	Point Defense Intercept
PTMS	Power and Thermal Management System
RAT	Ram Air Turbine
RDTE	Research, Development, Testing, and Evaluation
RFP	Request for Proposal
RTB	Return to Base
RTOS	Real-Time Operating System
S	Wing Area
SABR	Scalable Agile Beam Radar
SATCOM	Satellite Communications
SEP	Specific Excess Power
SEP	Specific Excess Power
TACAN	Tactical Air Navigation System
TSFC	Thrust Specific Fuel Consumption
TRL	Technology Readiness Level
NP	Neutral Point
NASA	National Aeronautics and Space Administration
STR	Sustained Turn Rate
ITR	Instantaneous Turn Rate
DATCOM	Digital Compendium
SM	Static Margin
VAC	Volts Alternating Current
UCAV	Unmanned Combat Aerial Vehicle
UHF	Ultra High Frequency
USAF	United States Air Force
VHF	Very High Frequency
VMS	Vehicle Management System Velocity at Takeoff
V_{max}	Maximum Velocity
WAAS	Wide-Area Augmentation System
GE	General Electric Aerospace Engines
PW	Pratt and Whitney
EJ	Eurojet

List of Figures

List of Tables

1 EXECUTIVE SUMMARY

The purpose of this report is to outline the objectives and design of *Project SPEAR*, in response to the 2025 American Institute of Aeronautics and Astronautics (AIAA) Undergraduate Team Design Competition. *SPEAR* addresses the need identified by the Request for Proposal (RFP) for a cost-effective, reliable, high-performance Homeland Defense Interceptor (HDI), capable of providing adequate force projection and maintaining homeland airspace sovereignty. The fleet of HDI aircraft must meet specific requirements, including a maximum flyaway unit cost per aircraft lower than $25 million 2025 USD while executing three key missions. This includes a Defensive Counter Air Patrol (DCAP) mission, a Point Defense Intercept (PDI) mission, and an Intercept/Escort mission. With intended use throughout the United States and its North Atlantic Treaty Organization (NATO) allies, the aircraft must be operable in all Instrument Meteorological Conditions (IMC) and deployable from all standard NATO runways. Maintenance must be cost-effective and require minimal specialized support equipment, ideally using Commercial Off The Shelf (COTS) parts. Current military platforms such as the F-16, F-22, and F-35 fail to offer a cost-effective and scalable solution to complete the necessary homeland defense missions. This creates a unique gap in the market for *SPEAR*, which, if un-filled, would leave NATO airspaces vulnerable as these platforms transition into retirement. *SPEAR* is an aircraft designed with low cost, simplicity, and scalability in mind that is capable of protecting all NATO homelands from emergent foregin threats. *SPEAR* is a remotely piloted Unmanned Combat Aerial Vehicle (UCAV) with planned Entry-into-Service (EIS) of 2032, utilizing innovative new combat-ready technologies to leverage the superiority of 5th generation fighter aircraft while maintaining low cost. *SPEAR* is structurally capable of sustaining a high-g load in clean configuration and holds a design service life of 2,000 hours while handling dynamic pressure loads up to Mach 1.2 at sea level. The fuel tank accommodates standard JP-8 or Jet-A fuel with self-sealing internal fuel tanks designed to withstand fire taken during combat. The aircraft is optionally equipped with up to four AIM-120D AMRAAM missiles and two AIM-9X Sidewinder missiles, with alternate configurations available. This ensures *SPEAR*'s combat versatility to meet the pressing needs for homeland defense.

SPEAR is capable of taking off and landing in under 4,000 ft from the icy runways at Fort Wainwright, AK, to the heat of Naval Air Weapons Station China Lake, CA. At altitude, it is capable of exceeding Mach 1.8 with an endurance and range greater than 5.5 hours and 2300 nm respectively, while reaching 35,000 ft from sea level in under 60 seconds. This combination of loiter time, range, and climb performance demonstrates *SPEAR*'s potential to redefine the meaning of rapid response to any foreign threat approaching the homeland. *SPEAR* utilizes strakes for vortex lift in combination with a double-delta wing configured for significant loiter time with minimal supersonic drag between Mach 0.7 and 1.8, allowing for long patrol missions and rapid dash segments simultaneously. The empennage features a conventional tail design sized for rapid maneuverability while the single General Electric F414-GE-400 engine supplies greater than sufficient thrust for all expected mission profiles while allowing for familiarity by maintainers due to its use on-

board the Navy's F/A-18 Super Hornets. By utilizing a combination of traditional materials such as aluminum and modern composites such as carbon fiber, *SPEAR* maximizes its performance while minimizing its weight to remain a low-cost modern UCAV. The side-mounted variable-aperture diverterless inlets reduce the probability of Foreign Object Debris (FOD) ingestion and ensures proper mass flow to the engine in all critical flight conditions. The tricycle landing gear is designed with future innovation in mind, capable of supporting loads and electrically driving an aircraft 125% larger than SPEAR, while retaining a low profile to facilitate quick accessibility for ground-level operations. By leveraging new, low-cost, and low-weight systems, *SPEAR* is equipped with the premium military avionics suites of today while remaining accessible for the systems of tomorrow. An advanced Power and Thermal Management System (PTMS) provides power and cooling to all systems, while a multitude of communication strategies enables seamless integration into a robust kill chain. Short-burst autonomous capabilities reduce operator workload, and redundant safety and critical flight systems provide exceptional reliability. *SPEAR* is capable and ready to protect the sovereignty of the United States and its allied nations with a feature set that characterizes the next generation HDI aircraft as a cost-effective, low-weight, high-performance, and maintainable solution to meet the demands of the AIAA RFP.

SPEAR Performance Capabilities

- Empty Weight: 12,674 lb
- Fuel Weight: 13,400 lb
- Maximum Takeoff Weight: 27,754 lb
- Maximum Mach at 35,000 ft: Mach 1.83
- Payload Capabilities:
  - 4x AIM-120D AMRAAM missiles
  - 2x AIM-9X Sidewinder missiles
- Time to Climb (Sea Level to 35k ft): 57 s
- Unit Cost Per Aircraft: $24.86 million
- Capable of Takeoff and Landing in Icy Conditions < 8000 ft
- 230 nm Radar Detection Range

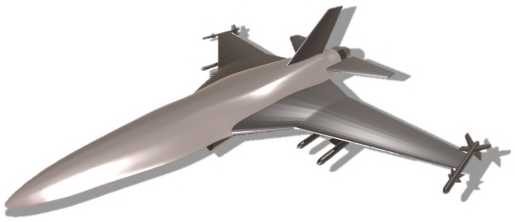

Figure 1: Project SPEAR

Table 1: Project Spear RFP Compliance Summary

Criteria	Requirement	Project Spear Compliance
Dash	Mach 1.6	**Mach 1.83 ✓**
Loiter	4 hours	**5.5 hours ✓**
Climb to 35k ft in 1 minute	>583 ft/s	**605 ft/s ✓**
All Specific Excess Power Requirements		✓
Sustained Load Factor Max Thrust: Mach = 0.9 @ 15k	>5.0 g's	**5.07 ✓**
Maximum Instantaneous Turn Rate @ 35k	>18 deg/s	**17.8 deg/s ✗**
Flyaway Cost Per Unit	<$25 million	**$24.86 million ✓**

2 INTRODUCTION

2.1 Problem Summary

The escalation of global conflicts in Europe, along with growing geopolitical tensions in Asia -particularly involving China, Russia, and North Korea - has heightened the United States' and its NATO allies emphasis on strengthening homeland defense airspace. These threats range from small cruise missiles to hijacked commercial aircraft. In response to rising tensions, existing assets such as the F-22, F-35, F-16, and F-18 currently serve as the main line of defense. While highly effective, these resources are not cost-efficient for scalable production for the purpose of homeland defense. A small, low-cost, and remotely piloted HDI aircraft could fill the market gap without drawing on excess Department of Defense funds. It is estimated that a fleet of 1,000 aircraft would be capable of protecting all NATO homelands from these threats.

2.2 Mission Profiles

The AIAA RFP specifies three missions, two of which are required for the design and one of which is used to evaluate the design.

2.2.1 Mission 1 Profile - Defensive Counter Air Patrol

Mission 1 (M1) is a Defensive Counter Air Patrol (DCAP) mission. *SPEAR* must be able to takeoff, climb to cruise altitude, cruise for 300 nm, perform a four hour loiter at 35,000 ft, dash at Maximum Velocity (V_{max}) for 100 nm, perform two 360° turns at Mach 1.2 and 0.9 respectively and fire all missiles, return to cruise altitude and cruise back to base before descending to sea level with 30 minutes of fuel reserves. M1 is a long endurance mission and was identified as the design-defining mission due to the long four hour loiter followed by a dash segment imposing a requirement for a large volume of fuel. The mission profile for M1 is shown in Figure 2. The breakdown of each flight segment's weight fraction as well as total mission weight fraction for M1 is shown in Table 3.

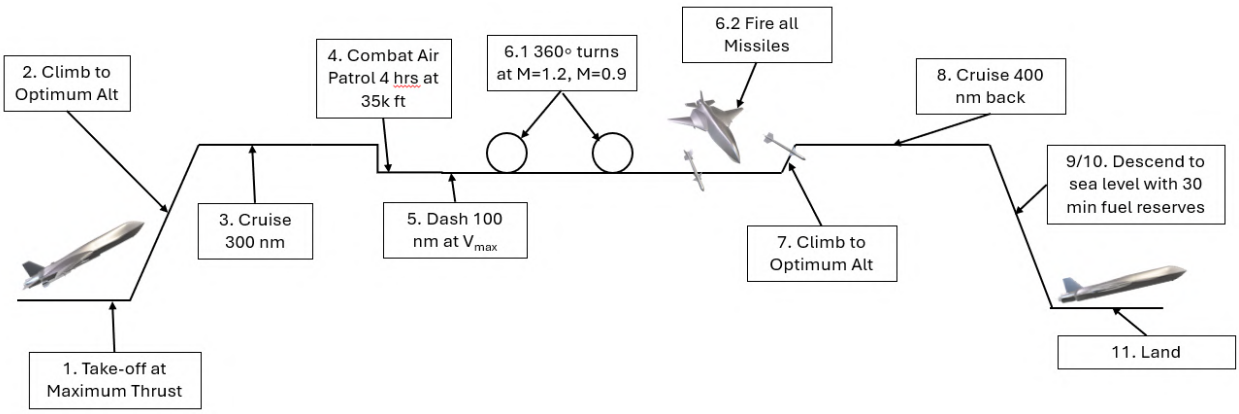

Figure 2: Mission 1 Profile

2.2.2 Mission 2 - Point Defense Intercept

Mission 2 (M2) is the Point Defense Intercept (PDI) mission. This mission is relatively similar to M1, with the early cruise and four hour loiter segments being removed and the dash segment changing to 200 nm. M2 was identified to not be a design-defining mission, since the characteristics necessary for the high speed segments and combat maneuvers overlap with M1 while requiring less fuel than M1 for the total flight. The mission profile for M2 is shown in Figure 3. The breakdown of each flight segment's weight fraction as well as total mission weight fraction for M2 is shown in Table 4.

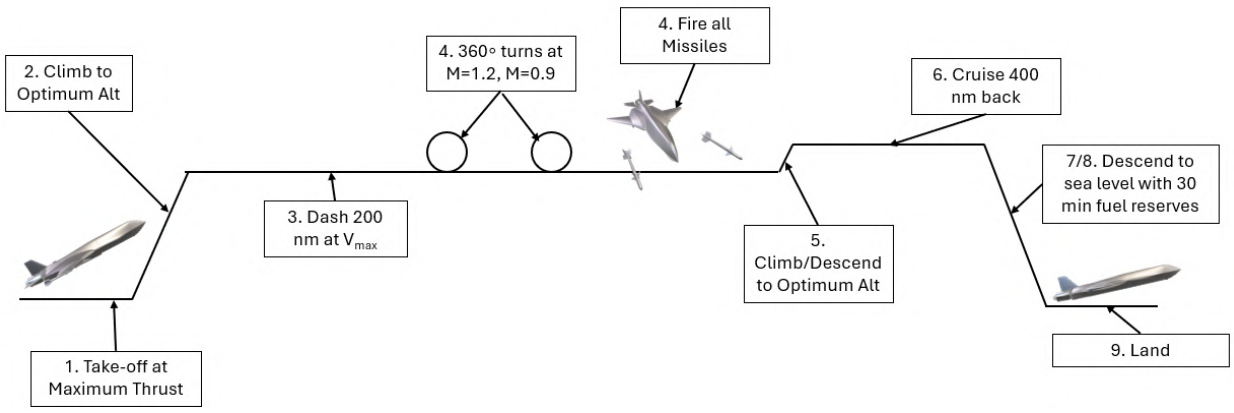

Figure 3: Mission 2 Profile

2.2.3 Mission 3 - Intercept/Escort

Mission 3 (M3) is not considered a design-defining mission. It is used to evaluate the aircraft performance with a slightly different mission profile. It is most closely similar to M2 with a change to perform a 300 nm escort at minimum practical velocity instead of a combat phase. All phases that had pre-defined segment lengths or times in M2 were undefined in length, resulting in M3 being a measure of merit mission. The mission profile for M3 is shown in Figure 4. The breakdown of each flight segment's weight fraction as well as total mission weight fraction for M3 is shown in Table 5.

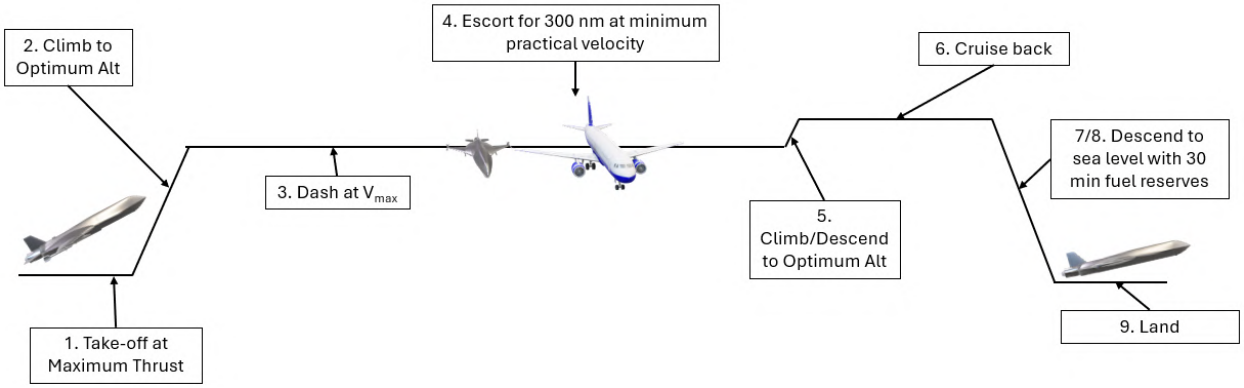

Figure 4: Mission 3 Profile

2.3 Customer Requirements - RFP and MIL-spec

The requirements for this design come from both the RFP and from relevant military specification (MILSPEC) documentation standards. The requirements from the RFP are as follows:

1. The aircraft must be able to complete all the segments of the missions described in Sec. 2.2.
2. The aircraft must be capable of being remote-piloted.
3. The major systems in the aircraft must be easy to access and maintain, to ensure a long service life while keeping the maintenance cost low.
4. With a factor of safety of 1.5, the aircraft must be able to withstand loads of +7 and -3 g's at 50% fuel and a dynamic pressure of 2133 psf. A high structural tolerance is important for the aircraft to have a good survivability.
5. The service life must be at least 2,000 hours.
6. The fuel tanks must be self-sealing in order to minimize the damage that could be caused if the aircraft is damaged.
7. The stability margin must be within a range of $\pm 10\%$.
8. The aircraft must be capable of taking off in under 8,000 ft in any weather condition. This guarantees that the aircraft can operate at any time in any NATO airbase.
9. The unit flyaway cost must be no greater than $25 million for 1,000 aircraft manufactured.
10. The aircraft must have a range of at least 200 nm. This enables the aircraft to stop threats before they breach the national borders.
11. The aircraft must be able to patrol a 300 nm radius for at least four hours.

12. The aircraft must be able to reach a Mach Number of 1.6 at an altitude of 35,000 ft.

13. The specific excess power with a load of 1-g and military thrust at a Mach Number of 0.9 has to be 200 ft/s at sea level, and 50 ft/s at 15,000 ft.

14. The specific excess power with a load of 1-g at maximum thrust and a Mach Number of 0.9 has to be 700 ft/s at sea level and 400 ft/s at 15,000 ft. At 5-g, the specific excess power for the same flight condition must be 300 ft/s and 50 ft/s.

15. The aircraft must be able to turn 18 $\deg/s$ at 15,000 ft. A high maneuverability ensures the aircraft is combat ready.

2.4 Concept of Operations

The 2025 AIAA RFP for a Homeland Defense Interceptor illustrates the need for a high-performance, rapid-response defense interceptor capable of intercepting threats approaching NATO domestic homelands. The past two years alone indicate the growing need for such an aircraft. On February 4th, 2023 a Chinese surveillance balloon flew across the US, eventually being shot down by a F-22 raptor off the coast of South Carolina [4]. On July 25th, 2024 NORAD intercepted a Chinese H-6 Xian in the Alaska Air Defense Identification zone in a United States/Canada joint operation using two CF-18s, two F-35s, and two F-16s [5]. Later that year on September 26th, the US intercepted the Russian Tu-95 Bear also off the coast of Alaska [6]. Scrambling high-value assets to intercept unknown threats is expensive in operational cost and dangerous to pilots should an actual risk arrive. A diagram of these occurrences over the United States, including flight paths, is shown in Figure 5.

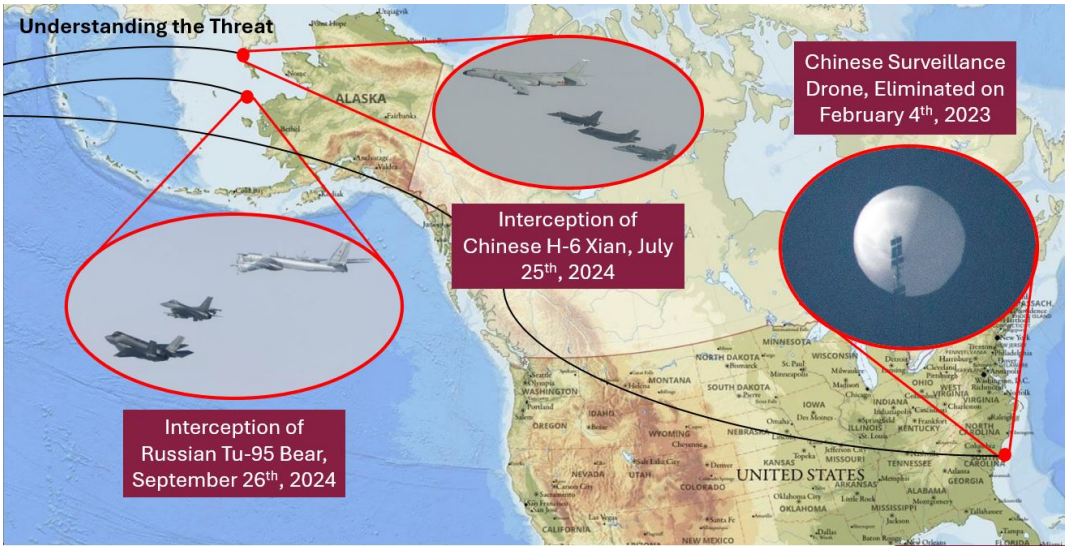

Figure 5: 2023-2024 United States Homeland Threat Map

To handle threats, such as those in Figure 5, the RFP states that *SPEAR* must operate in all IMC at all NATO bases. Expected operation ambient temperatures range from as cold as -45 °C in Fort Wainright, Alaska to as hot as 52 °C in Naval Air Weapons Station, China Lake, California. Specific material selection and thermal barrier coatings were considered in the design of the aircraft which will be described in 9.3.2. The aircraft needs a range of greater than 1000 nm at an altitude of 35,000 ft per the RFP's missions, more details about the mission breakdowns can be found in 2.2.

2.5 Deployment and Basing Strategy

During early production, *SPEAR* will operate with a minimum of 3 aircraft on any NATO base. Since the design of *SPEAR* allows for easy maintainability, there will always be at least two combat ready aircraft at all active bases. This will enhance mission performance by allowing multiple aircraft to be deployed for intercept or escort missions using the communications integration discussed in Sections 2.6 and 8.3. As production increases, *SPEAR* can utilize its swarm capabilities to a more full effect. Excellent climb and acceleration performance allows *SPEAR* to climb from sea level to 35,000 ft in under a minute.

2.6 Integration with Existing Infrastructure

SPEAR has been meticulously designed to integrate with all current and future assets of the United States military. A full outline of the systems and communication protocols is described in Section 8.3. By utilizing Intraflight Data Link (IFDL), *SPEAR* is equipped to be the best wing man to all modern and future assets in the arsenal.

SPEAR is also equipped to integrate seamlessly with all C2 stations, Satellite Communications (SATCOM), Airborne Warning And Control System (AWACS), naval assets, and other *SPEAR* aircraft. A diagram illustrating these relationships is shown in Figure 6.

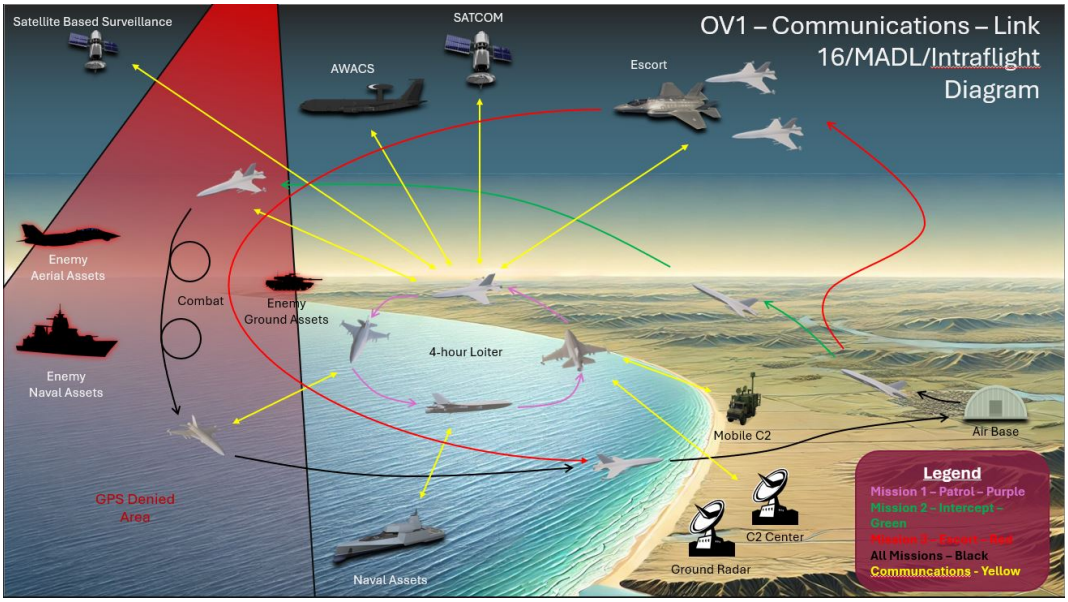

Figure 6: OV-1 Communications Diagram

The legend in the bottom right illustrates the different missions that the aircraft was designed around, 2.2. All of the systems mentioned above are present in the diagram. Significant redundancy was built into the communications system, more detail shown in Section 8.3.

To depict the regular operations expected of *SPEAR*, a Day in the Life diagram was constructed, shown in Figure 7.

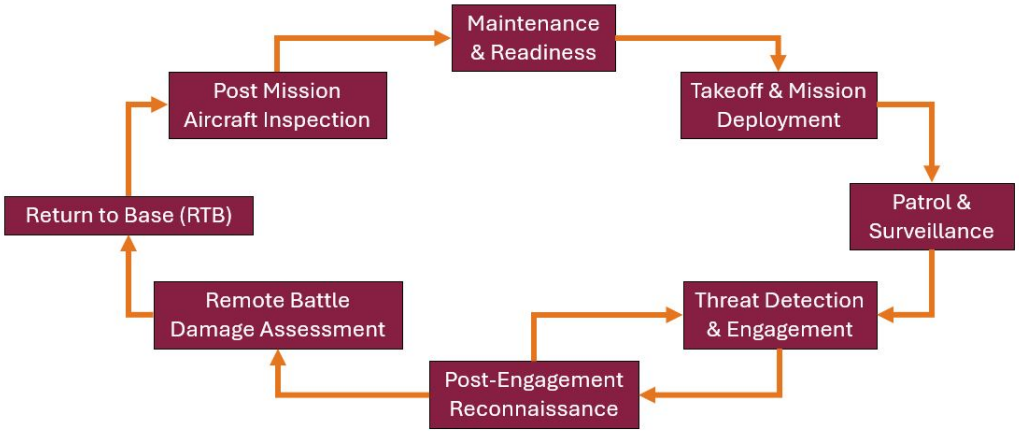

Figure 7: Day in the Life Diagram

A day in the life of *SPEAR* starts with maintenance and readiness, which will be constant and ongoing. With daily inspections, refueling, and combat inspections, *SPEAR* will be ready to get off the ground to intercept threats as quickly as possible while reducing downtime. The expected takeoff and mission deployment time for *SPEAR*'s is between 2-5 minutes. After climbing to altitude, *SPEAR* will patrol and perform surveillance, relaying real time data back to

command and monitoring the airspace for potential threats. If a threat is detected, our aircraft will identify, track, and intercept the hostile target. The aircraft, on the remote pilot's command, will engage the target and deploy weapons or countermeasures. The next block, post engagement reconnaissance, continues surveillance and determines if the threat was eliminated. If not, the aircraft will re-engage with the pilot's command. Remote battle damage assessment is *SPEAR's* vehicle health checkpoint, this will be occurring throughout all flight hours, but more in depth health assessment will occur after all engagements. If any flight plans or aircraft configuration changes need to occur to make it back to base, or improve its survivability, this will occur during this phase. *SPEAR* will return to base, and perform a post mission aircraft inspection to begin readiness for another day.

2.7 Key Design Drivers

When designing a concept to meet the requirement of the RFP, some important factors were taken into account that led to the design process. First of all, the customer demands for a low-cost aircraft, under $25 million. This constraint forces the use of standard, commercially available parts and prevents the use of new, complex technologies. Additionally, the aircraft was designed to have high climb rate and maneuverability to quickly respond to threats, to be operable at all NATO runways in all IMC weather conditions to be able to respond to a threat at any time, to have enough range and endurance for a four-hour long loiter phase, to be capable of remote pilot, to have a high structural capability, a multi-functional payload, and be easy to maintain.

2.8 Measures of Merit

For *SPEAR*, Measure of Merit (MoM) include weight summary, geometry, mission duration, takeoff and landing distances, and overall mission performance metrics such as maximum Mach number, thrust-specific excess power, and maneuverability. *SPEAR* emphasizes operational performance across different mission profiles while exceeding mission duration, takeoff and landing distance, and excess power expectations. The measures of merit for *SPEAR* are shown in Table 2.

Table 2: Measures of Merit for the HDI

Measure of Merit	Description	M1 Value	M2 Value	M3 Value
WEIGHT SUMMARY				
GTOW	Total Weight of the aircraft at takeoff	27,754 lbs	17,458 lbs	27,754 lbs
W_e	Weight of the aircraft without fuel or payload	12,674 lbs	12,674 lbs	12,674 lbs
W_f	Weight of the fuel carried	13,400 lbs	5,941 lbs	9,769 lbs
$\frac{W_{TO}}{S}$	Wing loading at Takeoff	97 $\frac{\text{lbs}}{\text{ft}^2}$	61 $\frac{\text{lbs}}{\text{ft}^2}$	97 $\frac{\text{lbs}}{\text{ft}^2}$
$\frac{T_{SL}}{W_{TO}}$	Ratio of thrust to weight at sea level	0.77	1.28	0.77
AIRCRAFT GEOMETRY AND SYSTEMS INTEGRATION				
S_w	Wing area	286 ft^2		
F_w	Fuselage width at horizontal tail intersection	5.5 ft		
D_{fus}	Fuselage structural depth	5.5 ft		
MISSION DURATION AND FUEL CONSUMPTION				
Endurance	Mission Duration	5.5 $hours$	3.1 $hours$	5.2 $hours$
Mission Radius or Range	Distance achieved for each mission	2,378 nm	1,330 nm	2,228 nm
COST ESTIMATES				
Flyaway Cost (1000 Units)	Estimated per-aircraft cost	$24.86 million		

2.9 Promising Technologies

One promising way to improve signal quality and cut down on aircraft weight is to move away from standard copper wiring and switch to fiber-optic cables. Since fiber optics transmit data through pulses of light rather than electrical current, they naturally offer stronger protection against Electro-Magnetic Interference (EMI) and Electronic Warfare (EW) tactics. This advantage is especially important in mission critical scenarios, where reliable communication can alter the chance of mission success. The Technology Readiness Level (TRL) of fiber optics for use in aircraft systems is 8 [7].

Another technology that complements a more effecient approach is Automated Fiber Placement (AFP), an additive manufacturing method designed for composite materials. AFP uses robotic systems to place fibers exactly where they're structurally needed, which reduces waste and increases structural integrity. By carefully aligning fibers along known load paths, AFP allows for the optimization of component strength and minimization of total weight. The TRL of AFP for use in aircraft production is 10.

When fiber-optic wiring is combined with AFP-based composite structures, the result can be a substantial boost in weight savings, EMI protection, and overall efficiency. Both technologies align well with *SPEAR's* aim of delivering a cost-effective, high-performance interceptor that remains dependable without inflating expenses. As these technologies continue to mature, early integration of fiber optics and AFP can help achieve greater mission capabilities while lowering long-term maintenance and upgrade costs.

2.10 Design Strategy

To ensure proper completion of a Preferred System Concept (PSC) that met all design requirements, objectives, and measures of merit, *SPEAR* was designed using an iterative process. This process started by identifying different aircraft features associated with comparator aircraft, such as those described in section 12. Four concepts were created using a variety of these features as well as un-traditional features not found on combat aircraft or UCAVs, such as a flying-wing concept. These four concepts are highlighted in Section 3.1. Further analysis was conducted on each of these four concepts by the team members based on sub-team roles. The overall design direction of each of the four concepts was determined through the use of design meetings as well as performance evaluation of each change made. Each of the original concepts and the final concept are shown together as part of Section 3.1. The final concept was developed based on desirable features from Concepts 1 and 2 and more detailed analysis was conducted on this concept. Comparisons of the final concept to the initial four concepts is shown throughout the appendices.

3 Preferred Solution Concept

The design process started with four original concepts, each created independently to have as many unique ideas and perspectives as possible.

3.1 Initial Viable Concepts

The initial concepts presented a diverse range of approaches. Concept 1, depicted in Figure 8a, was designed with the primary objective of maximizing loitering duration. Featuring a high aspect ratio, it was optimized to achieve an exceptional lift-to-drag ratio. This design incorporates a single inlet and engine, with stability provided by a V-tail and two differential stabilators. The second concept shown in Figure 8b is a more traditional fighter jet, inspired by the F-15. It is the only concept featuring two engines and is stabilized by a single vertical tail and horizontal stabilators. The high thrust would allow this concept to carry all of its armaments externally. Concept 3, shown in Figure 8c, is a delta wing, single inlet design. The delta wing would optimize this design for high Mach mission phases such as the dash phase, as the delta wing would lower the wave drag. This design features a V-tail for stability. Concept 4, shown in Figure 8d is a blended wing body concept. Optimized for weapon carriage, this concept has a single inlet and horizontal tail. It is also the only design to feature a canard setup as well as thrust vectoring to optimize its mobility.

(a) Concept 1 Geometry

(b) Concept 2 Geometry

(c) Concept 3 Geometry

(d) Concept 4 Geometry

Figure 8: Initial 4 Viable Concepts

3.2 Concept Downselection

The process of selecting which concept to focus on was done with a House of Quality (HoQ). The requirements and MoMs were weighted based on how important they were to the team. The three most important requirements, in order of decreasing importance were chosen to be the low cost, the high climb performance to ensure rapid threat interception, and high range to help meet the loiter requirement. All the requirements and the weight they were given are shown in the first HoQ shown in Figure 9.

Customer Needs	%Weight	Concepts	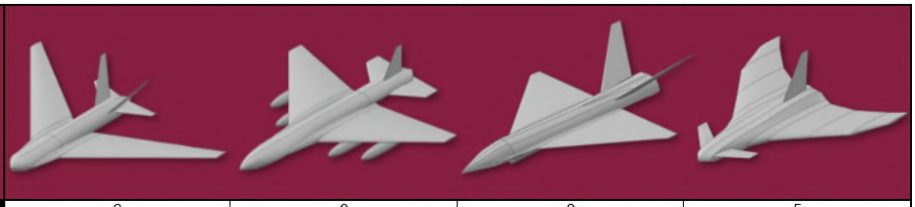			
Low Cost	12.87		6	8	8	5
High Climb Performance	10.55		8	7	5	7
Range	9.01		8	4	4	6
Operable in all meteorological conditions and at all NATO bases	8.88		10	10	10	10
Endurance	8.12		8	5	4	5
High Max Speed	7.98		4	5	9	5
High Structural Load	7.72		5	7	7	8
Light Weight	7.21		6	6	7	4
Multifunctional Payload	6.95		4	8	5	6
High Maneuverability	6.56		5	6	8	6
Remote Pilot	4.50		10	10	10	10
Long Service Life	4.38		8	8	8	6
Low Radar Cross Section	3.35		7	6	7	5
Short Field Takeoff Performance	1.93		7	6	5	7
Totals	100.00		678.8	686.1	689.7	634.7

Figure 9: First House of Quality

The initial HoQ analysis resulted in a close competition between Concepts 2 and 3, both achieving scores exceeding 680. Concept 4 was eliminated due to the high cost associated with thrust vectoring, as well as the increased drag from its large wing, which reduced its range and endurance. Concept 1 was discarded because its high aspect ratio wings made it too costly, slow, and difficult to maneuver. This HoQ also led to the creation of a new concept, which was subsequently evaluated alongside the other four in a revised HoQ, as shown in Figure 10. The new concept features a single engine to reduce costs, leading-edge extensions for improved climb performance, and low aspect ratio wings to enhance maneuverability.

Customer Needs	%Weight	Concepts					
Low Cost	12.87		7	7	7	8	7
High Climb Performance	10.55		7	8	6.5	5	6.7
Range	9.01		5	7	5	9	5
Operable in all meteorological conditions and at all NATO bases	8.88		10	10	9	10	10
Endurance	8.12		8	9	8	10	8
High Max Speed	7.98		8	8	8	8	8
High Structural Load	7.72		5	8	6	3	9
Light Weight	7.21		8	4	8	8	8
Multifunctional Payload	6.95		4	9	5	6	9
High Maneuverability	6.56		5	9	8	1	8
Remote Pilot	4.50		10	10	10	10	10
Long Service Life	4.38		8	8	8	6	9
Low Radar Cross Section	3.35		7	6	7	5	9
Short Field Takeoff Performance	1.93		8.5	9	7	8	9
Totals	100.00		703.3	792.9	720.6	703.1	797.5

Figure 10: Final House of Quality

The weights of the requirements remained the same in the final HoQ, but the given values minimally changed, as more in-depth analysis was conducted. The final scores were very similar, Concepts 2 and 3 scored much higher than Concepts 1 and 2 for the same reasons as listed above. In Figure 10, the highest scoring concept in each requirement is highlighted in green, and a poor performance in red. The new concept was found to be better than the original four in most categories, while having high enough scores in the others to end with much higher total score than Concepts 2 and 3, and was therefore chosen for further development.

3.3 Preferred Solution Initial Sizing

Initial sizing was performed using the iterative method outlined in Chapter 5 of Nicolai's textbook [2]. This method involves estimating the weight ratio at the beginning and end of each mission segment, utilizing historical data, fuel burn estimations, and known weight losses such as the use of missiles. The final aircraft weight is determined by applying the total weight ratio to an estimated take-off weight. The resulting available empty weight is then compared to the required empty weight, which is based on historical trends. If the available and required empty weights do not fall within an acceptable range, a new take-off weight estimate is made, and the process is repeated until a solution is found. This method is also used to obtain preliminary values for wing loading and thrust-to-weight ratios.

This method was applied to every initial aircraft concept, which allowed for a more accurate estimation for the HoQ shown in Figure 10. Additionally, the preliminary concept guided many of the initial design choices, including engine selection, wing sizing, and fuel storage.

A preliminary weight breakdown analysis was performed from the Maximum Takeoff Weight (MTOW) and Wing Area (S) optimization outputs. This breakdown was calculated using weight estimations from Nicolai [2]. Below are the fuel fraction breakdowns for each of the mission outlined in the Tables 3- 5.

Table 3: Mission 1 Weight Fraction

Segment	Description	Fuel Fraction
Takeoff	Warmup and Takeoff	0.98
Climb	Climb to Optimum Altitude	0.977
Cruise	Cruise 300 nm	0.935
Combat Air Patrol	Climb to 35,000 and 4 hr. Loiter at Optimal Speed	0.646
Dash	Dash 100 nm at 35,000 ft	0.948
Combat 1	Combat Maneuver at Mach 1.2	0.99
Combat 2	Combat maneuver at Mach 0.9	0.991
Climb	Climb/Descend to Optimum Altitude	0.984
Cruise	Cruise 400 nm	0.912
Descend	Descend to Sea Level	1.0
Loiter	30 minute Fuel Reserve Loiter	0.659
Land	Land	0.995
Total Mission	-	0.318

Table 4: Mission 2 Weight Fraction

Segment	Description	Fuel Fraction
Takeoff	Warmup and Takeoff	0.98
Climb	Climb to 35,000 ft and Accelerate to V_{max}	0.977
Dash	Dash 200 nm	0.919
Combat 1	Combat Maneuver at Mach 1.2	0.993
Combat 2	Combat maneuver at Mach 0.9	0.997
Climb	Climb/Descend to Optimum Altitude	0.959
Cruise	Cruise 200 nm	0.997
Descend	Descend to Sea Level	1.0
Loiter	30 minute Fuel Reserve Loiter	0.883
Land	Land	0.995
Total Mission	-	0.718

Table 5: Mission 3 Weight Fraction

Segment	Description	Fuel Fraction
Takeoff	Warmup and Takeoff	0.98
Climb	Climb to 35,000 ft and Accelerate to V_{max}	0.977
Dash	Dash 200 nm	0.811
Escort	Escort at Minimum Practical Airspeed 300 nm	0.954
Climb	Climb/Descend to Optimum Altitude	0.977
Cruise	Cruise at Optimum Speed and Altitude	0.90
Descend	Descend to Sea Level	1.0
Loiter	30 minute Fuel Reserve Loiter	0.803
Land	Land	0.995
Total Mission	-	0.513

3.4 Constraint Plot

SPEAR must adhere to various performance requirements specified in Section 4 of the RFP. To begin determining the aircraft size that meets these requirements, each condition was plotted against wing loading and thrust-to-weight ratio. The design space where the aircraft can satisfy all these requirements is defined by the intersection of these two curves. To ensure the curves accurately represent the requirements, they are normalized to the takeoff condition using the weight fractions calculated in the previous section. In Figure 11, only the most critical requirements are shown in the constraint diagram.

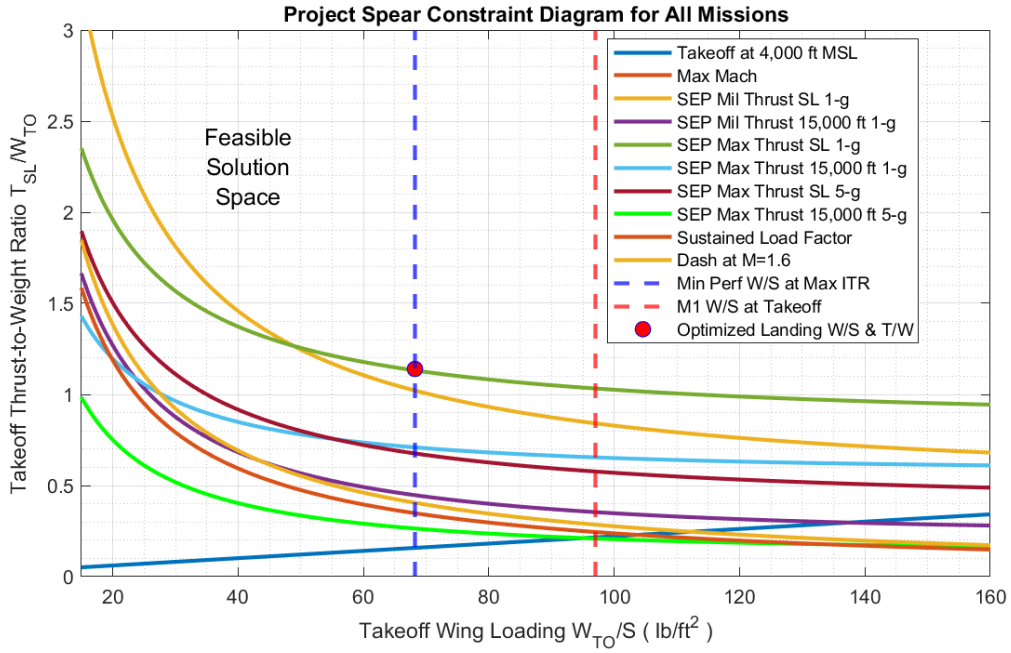

Figure 11: Initial Sizing Constraint Diagram

3.5 Operating Procedures

Understanding the operating procedures of SPEAR enhances the Air Force's feedback throughout the design, testing, or manufacturing process. Surveillance and engagement diagrams have been developed to enhance customer understanding of the systems and processes on board SPEAR. Figure 12 depicts the surveillance OV-5 diagram.

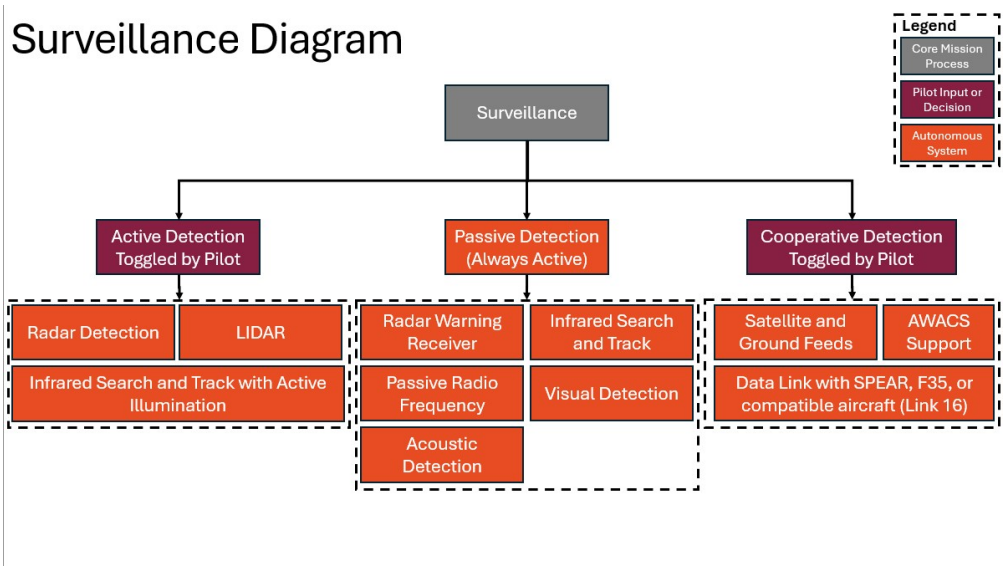

Figure 12: Surveillance OV-5 Diagram

The legend in the top right of the diagram is broken into gray for core processes, maroon for pilot input, or orange for

autonomous systems. Three key detection modes exist in SPEAR, active detection, passive detection, and cooperative detection. Active detection must be toggled by the pilot as it leaves the aircraft more vulnerable with this system activated. SPEAR has radar detection, Light Detection and Ranging (LIDAR), and infrared search and track with active illumination Infrared Search and Track System with Laser Ranging (IRSTS). All of these systems send signals, waves, and lasers. The detection radius of SPEAR using active radar detection is 230 nm.

Passive detection will be always active on the aircraft. This system does not output any signals, waves, or anything else. SPEAR will have visual detection, radar receivers, IRSTS, and radio frequency receivers. These systems lead to a significantly lower detection radius, but SPEAR is less detectable.

Finally, cooperative detection involves using external military assets to map the area and detect threats. SPEAR has been meticulously designed to integrate with all of these systems. By fabricating a mesh of threat geospatial information, SPEAR will be well equipped to detect all threats. Surveillance is one piece of SPEAR's engagement. A second OV-5 shown in Figure 13 was created to illustrate the engagement procedure.

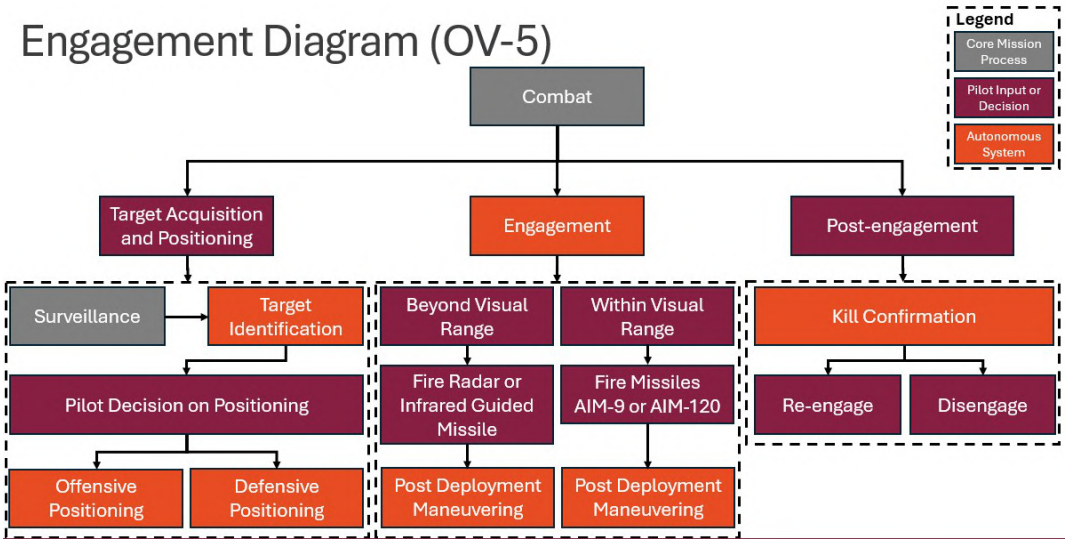

Figure 13: Engagement OV-5 Diagram

Similar to Figure 12, there are three core components of SPEAR's engagement, target acquisition and positioning, engagement, and post engagement. Surveillance is the first step to target acquisition and positioning, a threat's location can be discovered during flight or known on the ground as the aircraft are scrambled. An autonomous system will identify the threat, the pilot will then make a decision on SPEAR's positioning. Offensive positioning will ready the aircraft for engagement and armament deployment. Defensive positioning can be a relay for other assets, or continue reconnaissance of the threat.

There are two additional modes of engagement the pilot will make a decision on, within visual sight and beyond visual

sight. SPEAR is equipped with four AIM 120D and two AIM 9X, further description can be found in 8.2. If fired beyond visual sight, these missiles will be guided by their own on board Guidance, Navigation, and Control (GNC). SPEAR will then perform a post deployment maneuver, likely a turn and burn. If the combat is within visual sight, SPEAR will use the more traditional target lock system typical of fighter aircraft. After deployment of the armament, SPEAR will perform a similar post deployment maneuver. With the likelihood of the target being much closer, SPEAR may make a more involved turn or combat maneuver. Finally, the aircraft will confirm the elimination of the threat. If the target was not eliminated, the engagement process can begin again.

4 Aerodynamics

The RFP specifies multiple dash segments between M1 and M2 and an extended four hour loiter in the DCAP mission. To be able to complete a high speed dash at a Mach number of at least 1.6 while still being able to complete the loiter segment, the wing design must be aerodynamically efficient in both the subsonic and supersonic regimes.

4.1 Wing Planform

From the original preliminary sizing and constraint analysis, a M1 take-off wing loading of 97 psf was used to size the wing as it is the highest wing loading expected for the aircraft. This led to a wing area selection of 286 ft^2. The M1 loiter requirement is considered to be the most difficult to meet requirement based on traditional aircraft sizing. To be able to ensure an extended loiter capability, a wing with a larger aspect ratio would be preferred to increase aerodynamic efficiency and reduce fuel consumption. Conversely, the necessity to dash at a high speed means a low aspect-ratio highly swept wing with a smaller span would be preferred. A variety of solutions were considered to allow for both the high-speed dash and lower-speed loiter to be completed, including a variable-swept wing and different planform designs. A comparison of planform designs to meet the wing area requirement from initial sizing are shown in Figure 14.

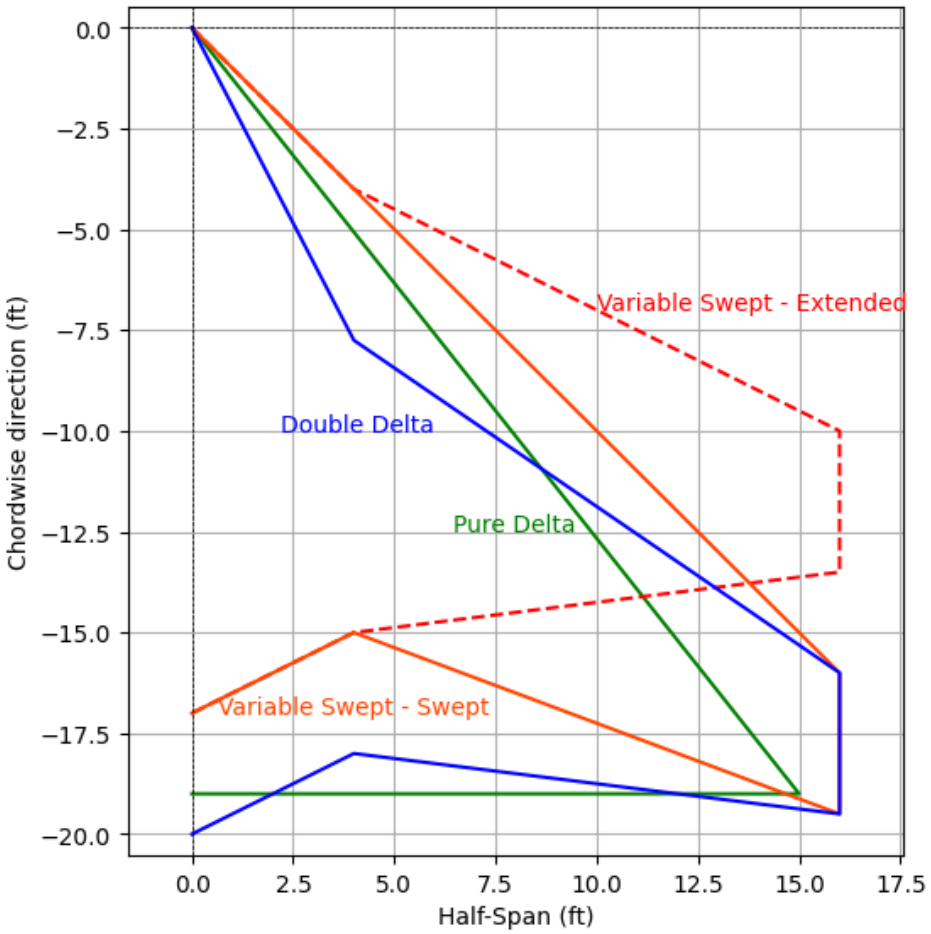

Figure 14: Planform Geometry Comparison

The variable sweep wing, shown in Figure 14, was considered to be capable of completing the necessary mission segments but was determined to be cost-prohibitive, adding millions to the expected total cost as well as necessitating more structural weight. The delta wing was considered to be simple and well-understood aerodynamically but would not have excellent efficiency in either subsonic or supersonic regime. The double delta wing is designed to handle both supersonic dash segments with highly swept Leading-Edge Extension (LEX)s while also having a higher aspect ratio wing outboard section to increase efficiency in the loiter phase. This design also allowed for reduction in expected wave drag, allowing for more efficient dash segments. The LEX on the double delta generate powerful vortices during high angle of attack maneuvers, which generates a powerful vortical lift and delays separation. The large root section also allows for better structural integration with the fuselage structure, resulting in a stiffer structure and lighter wing. The combination of all these beneficial characteristics led to the decision to make the final wing planform a double

delta configuration, shown in Figure 15.

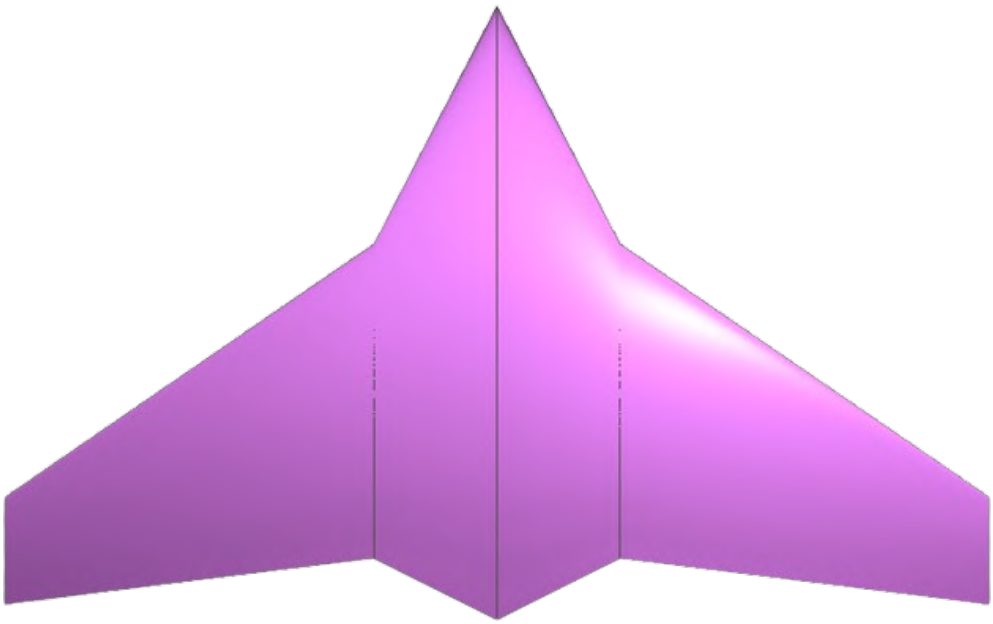

Figure 15: Wing Planform Top-View

Double delta wing configurations featuring leading edge extensions have become more common in current-generation fighters which allows for more design familiarity and known negatives. Double delta wings have a characteristic pitch instability that can be minimized by the shaping of the leading edge extensions. To determine optimal inboard and outboard sweep, a historical study was conducted on modern fourth and fifth generation fighters, such as the F-16 and F-18. The in-board sweep angle of the F-18 is approximately 60 degrees. The LEX on *SPEAR* are 63 degrees to induce vortices that would avoid or dissipate before reaching the horizontal tail to maintain as much control authority to handle the inherent instability. This sweep angle also allows a substantial increase in lift due to the associated vortex lift. This increases the maneuverability of the aircraft and allows for shorter take-off and landing distances. The outboard section of the wing's design was based on historical trends and design principles outlined in Raymer's textbook. The historical trend of leading edge sweep versus design max mach is shown in 16a. The historical trend of taper ratio vs. quarter-chord sweep is shown in 16b.

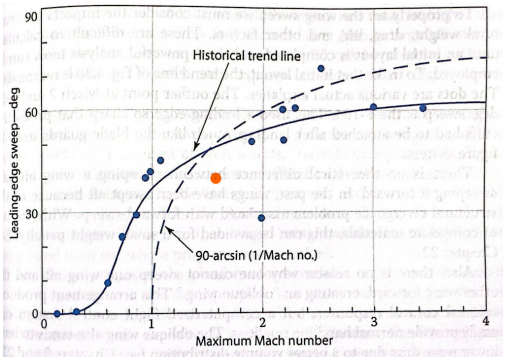

(a) Historical Trend Leading Edge Sweep vs. Design Max Mach

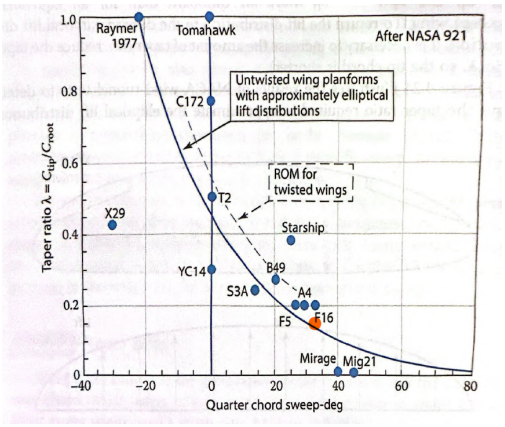

(b) Historical Trend Taper Ratio vs. Quarter-Chord Sweep.

Figure 16: Historical Trendlines for Wing Design (Spear in Orange) [1]

After analyzing historical trends and conducting preliminary analysis, the outboard section of the wing was selected to have a sweep angle of 34 degrees, ensuring it remains inside the entire Mach cone in the entire expected flight envelope. The root and tip chord lengths were determined using an iterative process with hundreds of variations to reduce induced drag and maximize lift using *XFLR5* with Karman-Tsien second order compressibility corrections. This allowed for rapid configuration changes and a quick approximation of wing aerodynamic characteristics prior to additional analysis. The final planform has a LEX root chord of 20 ft, an outboard section tip chord of 3 ft, and a junction chord of 8.25 ft at the connection between the LEX and outboard wing section. The final planform parameters after initial planform selection are shown in Table 6.

Table 6: Final Planform Characteristics

Planform Characteristic	Value
Wing Area	286 ft^2
Half-Span	16 ft
LEX Sweep	66 °
Outboard Section Sweep	34 °
Aspect Ratio	3.58
Mean Geometric Chord	8.94 ft
Mean Aerodynamic Chord	10.91 ft
Taper Ratio	0.17

4.2 Airfoil Selection

With initial planform selection complete, the next step was to select airfoils for both the LEX and outboard section. A historical survey was conducted on supersonic aircraft as well as modern fighters to start the initial airfoil selection

[1]. It was found that supercritical airfoils, such as the NACA 6-series airfoils, were commonly used in fighter aircraft with small modifications made depending on the use case. Supercritical airfoils are designed to remain laminar for a greater chordwise distance than traditional subsonic airfoils. An adverse pressure gradient forms much later leading to less overall turbulent flow over the wing when using a supercritical airfoil.

To ensure the aircraft retained control authority at near-stall conditions, it was determined that the out-board section would need a thinner airfoil than that of the root of the wing. To make sure that *SPEAR* had enough lift in the subsonic regime the airfoil at the root needed to be thicker. To determine the ideal thickness for both sections, the overall wing had to be considered. From preliminary design, the 2D design lift coefficient for each mission phase was determined for both M1 and M2 for a constant airfoil along the entire wing. Different airfoils were tested in *XFLR5*'s 2D mode, based on *XFOIL*, that would allow the aircraft to meet the necessary overall design lift coefficient while minimizing drag. The results from *XFLR5* were compared against publicly available NACA 6-series testing data from [1]. The comparison showed good agreeance between data sets. Based on the historical survey as well as the publicly available testing data, it was determined that a modified NACA 64-210 and NACA 64-206, at the root and tip respectively, would be able to meet the design requirement. The second digit of the NACA 6-series airfoils indicates that maximum thickness occurs at a normalized chord of x/c=0.4 for both airfoils. The third digit indicates the design lift coefficient of 0.2 for both airfoils. The last two digits indicate the percent thickness. These selections compared well against the F-16, which used a modified NACA 64-204 at the wing root and tip [8]. The F-16 was designed to fly at a higher Mach number and for a lower loiter period. *SPEAR* is able to have a lower drag at its design Mach when compared to the F-16 planform and lower thickness airfoil at its design Mach. The thicker airfoils allows for retention of higher lift generation characteristics increasing loiter performance at subsonic speeds. The initial section analysis was conducted at 35,000 ft and a Mach number of 0.8 with appropriate second-order compressilibity corrections. The 2D geometry and pressure profiles at a zero angle of attack for each airfoil are shown in Figure 17.

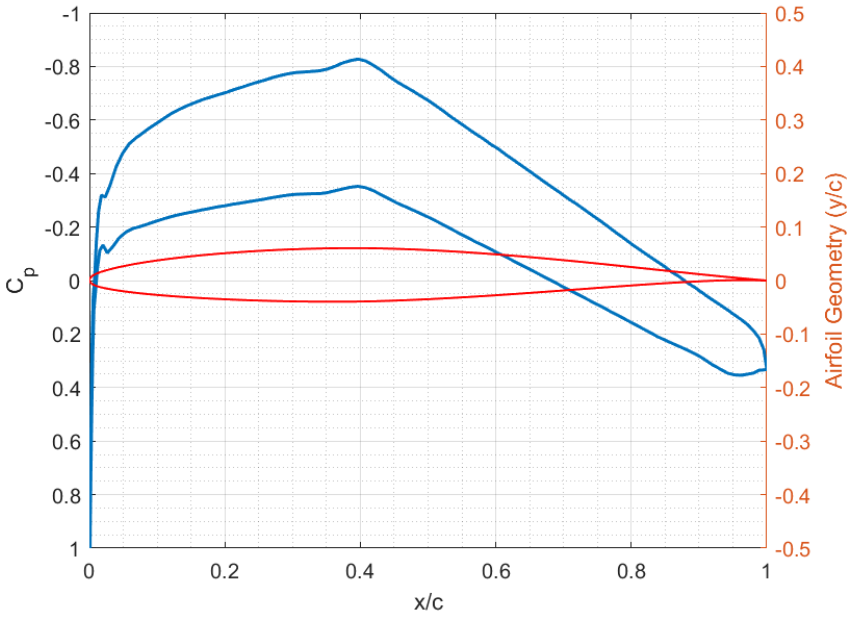

(a) Pressure Profile - NACA 64-210

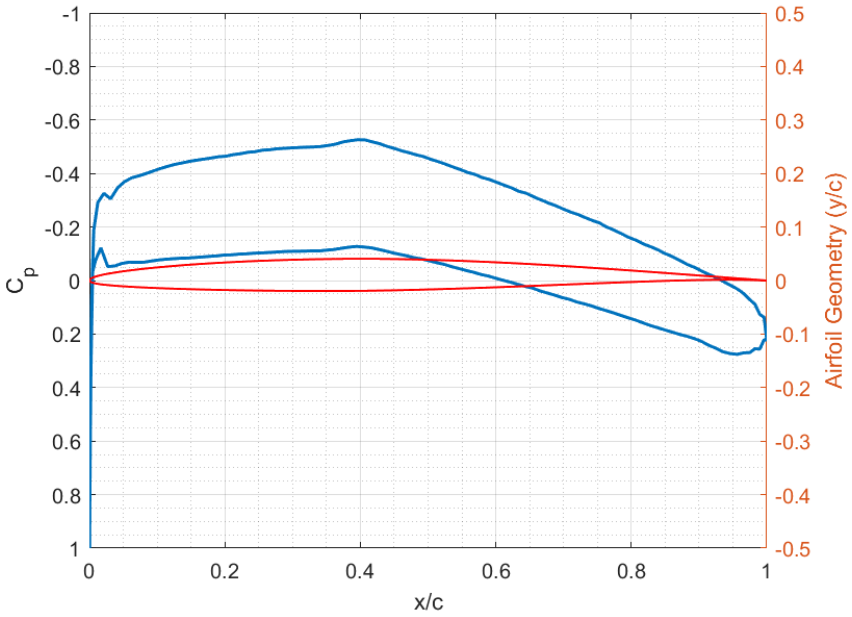

(b) Pressure Profile - NACA 64-206

Figure 17: Pressure Distributions at Zero Angle of Attack, Mach=0.8

The airfoils used on *SPEAR* have different characteristics that were important in determining lift capabilities during the loiter and supersonic dash phases. The lift slope and zero-lift angle-of-attack were important to understand what angle-of-attack would be necessary during the loiter phase. It was also important to determine the maximum 2D and 3D lift coefficients. These characteristics are summarized in Table 7.

Table 7: Aerodynamic Characteristics of NACA 6-series Airfoils during Loiter

Characteristic	NACA 64-210	NACA 64-206
Lift Slope (C_{L_α})	0.105/deg	0.110/deg
Maximum 3D Lift Coefficient ($C_{L_{max}}$)	1.44	1.03
Zero-Lift Angle of Attack ($\alpha_{L=0}$)	$-1.5°$	$-1.0°$

To better understand the boundary layer in important regions, such as close to the inlet for ingestion analysis, an implicit turbulent boundary layer finite difference method was used to determine boundary layer thickness and momentum thickness as well as skin friction at Mach 0.8, 1.6, and 1.8. The primary modifications made to the code involved changes to the eddy viscosity formulation for vortex separation. All analysis was conducted at 35,000 ft using the standard atmosphere model with viscosity calculated from Sutherland's Law. The plots showing skin friction, boundary layer thickness, and momentum thickness for Machs 0.8, 1.6, and 1.8 are shown in Figure 18.

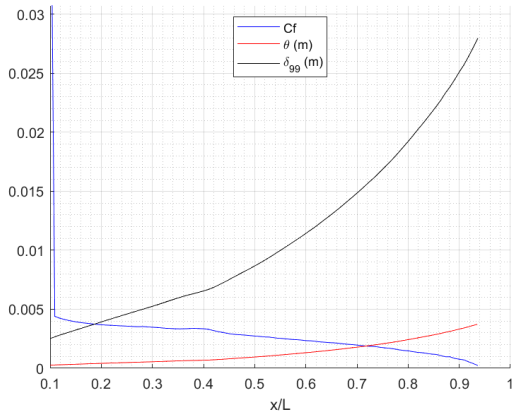

(a) Mach 0.8 - NACA 64-210

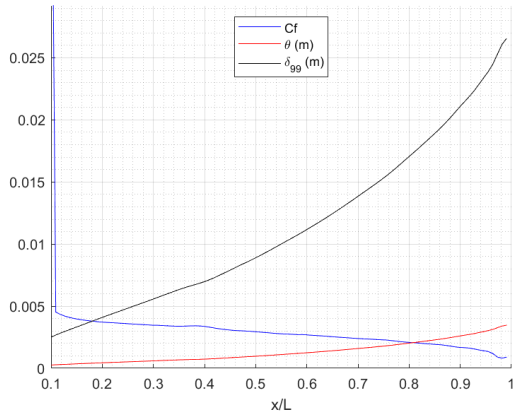

(b) Mach 0.8 - NACA 64-206

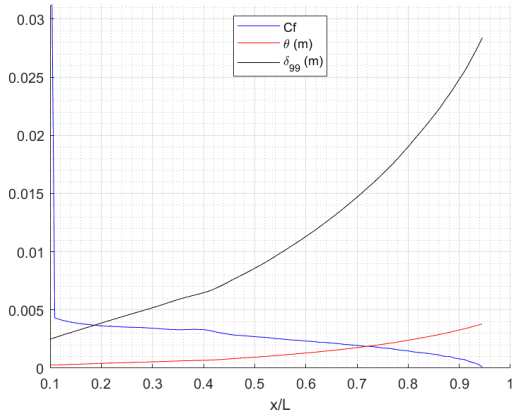

(c) Mach 1.6 - NACA 64-210

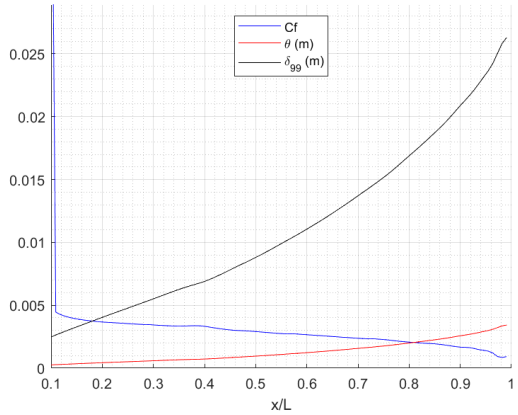

(d) Mach 1.6 - NACA 64-206

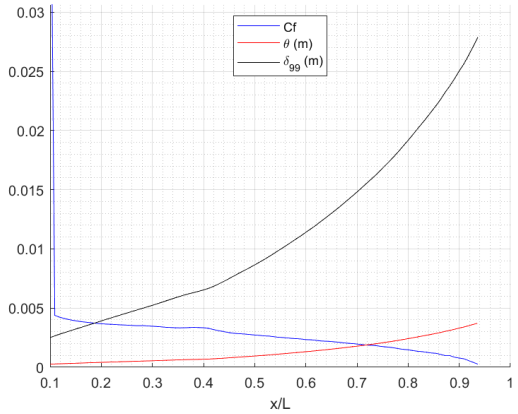

(e) Mach 1.8 - NACA 64-210

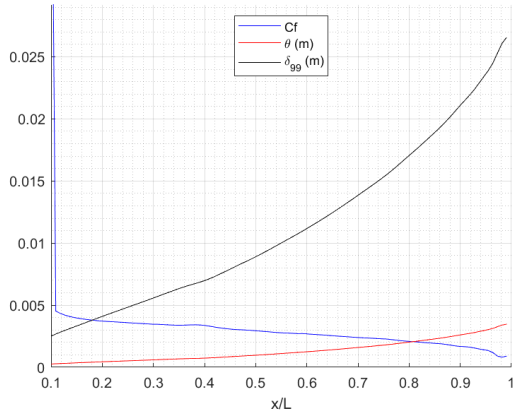

(f) Mach 1.8 - NACA 64-206

Figure 18: Turbulent Boundary Layer Characteristics of Airfoils on *SPEAR*

This boundary layer analysis was used to determine the offset from the fuselage to avoid boundary layer ingestion in the design of the intake, discussed in Section 5. This analysis was also used to determine turbulent boundary layer separation. For the NACA 64-210 at the root, additional vortex turbulence delayed separation while the NACA 64-206

had not additional separation delay applied. A summary of the separation location at the root and tip is shown in Table 8.

Table 8: Normalized x/c Separation Location Summary

	NACA 64-210	NACA 64-206
Mach	**Separation Location (x/c)**	
0.8	0.9411	0.9965
1.6	0.9465	0.9969
1.8	0.9424	0.9968

Table 8 shows that separation is not expected until nearly the end of each airfoil. While 3D effects may lead to variation, this initial analysis was important to understand the zero angle of attack boundary layer for the loiter and dash segments of flight. This analysis was used to offset the inlet as well as place the horizontal tail outside of the large vortices and boundary layer formed from the wing.

4.3 Span Load Distribution

With a planform and initial airfoil geometry selected, it was necessary to increase the aerodynamic efficiency of the 3D wing. With a low-aspect ratio wing the wing tips experience high-loading, which is not ideal for maneuvering, efficiency, or drag. Adding geometric twist enables the reduction of tip loads on the wing. The spanwise spanload is a common metric used to compare wings to elliptical wings, which are known for the efficiency and tip load reduction. The local lift coefficient is used to evaluate spanwise spanload as a function of local lift coefficient and mean aerodynamic chord. A custom twist optimizing code was used with the specified geometry planform and local lift coefficient from *XFLR5* to find approximations for ideal twist at the root, junction, and tip of the wing. This resulted in a twist of -0.7° at the root, 0.2° at the junction, and 3° at the tip of the outboard wing section. A comparison of the local lift coefficient versus half span before and after twist optimization is shown in Figure 19.

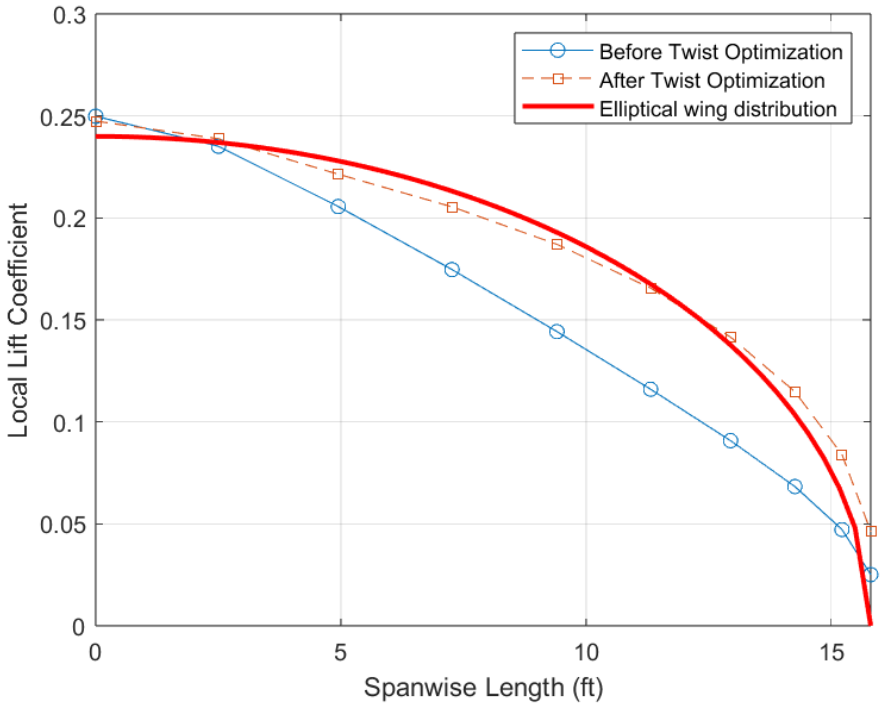

Figure 19: Twist Optimization Spanload Distribution Effect

4.4 Loiter Lift Analysis

To verify capability for the wing to generate enough lift for an extended loiter phase, the exact speed and angle of attack needed to be determined to maximize aerodynamic efficiency. Additionally, it was important to understand low-speed characteristics to size high lift devices for take-off and landing. The geometry of the wing, including the airfoils, was put in *XFLR5* to determine the lift characteristics during loiter. Additional compressibility corrections were applied and analysis was conducted at the loiter condition described in Section 6. To generate the lift to sustain the expected loiter weight of the aircraft, an angle of attack of 1.1 degrees was determined to be necessary at the start of the loiter phase that gradually reduced as fuel weight decreased.

4.4.1 High Lift Devices

High lift systems on-board traditional fighter aircraft typically include leading edge flaps or slats and trailing edge flaps. This is to reduce necessary velocity to achieve the same amount of lift at various points in the flight regime and, importantly, during take-off and landing.

There are other reasons to consider the use of high lift devices at certain points in the flight regime. Leading edge slats function the same as point vortices, seeking to reduce the speed on the main element and reducing the chance of separation. By using a leading edge element, the boundary layer coming off the leading edge element is at a higher velocity than the freestream velocity, meaning the boundary layer does not have to slow as much to remain attached to each surface. This takes pressure off the boundary layer and avoids early flow separation, allowing the wing to

generate more lift. The suction lift generated as a result of this is proportional to the square of the trailing edge velocity, meaning large benefits to overall lift can be gained through the using of a leading edge element.

The use of a trailing edge element causes a higher velocity to be seen in the upstream region, inclined to the mean line. To meet the Kutta condition, circulation is increased over the whole section, increasing lift. Additionally the boundary layer leaves the trailing edge element faster than the relative free stream to form a wake which is more efficient energy-wise when using a trailing edge element. This efficiency gain, as long as the wake remains separate from the local boundary layer, is even greater as the number of local trailing edge elements increase. The use of multi-element high lift devices allows for multiple thinner boundary layers to form rather than a single larger boundary layer, reducing drag.

A multi-element high lift device system was determined to be necessary on-board *SPEAR*'s wing. Leading edge slats and double slotted flaps were selected to be the high-lift devices to minimize additional integration weight while maximizing lift. Empirical estimations of the coefficient of lift associated with the airfoils used on *SPEAR* were found in Nicolai's textbook, which was then used to form the overall lift profile of the wing [1].

The slats were selected to occupy the forward 15% of the leading edge of the outboard section of the wing while ending spanwise 1.5 ft before the tip of the wing to avoid integration issues with a wing tip-mounted missiles. The trailing edge flaps occupy the last 30% of of the chord on the trailing edge, starting 0.2 ft from the outboard section of the LEX and ending after 4.11 ft. This leaves enough spanwise space on the outboard section for ailerons as discussed in Section 7.

4.5 Drag Build-Up Methodology

4.5.1 Subsonic Drag

To compute drag in the subsonic regime, estimations for induced drag and parasite drag are necessary to find the total coefficient of drag. To find induced drag, the vortex lattice method was used with a second-order Karman-Tsien compressibility correction to find the component drag for the wing, vertical tail, and horizontal tail. The fuselage induced drag was estimated using a Virginia Tech subsonic drag code estimator developed by Dr. William Mason. Weapons drag was added using historical coefficient of drag estimations for traditional missiles of approximate size to the AIM-120D and AIM-9X on-board *SPEAR* [9]. To find the parasite drag over all bodies, another Virginia Tech code developed by Dr. Mason was used [10]. This code allowed for input of the wing, vertical tail, horizontal tail, and fuselage at any specified flight conditions.

4.5.2 Supersonic Drag

In the supersonic regime, wave drag becomes dominant over both parasite and induced drag. Wave drag is predominantly associated with volume so minimization of drag area distributions and a large fineness ratio become essential. The fineness ratio is the ratio of a streamlined body's length to its maximum diameter. Based on slender body theory, the wave drag associated with a specified geometry based on multi-axis cross sectional are is shown in Equation 1.

$$D_{wave} = \frac{-q_\infty}{2\pi} \int_0^l \int_0^l S''(x_1) S''(x_2) \log|x_1 - x_2| dx_1 dx_2 \tag{1}$$

Equation 1 indicates that for a slender axisymmetric body, such as *SPEAR* wave drag is independent of Mach number. Minimizing total volume while maximizing body length leads to a reduction in wave drag. Although the Sears-Haack body does not give a minimum wave drag solution for a given maximum cross-sectional area, it provides a good estimate of area rule shaping, which could be adjusted to minimize overall wave drag. After initial fuselage shaping, an effort was made to accomodate internal systems while trying to match the area distribution of a Sears-Haack body. The initial fuselage, wing, and tail used in wave drag analysis is shown in Figure 20.

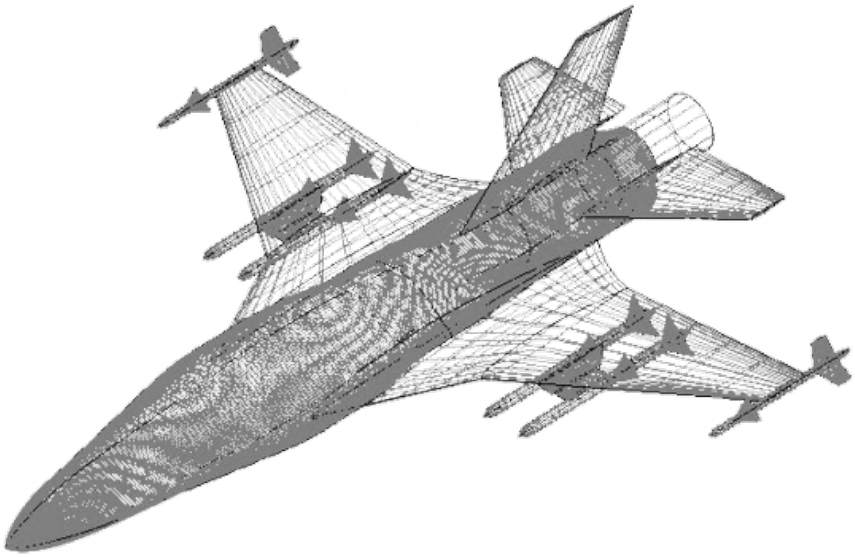

Figure 20: Wing-Body Used in Wave Drag Analysis

A comparison of the area distribution of *SPEAR* and the Sears-Haack Body of equivalent total cross sectional area is shown in Figure 21.

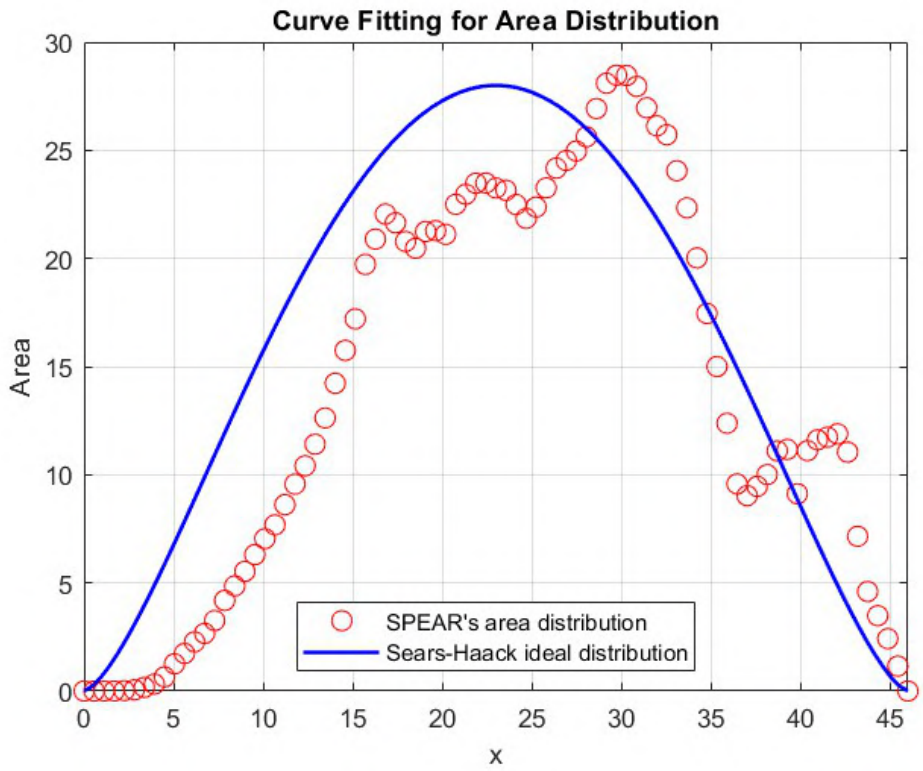

Figure 21: Sears-Haack vs. *SPEAR*'s Area Distribution

While *SPEAR*'s area distribution does not perfectly mimic the Sears-Haack body, which has a known coefficient of wave drag for a specified length and diameter (or a known wave drag value for a known volume, length, and dynamic pressure), it is possible to estimate wave drag based on deviation from the Sears-Haack body. Raymer provided an equation to estimate total wave drag for a non-slender body using a shape factor to differentiate from the Sears-Haack distribution [1]. This formulation includes Mach number as a dependency and is found in Equation 2.

$$(D/q)_{wave} = EWD * ((1 - .386(M - 1.2)^{.57})(1 - \frac{\pi\Lambda_{deg}^{.77}}{100}))(D/q)_{Sears-Haack} \tag{2}$$

The EWD shape factor used in equation 2 depends on how close the area distribution of the aircraft matches that of the Sears-Haack. It is assumed that *SPEAR* has a similar shape factor to that of the F-16, which is a value of 2.2. This scales the wave drag by a factor of 2.2 compared to the optimal wave drag body with the same cross-sectional area and length. To find induced supersonic drag, a program called *Arrow* is used [10]. *Arrow* takes in the aircraft geometry modeled by an arrow wing and the flight condition, and outputs a zero and one-hundred percent suction coefficient of lift and induced drag. By adding the wave, supersonic induced, and parasite drag, the total supersonic drag is estimated. The supersonic drag build-up was used to estimate the maximum Mach number from aero-propulsive forces in Section 6.

5 Propulsion

Engine selection can largely define the capabilities of an aircraft throughout its mission profiles. It is common that engine weight is 10-15% of the empty weight. Due to the long loiter section highlighted in the RFP, an affordable, light, and highly efficient engine was important to find. To combat the immense costs and time of developing an aircraft engine of this caliber, a COTS engine, without any modification, is a requirement. Drawbacks of using a COTS engine is the imperfect fit for the performance required of the engine. *SPEAR* accepts the imperfect fit and achieves a higher Mach as a result of the slightly over sized engine.

5.1 Engine Selection

The engine was selected based on careful definitions of the requirements from the RFP and preliminary sizing on the aircraft's required thrust and fuel efficiency. The engine must be able to provide high afterburning thrust to meet the Mach 1.6 dash and be very fuel efficient at its loiter to meet the four-hour loiter. Research was conducted for a variety of medium to small-size low-bypass turbofan engines that would reach the thrust-to-weight ratio needed for all three missions and the minimum performance requirements specified in the RFP. The three engine companies are well known to the aerospace industry and their contributions were compared against each other. Pratt and Whitney (PW) and General Electric Aerospace Engines (GE) are both American companies that have been providing jet engines to the United States military for nearly 80 years. PW has provided key contributions to the military in their J57 used in the B-52, F100 used in the F-15 and F-16, F119 used in the F-22 Raptor, F135 powering the F-35, and more larger engines for tankers and other cargo aircraft. GE developed revolutionary engines in the J47 used in the B-47, F101 used in the B-1, F110 used in the F-15 and F-16, F404 used in the F-18 legacy hornets, F414 used in the F-18 super hornets, as well as much larger commercial engines. Eurojet was formed by the European companies: Rolls-Royce, MTU Aero Engines, Avio Aero, and Industria de Turbo Propulsores to develop a military grade turbofan engine separate of the US. Though all of these companies have their own history, their joining for this engine program has yielded a single engine, the Eurojet (EJ)200. Though it is unlikely that a European engine manufacturer would be selected for an American homeland defense interceptor, the comparison provides valuable benchmarks and greater selection.

Three engines of choice were chosen for further analysis: the PW F100-220, the GE F414-400, and the EJ200. The properties of these engines including thrust, Thrust Specific Fuel Consumption (TSFC), engine dimensions, and weight are shown in Table 9. The PW F100-220 is the most fuel efficient without afterburner of the three options. The thrust of all three engines is very comparable which was a key factor in narrowing down the field of engines. *SPEAR* aims to minimize weight while maximizing onboard system integration, which would not have been feasible with the PW F100-220 due to its size. The EJ200 is the smallest of the three in both weight and sizem and its compact, lightweight design enables a thrust to weight ratio of 8.77. Unfortunately, the unit cost of $7 million for this engine was too great to

overcome great performance. The GEF414-400 was selected for its ideal thrust-to-weight ratio, size, weight, and cost. This engine powers all of the Navy's F/A-18 E/F Super Hornet boosting Project *SPEAR*'s confidence in the reliability and performance of this engine.

Table 9: Comparison of Candidate Engines

Specification	F100-220	F414-400	EJ200
Dry Thrust [lbf]	14,100	14,447	13,500
Afterburning Thrust [lbf]	23,770	21,496	20,000
Dry TSFC $\left[\frac{\text{lbm}}{\text{lbf}\cdot\text{h}}\right]$	0.7	0.82	0.81
Afterburning TSFC $\left[\frac{\text{lbm}}{\text{lbf}\cdot\text{h}}\right]$	2.1	1.844	1.73
Engine Weight [lb]	3,234	2,512	2,280
Engine Diameter [in]	46.5	39	29
Engine Length [in]	206.1	153.4	157
Thrust-to-Weight Ratio	7.35	8.56	8.77
Cost [2025 USD per engine]	6.5M	5M	7M

SPEAR is equipped with a single General Electric F414-AE-400 turbofan engine placed in the rear of the fuselage. This engine weighs 2512 pounds and has a thrust-to-weight ratio of 8.56, costing approximately $5 million US dollars, scaled for 2025. The F414-400 produces 14447 lbs of dry thrust and 21496 lbs of afterburning thrust with a TSFC of 0.82 and 1.844 $\frac{\text{lbm}}{\text{lbf}\cdot\text{h}}$ respectively, all at sea level static conditions.

5.2 Engine Analysis

Off-design analysis plots are included in the form of two carpet plots, the first for dry and the second for afterburning in Figures 22 and 23.

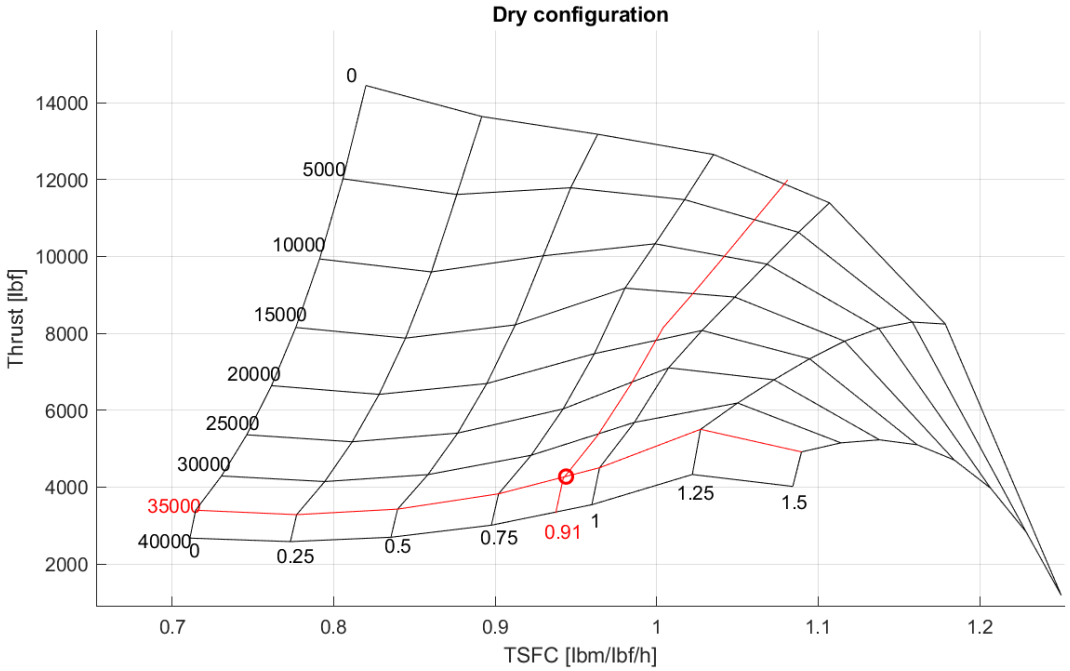

Figure 22: Propulsion Engine Deck Carpet Plot for Dry Run

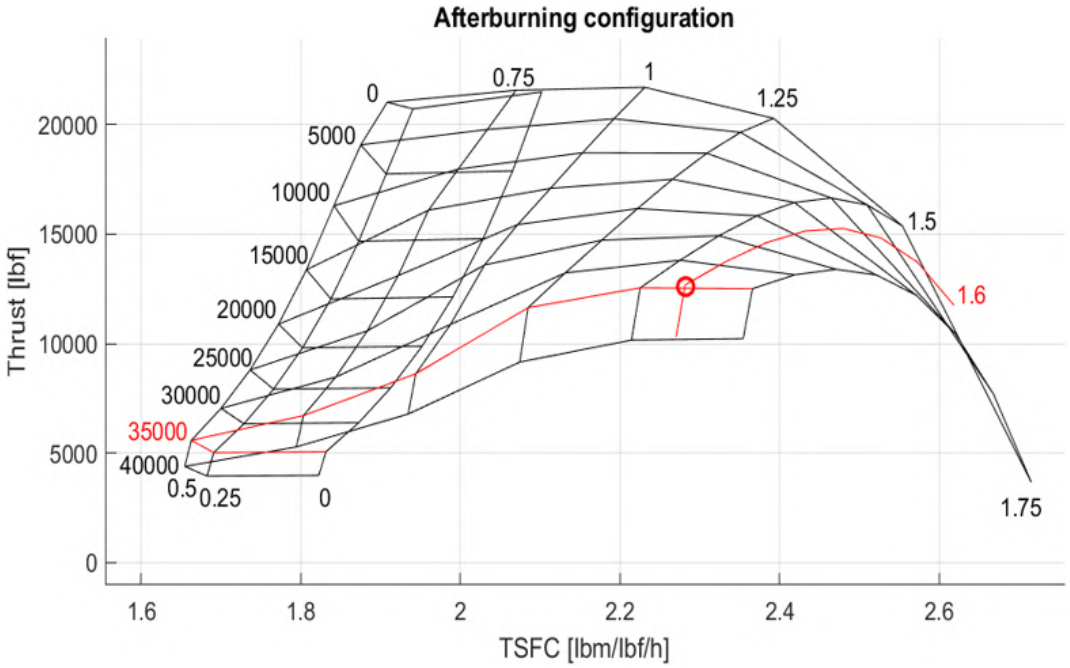

Figure 23: Propulsion Engine Deck Carpet Plot for Afterburning Run

The carpet plots show TSFC measured in $\frac{\text{lbm}}{\text{lbf}\cdot\text{h}}$ on the x-axis and thrust measured in lbm on the y-axis, where lbm is the measure of fuel mass consumed, lbf is pounds of force produced, and h denotes hours. The "vertical" lines on the mesh grid denote the Mach number, and the "horizontal" lines on the mesh grid denote altitude, measured in feet. The red lines with the circle at the intersection are important design points for SPEAR. The intersection for 22 shows

SPEAR's loiter condition at 35,000 ft at a Mach number of 0.91. At these conditions, SPEAR produces up to 4,225 lbf of thrust with a TSFC of 0.94 $\frac{\text{lbm}}{\text{lbf}\cdot\text{h}}$. Pairing this thrust with the drag described in Section 4.5, SPEAR has more than enough thrust to perform the 4 hour loiter mission, while burning 6,330 lbs of fuel.

Afterburning engine performance, denoted in Figure 23, has an intersection of red lines at *SPEAR*'s second design condition, dash. At an altitude of 35,000 ft and a Mach of 1.6, SPEAR can produce 12,600 lbf of thrust with a TSFC of 2.28 $\frac{\text{lbm}}{\text{lbf}\cdot\text{h}}$. Combined with the wave drag analysis performed in 4.5, our aircraft can reach a maximum Mach of 1.83. By completing the engine analysis, *SPEAR* is confident the engine selected is the best option for the size and mission performance of the aircraft with no further improvement or development.

5.3 Intake Design

The overall performance of an air-breathing engine is strongly governed by the design and effectiveness of its intake system. At supersonic flight speeds, a variety of inlet designs can be chosen to make a more efficient inlet. The design Mach number of the aircraft largely defines the intake selected. By using oblique shocks to slow and increase the pressure of the flow before entering the engine, significant efficiency can be gained. Fig. 24 shows various inlet designs and which are more suitable at different flight Mach Numbers [1]. A red line was added to show *SPEAR*'s design Mach Number of 1.6, as required by the RFP. It is clear that the two or three shock external compression inlets are the best choices.

At supersonic speeds, some pressure loss is inevitable due to shocks, it is important to determine how much loss the inlet type will produce. Fig. 25 shows how different inlet designs affect that pressure recovery efficiency. A red and green line were added to Fig. 25 at the design Mach Number of 1.6 and *SPEAR*'s max Mach of 1.83. The pressure ratios for the design and max Mach are 0.97 and 0.96 respectively. To retain the highest total pressure a two or three shock inlet must be used for *SPEAR*. Although a pitot inlet (one shock in Fig. 25) is less complex and cheaper, it also causes a far greater loss in total pressure, especially at *SPEAR*'s max Mach. To accurately compare the two versus three shock inlets, additional metrics such as the weight must be taken into account. On the other hand, the minimal increase in efficiency of three-shock inlet was determined not to be sufficient to outweigh the complexity and cost associated with it.

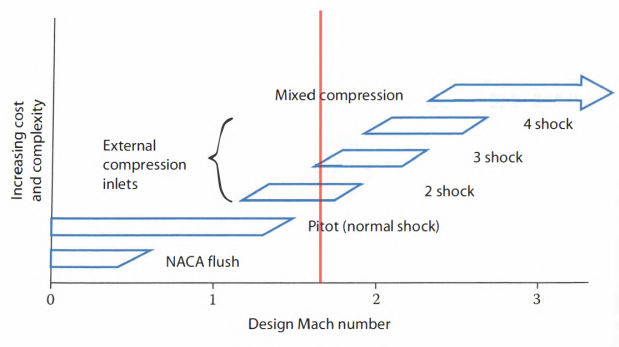

Figure 24: Inlet Type

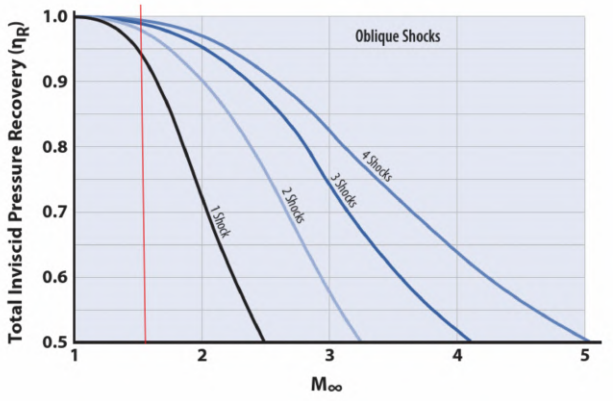

Figure 25: Pressure recovery at different Mach Numbers for different Inlet types

The stagnation pressure of the freestream flow can be thought of as the highest potential pressure achievable, without losses. Pressure losses will be present in all flows due to its non isentropic existence in nature.

The intake system consists of two inlets, each with an area of 2.813 ft^2. This area was calculated using equations 3 and 4 [1], knowing the GE F414-400 runs with a static, sea level mass flow rate 170 lb/s of air. The term $\frac{A_{BLB}}{A_c}$ is a correction factor dependent on Mach Number. That relationship is displayed in Figure 26. At the dash condition of M = 1.6, the correction factor is 0.003. Equations 3 and 4 were applied at the dash condition, where the engine runs at highest capacity.

$$A_{\infty E} = \frac{\dot{m}_E + \dot{m}_s}{32.17 \rho_\infty V_\infty} \tag{3}$$

$$A_c = A_{\infty E} + A_{\infty E} * \frac{A_{BLB}}{A_c} \tag{4}$$

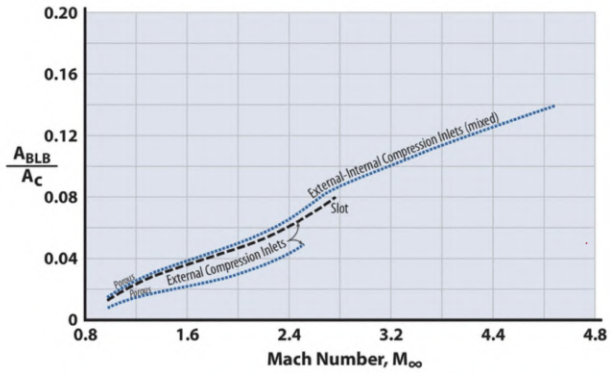

Figure 26: $\frac{A_{BLB}}{A_c}$ as a function of Mach number [2]

The $\dot{m}_s$ term in equation 3 represents the extra mass flow allocated for other systems on the airplane. Table 10 shows which systems were accounted for, and what extra percentage of the mass flow had to be accounted for. The final required intake area is 5.625 ft^2, which is divided into two equal area inlets. A fully remote aircraft removes the need for life support, allowing for a smaller inlet and more efficient engine.

Table 10: Mass flow required for aircraft systems

System	Percent extra mass flow
Engine Oil Cooling	1.5%
Engine Nacelle Cooling	4%
Ejector Nozzle	1.5%
Hydraulics	0.5%
Environment Control	2%

The environmental control system must have 2% of the engine's airflow and provide 50 kW of power. *SPEAR* utilizes a PTMS to eliminate engine bleed air. By eliminating the need for bleed air, the engine performs more efficiently, allowing *SPEAR* to loiter and dash for longer periods of time. More information about the PTMS can be found in 8.4. The inlet system is an S-duct with the inlets themselves located along the fuselage, slightly ahead of the wings to avoid the shock and turbulent air caused by the wing. The outline of that double-inlet design is displayed in Figure 27. The intakes merge before entering the engine and air flows in a single duct before entering the engine.

The front face of the S-Duct is a half-ellipse with a semi-minor axis of 0.5046 ft and a semi major axis of 0.757 ft, the major axis being flat along the fuselage of the aircraft. The length of the inlet ramp is 4.541 ft, which is calculated using a ramp length to inlet height ratio of 9 to minimize diffuser loss, as indicated by Figure 28.

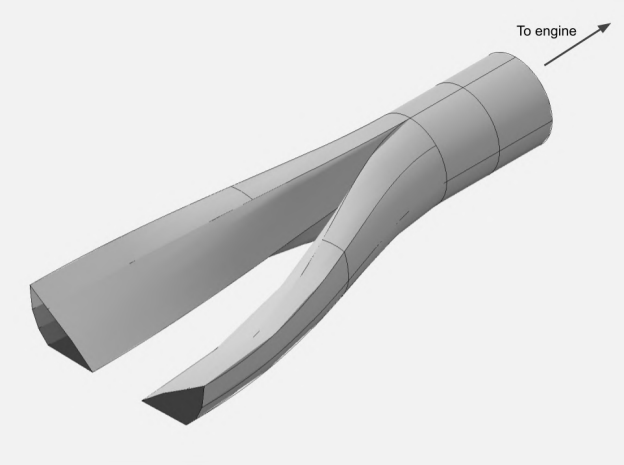

Figure 27: SPEAR's S-duct inlet design

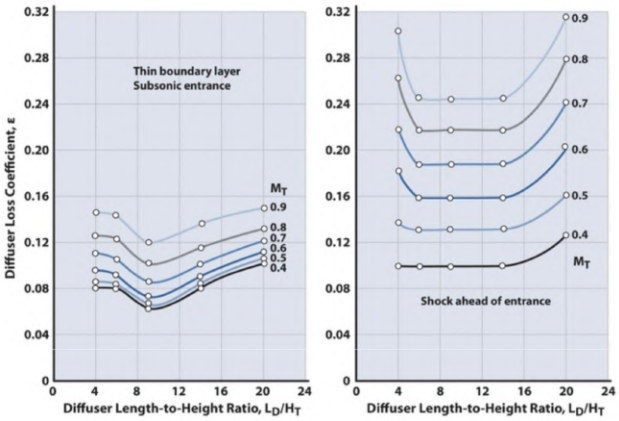

Figure 28: Length to Height ratio of the inlet ramp [2]

5.3.1 Boundary Layer Ingestion

Turbulent boundary layer ingestion is a necessary design consideration for all aircraft due to its impact on engine performance. Boundary layer ingestion occurs when the flow attached, or detached, to the body enters the intake. The flow in the boundary layer is traveling at slower speeds with higher vorticity. This results in the engine effectively having a smaller effective inlet area, reducing airflow to the engine. Airflow to an air-breathing engine is of vital importance and must be as undisturbed as possible. Figure 29 illustrates the boundary layer ingestion being described above. The slower moving boundary layer, shown in blue, is entering the engine along with the free stream. Since the flow on one side of the slower than that of the freestream, there will be turbulence and distortion, potentially causing damage to the fan. Based on the turbulent boundary layer analysis conducted between Mach 0.8 and 1.8, an offset of the fuselage was determined to be necessary to avoid boundary layer ingestion. The intake is offset from the fuselage by 0.787 inches to avoid any ingestion.

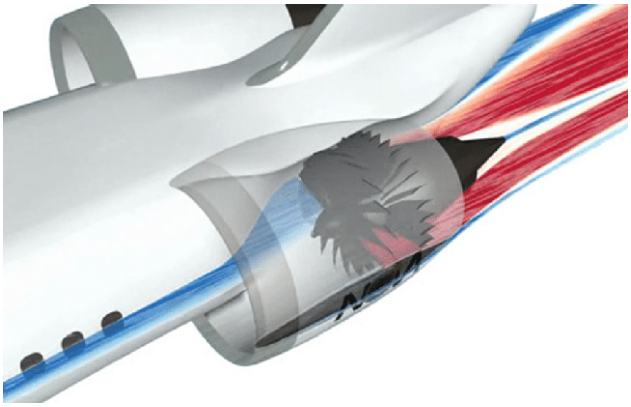

Figure 29: Boundary Layer Ingestion in Turbofan Engine [3]

5.4 Thrust Vectoring

Thrust vectoring is a modern system integrated with the propulsion device on few fighter aircraft designed to enhance maneuverability and performance. The F-22A is the only historical fighter with thrust vectoring. The F-22A was developed as a stealthy air superiority fighter and is the most lethal dog fighter in the United State's Arsenal. The F119-PW-100 engine is an integral part of the F-22's dominance. Exact unit cost is not available for acquisition costs, though PW was awarded a contract this year, 2025, for $1.5 billion to maintain over 400 engines for three years. Maintenance of this engine costs $1.25 million annually per the most recent contract [11]. Additional maintenance contracts have been given for the maintenance of this engine at a price point of $2+ million per year [12].

Thrust vectoring in *SPEAR* could improve maneuverability and climb performance. Specifically, the low speed, high angle of attack maneuverability would see significant improvements. Through complex engineering, the nozzle diverts the thrust of the engine a few degrees to give the thrust influence with the other forces the aircraft is experiencing. Figure 30 illustrates a comparison between two dimensional and axisymmetric nozzles. In the two dimensional nozzle, the exhaust can be deflected to supply the propulsive force of the engine in a direction not parallel with the length of the engine. This has been used in the F-22 and Su-37 to improve pitching ability.

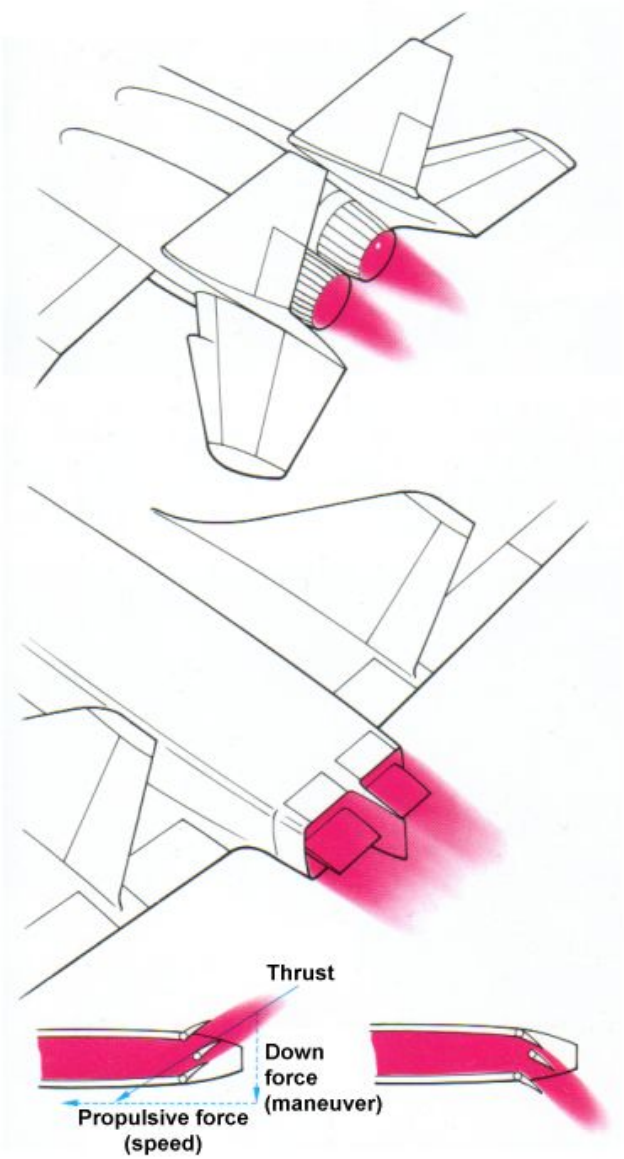

Figure 30: Comparison of 2D Vectored and Axisymmetric Nozzle [3]

Significant weight would be added to the propulsion system to include thrust vectoring. In the 1980s and 1990s, National Aeronautics and Space Administration (NASA) conducted a research program using a F-18 Hornet known as the High Alpha Research Vehicle (HARV) program. The combination of strakes, thrust vectoring, and a flight control system provided stability in a previously dangerous flight regime. The total weight of all these systems and a spin recovery parachute was 4,119 lbs [13]. It can be safely assumed that the thrust vectoring on both engines was approximately 2,000 lbs, or 1,000 lbs per engine. Adding weight to the aircraft can reduce fuel efficiency in the loiter and reduce maneuverability.

Due to the overwhelming acquisition and maintenance costs associated with thrust vectoring, *SPEAR* will not feature

this technology. The priority of *SPEAR* is to deliver a high performance, low cost interceptor. Utilizing this complex, expensive technology was therefore avoided.

6 Performance

As mentioned in Section 2.3, the RFP lists requirements that *SPEAR* needs to meet. This section demonstrates where *SPEAR* meets, or closely approaches, all of those requirements.

6.1 Dash and Max Mach

To determine the aircraft's maximum speed for the dash segment at 35,000 ft, the aircraft's required thrust was plotted against the available thrust across a range of Mach numbers. The thrust required and available for this flight phase are shown in Figure 31. Notably, these curves predict the thrust from a purely performance perspective.

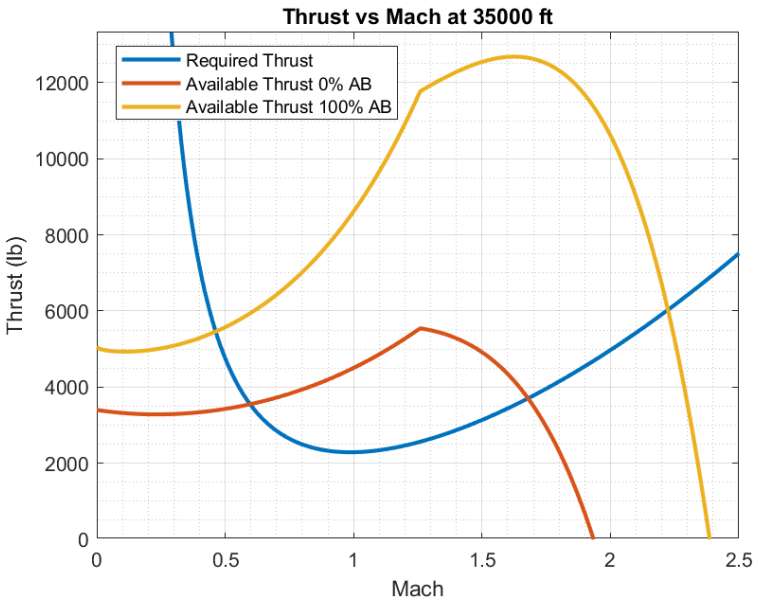

Figure 31: Thrust vs Mach at 35k ft

After additional aerodynamic and propulsion analysis was conducted that looked at supersonic drag effects, the maximum Mach values attainable across a range of altitudes were found. Shown in Figure 32, the maximum Mach value for an altitude of 35,000 ft. is Mach 1.83.

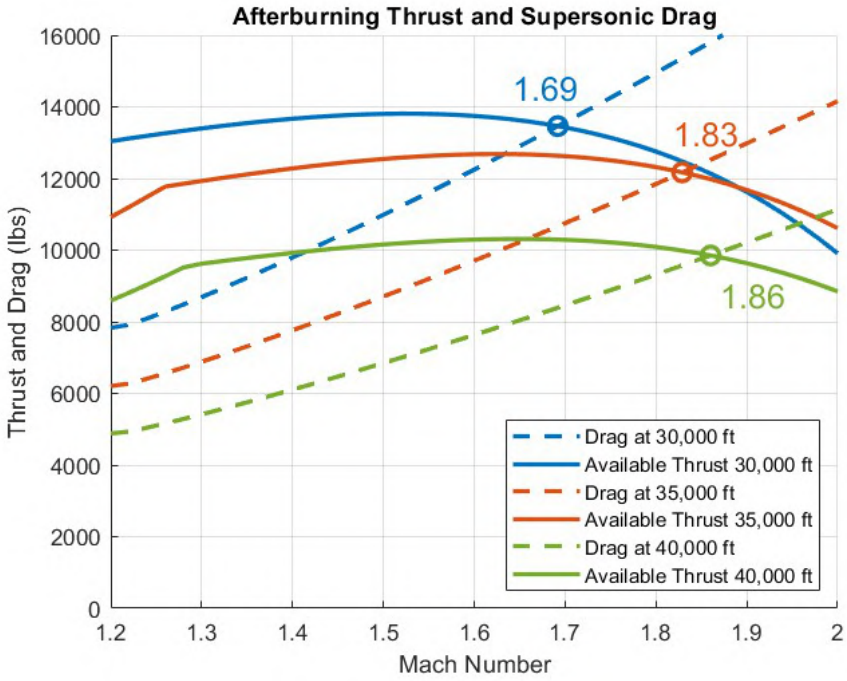

Figure 32: Wave drag and afterburning thrust plotted at different altitudes

Although the maximum Mach at 35,000 ft. exceeds the RFP requirement by Mach 0.23, this extra capability allows *SPEAR* to reach its target faster while not degrading its propulsive efficiency.

6.2 Loiter and Cruise

For the loiter and escort mission segments, the maximum endurance Mach number is found by locating the lowest point on the required thrust curve. This optimum Mach number is Mach 0.91 at 35,000 ft as shown in Figure 31. Since the cruise altitude is undefined in the RFP, the best cruise altitude is calculated by analyzing the maximum Mach number of a range of mission phase altitudes. For *SPEAR*, this altitude is 26,730 ft at a best cruise Mach of 0.76 as seen in Figure 33.

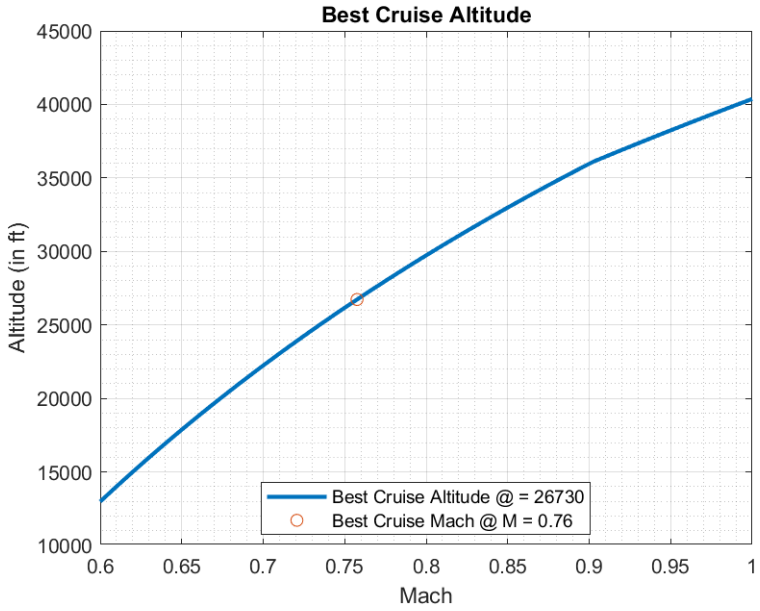

Figure 33: Best Cruise Altitude

At the best cruise altitude, the lowest speed the aircraft can operate at before stall is Mach 0.34. Because the escort phase occurs at 26,730 ft and the stall speed is approximately Mach 0.34, the best escort Mach for *SPEAR* is 0.4. This speed avoids stall conditions while minimizing fuel burn. This is shown in Figure 34, where the lowest Mach Number is represented by a blue dot.

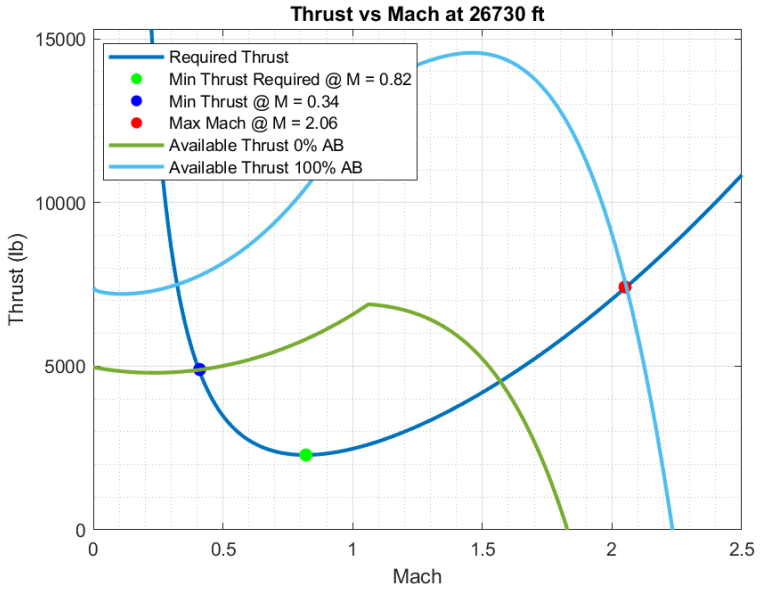

Figure 34: Minimum Thrust at Best Cruise Altitude

A maximum range Mach number is determined by plotting the thrust against Mach curves for the cruise flight segment. The maximum Mach is 2.06 as shown by the red dot in Figure 34. It should be noted that this Mach value is

independent of the RFP missions. It does not account for the structural effects of flying at this speeds at best cruise altitude, and is solely based on thrust performance.

6.3 Specific Excess Power

The RFP required *SPEAR* to perform several specific excess power metrics across varying altitudes and load factors with a 50% fuel weight. Figure 35 provides Specific Excess Power (SEP) curves for sea level and 15,000 ft. conditions. The RFP specific requirements at sea level and 15,000 ft are represented as circles in Figure 35, and correspond to a specific SEP curve on the graph. *SPEAR* meets all of these SEP requirements.

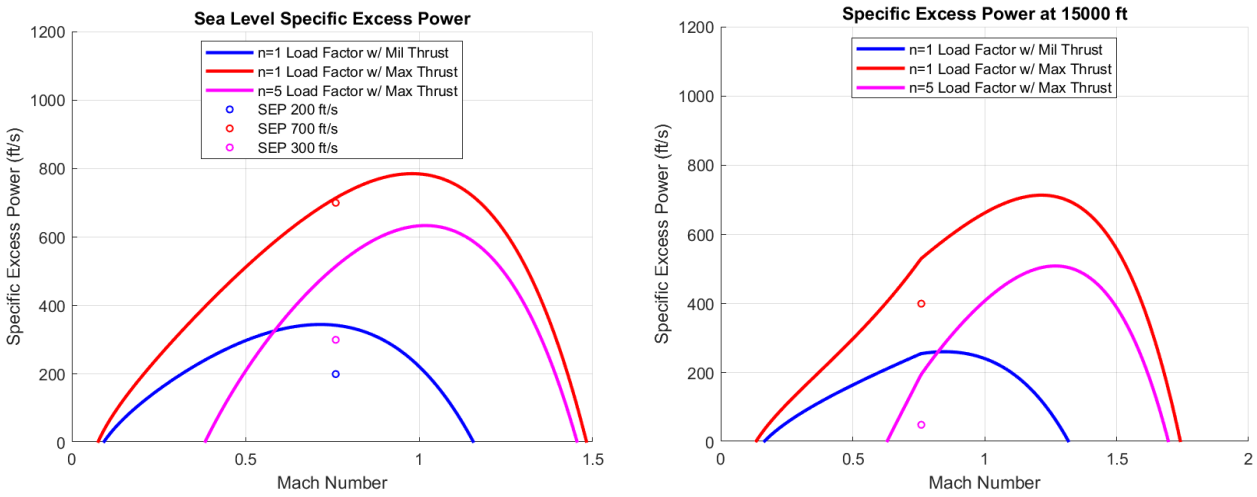

(a) Sea Level SEP (b) 15,000 ft SEP

Figure 35: Specific Excess Power at Sea Level and 15,000 ft. conditions

As shown in Figure 35(a), the SEP requirements at sea level are well within the specific excess power curves. In Figure 35(b), the RFP requirements also fall well within the SEP curves, with the requirements for 1-g at military thrust and 5-g maximum thrust having the same value.

6.4 Maximum Instantaneous Turn Rate

The maximum instantaneous turn rate (ITR) is the highest numbers of degrees aircraft can turn per second at optimum settings at the beginning of its turn. This rate is constrained by the aircraft's maximum structural load factor, which is defined in the RFP to be $n = 7$. For *SPEAR*, this results in a maximum Instantaneous Turn Rate (ITR) of $17.8\frac{deg}{s}$ at a Mach of 0.76, as shown in Figure 36.

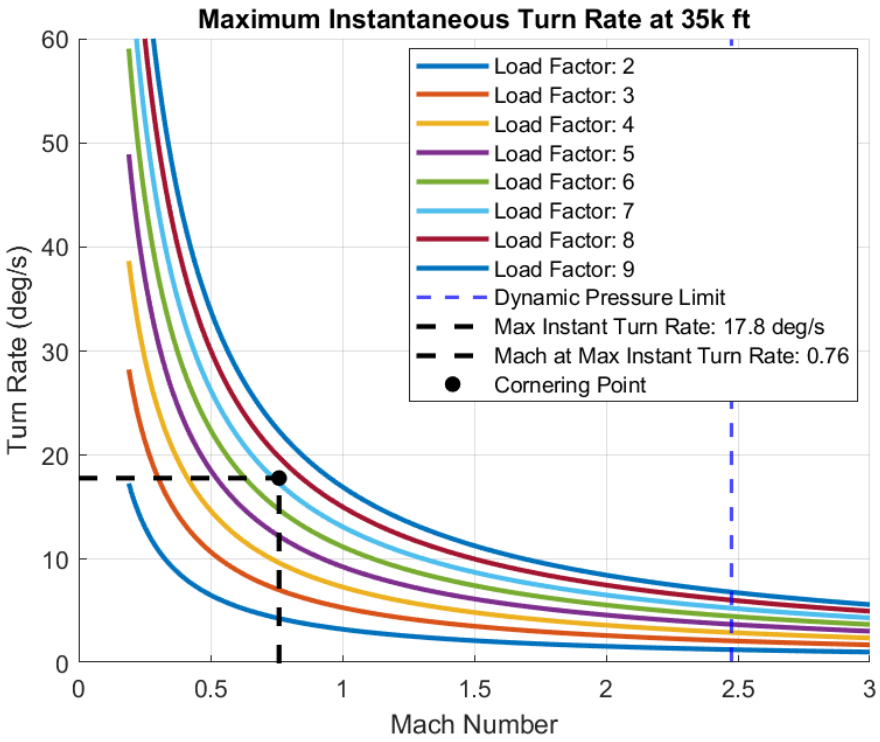

Figure 36: *SPEAR* Maximum Instantaneous Turn Rate at 35,000 ft

SPEAR fails to meet the RFP requirement by $0.2\frac{deg}{s}$. However, this is a direct result of the aircraft flying at the best cruise Mach. If the maneuvering Mach Number is lowered by 0.02, *SPEAR* can meet the RFP requirement.

6.5 Sustained Turn Rate

The sustained turn rate (STR) is defined as the maximum rate at which an aircraft can continuously turn without loss of airspeed or altitude. According to the RFP, the aircraft must be capable of achieving a 5-g STR at an altitude of 15,000 ft at Mach 0.9. To determine whether *SPEAR* meets this requirement, its STR envelope is computed as a function of Mach number. The maximum achievable load factor at each Mach number is then converted into a corresponding turn rate and is presented in Figure 37 following the same format as the ITR analysis.

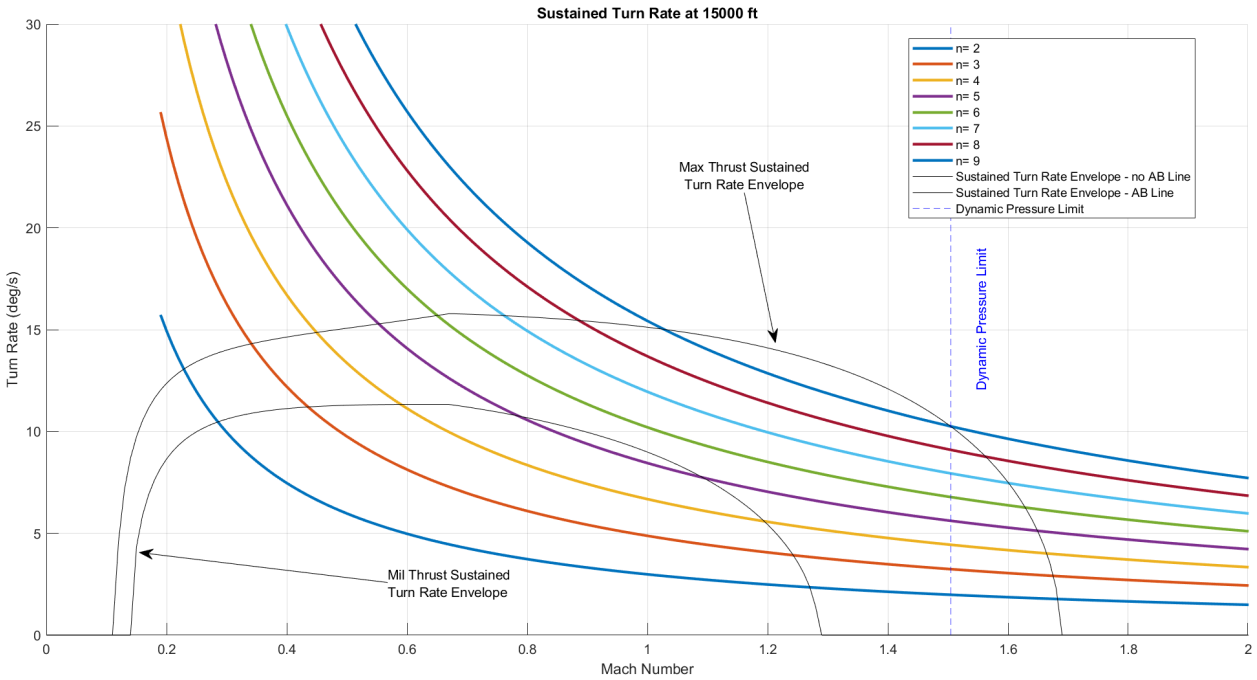

Figure 37: *SPEAR* Sustained Load Factor at 15,000 ft

The lower part of the envelope is the non-afterburning Sustained Turn Rate (STR). It slightly rises above $n = 5$ around Mach 0.9, which means that *SPEAR* can pull a 5.06-g sustained turn at Mach 0.9. Because the afterburning turn rate is limited by the structural load capability of the aircraft, *SPEAR* can pull a maximum of 7-g sustained turn at Mach 0.9.

6.6 Takeoff and Landing

The RFP specifies that both takeoff and landing distances must exceed 8,000 ft, corresponding to standard NATO runway lengths. The following analysis confirms that *SPEAR* meets these requirements under dry and icy sea level conditions or all mission configurations. In addition, the balanced field length and landing field lengths across each mission is entailed in the section below. The performance analysis for the additional RFP for a 4,000 MSL takeoff and landing altitude is located in 6.8.

Takeoff parameters was calculated using Nicolai [2]. Takeoff distance is broken into four segments, including a 50 ft obstacle clearance, and is summed in the total takeoff distance. It is analyzed using aircraft lift and drag values during takeoff.

Table 11 presents the takeoff distances across all missions in dry sea-level conditions. *SPEAR* meets the distance requirement in the RFP across all missions, having a maximum takeoff distance of 2,012 ft in Mission 1, well below the RFP 8,000 ft limit. Missions 1 and 3 yield identical performance due to identical maximum possible internal fuel

and weapons carriage loading.

Table 11: Dry Condition Takeoff Performance at Sea Level

Metric	Mission 1	Mission 2	Mission 3
Ground Roll (ft)	1,426	593	1,426
Rotation Distance (ft)	410	342	410
Transition Distance (ft)	106	73	106
Clearing Obstacle Distance (ft)	74	74	74
Total Takeoff Distance (ft)	2,018	1,083	2,018
Balanced Field Length	15,740	14,441	15,740

To model icy runway takeoff performance, a takeoff friction coefficient of 0.01 was used, based on historical fighter data found in Nicolai [2]. Icy runway takeoff performance is shown in Tables 12 and 14. The worst-scenario takeoff distance is 2,020 ft and the corresponding maximum landing distance is 4,367 ft. Even under these more demanding surface conditions, all distances remain significantly below the 8,000 ft limit.

Table 12: Icy Condition Takeoff Performance at Sea Level

Metric	Mission 1	Mission 2	Mission 3
Ground Roll (ft)	1,428	593	1,428
Rotation Distance (ft)	410	342	410
Transition Distance (ft)	106	73	106
Clearing Obstacle Distance (ft)	74	74	74
Total Takeoff Distance (ft)	2,020	1,095	2,020
Balanced Field Length	16,538	15,425	16,538

SPEAR meets all RFP takeoff and landing requirements for dry and icy conditions.

Landing performance under dry conditions is presented in Table 13. Distances are segmented by approach, free roll, braking phases and are calculated based on 50% fuel weight remaining. The maximum landing distance observed is 1,996 ft, well within the RFP limits.

Table 13: Dry Condition Landing Performance at Sea Level

Metric	Mission 1	Mission 2	Mission 3
Approach Distance (ft)	888	1,004	888
Free Roll Distance (ft)	487	509	487
Brake Distance (ft)	539	481	539
Total Landing Distance (ft)	1,915	1,996	1,915
Landing Field Length	3,197	3,332	3,197

Additionally, *SPEAR* icy condition landing analysis was conducted. The results of this analysis are shown in Table 14. To model icy runway landing performance, a landing friction coefficient of 0.1 was used, based on historical fighter data found in Nicolai [2].

Table 14: Icy Condition Landing Performance at Sea Level

Metric	Mission 1	Mission 2	Mission 3
Approach Distance (ft)	888	1,004	888
Free Roll Distance (ft)	487	509	487
Brake Distance (ft)	2,657	2,852	2,657
Total Landing Distance (ft)	4,033	4,367	4,033
Landing Field Length	6,735	7,293	6,735

SPEAR meets all RFP takeoff and landing distance requirements, even in degraded runway conditions.

6.7 Performance Measures of Merit

In addition to the RFP MoM pertaining to the mission performance, Section 4 of the RFP outlines several additional maneuverability MoM the aircraft must perform. All of these MoM are simulated at 50% fuel weight required for each mission. The results for all three missions, at each of the design points is presented in 6.8. The maneuver weights and missile capacity used for this analysis are specified in Table 15. Since Missions 1 and 3 are simulated with the maximum possible internal fuel and weapons carriage capacity, their results will look similar.

Table 15: Maneuver Weights

Metric	Mission 1	Mission 2	Mission 3
Weight (lb)	21,054	14,487	21,054
Missile Capacity	6	2	6

6.8 Performance Foldout

Mission 1 & 3 Sustained Load Factor Envelopes

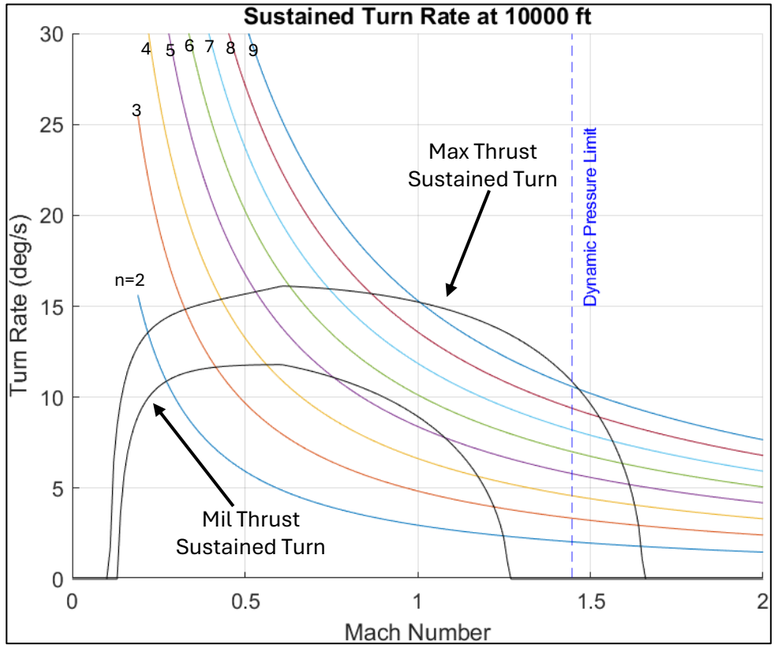

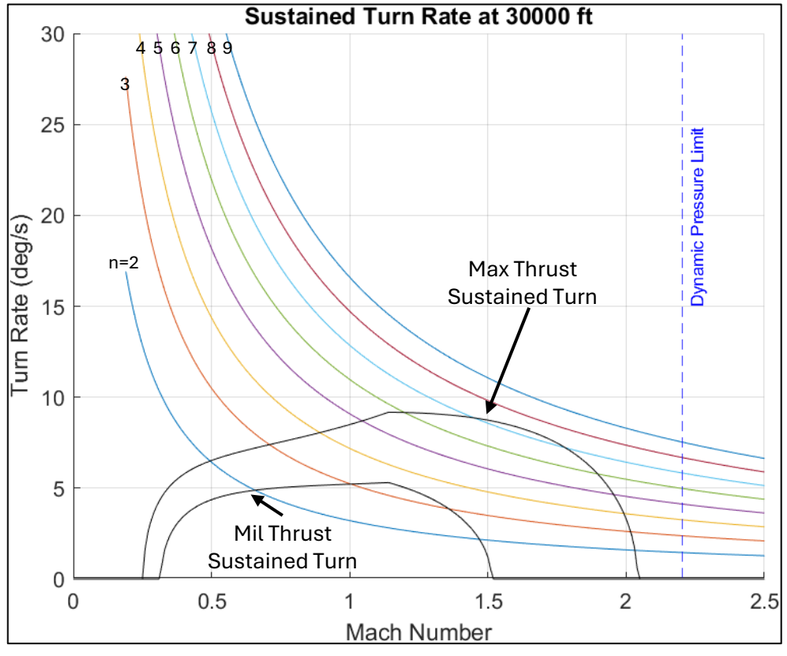

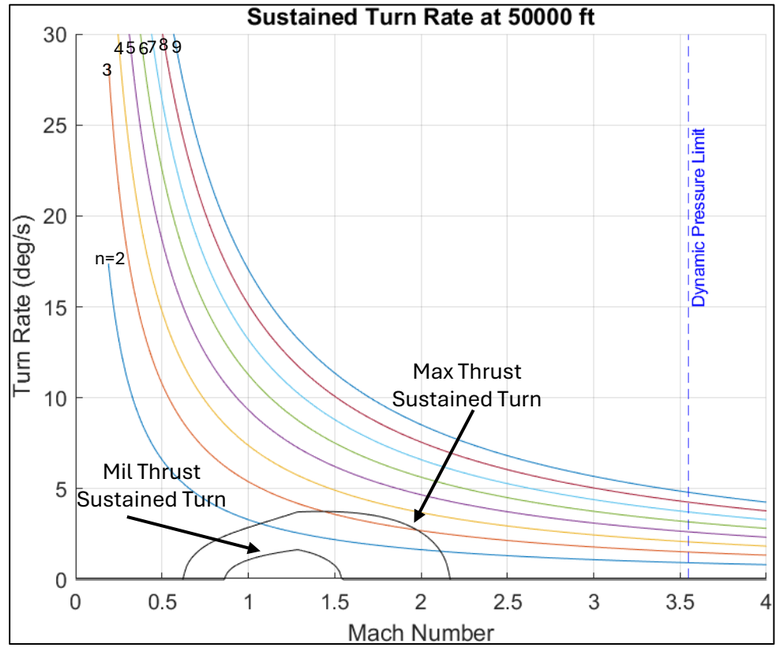

Mission 2 Sustained Load Factor Envelopes

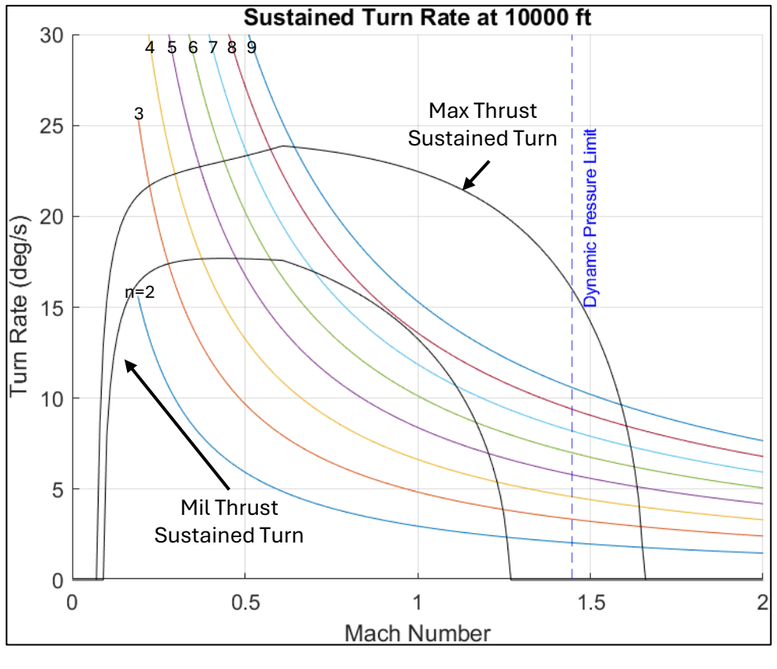

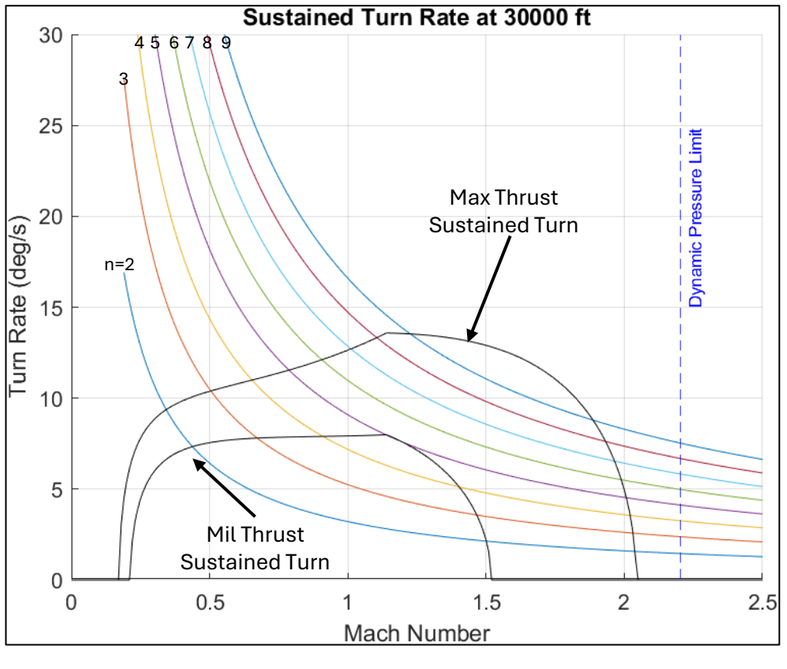

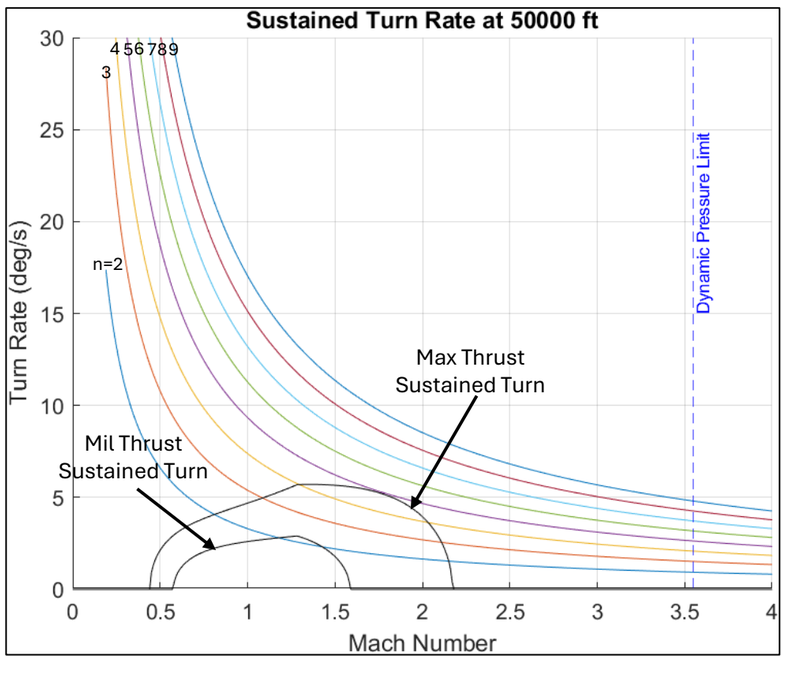

Mission 1-3 Takeoff and Landing Analysis

Takeoff Analysis

Sea Level Dry Conditions			
Metric	**Mission 1**	**Mission 2**	**Mission 3**
Ground Roll	1426	593	1426
Rotation	410	342	410
Transition	106	73	106
Clearing Obstacle	74	74	74
Takeoff	2018	1083	2018
Balanced Field	15740	14441	15740

Sea Level Icy Conditions			
Metric	**Mission 1**	**Mission 2**	**Mission 3**
Ground Roll	1428	593	1428
Rotation	410	342	410
Transition	106	73	106
Clearing Obstacle	74	74	74
Takeoff	2020	1095	2020
Balanced Field	16538	15425	16538

4,000 MSL Dry Conditions			
Metric	**Mission 1**	**Mission 2**	**Mission 3**
Ground Roll	1578	652	1578
Rotation	434	361	434
Transition	118	81	118
Clearing Obstacle	74	74	74
Takeoff	2205	1170	2205
Balanced Field	14592	13569	14592

4,000 MSL Level Icy Conditions			
Metric	**Mission 1**	**Mission 2**	**Mission 3**
Ground Roll	1580	653	1580
Rotation	434	361	434
Transition	118	81	118
Clearing Obstacle	74	74	74
Takeoff	2207	1170	2207
Balanced Field	15199	14340	15199

Landing Analysis

Sea Level Dry Conditions			
Metric	**Mission 1**	**Mission 2**	**Mission 3**
Approach	888	1004	888
Free Roll	487	509	487
Braking	539	481	539
Landing	1915	1996	1915
Level Field Length	1397	3332	1397

Sea Level Icy Conditions			
Metric	**Mission 1**	**Mission 2**	**Mission 3**
Approach	888	1004	888
Free Roll	487	509	487
Braking	2657	2852	2657
Landing	4033	4367	4033
Level Field Length	6735	7293	6735

4,000 MSL Dry Conditions			
Metric	**Mission 1**	**Mission 2**	**Mission 3**
Approach	1100	1232	1100
Free Roll	518	541	518
Braking	520	440	520
Landing	2139	2214	2139
Level Field Length	3573	3698	3573

4,000 MSL Level Icy Conditions			
Metric	**Mission 1**	**Mission 2**	**Mission 3**
Approach	1100	1232	1100
Free Roll	518	541	518
Braking	3004	3211	3004
Landing	4623	4985	4623
Level Field Length	7721	8325	7721

Maneuverability Capabilities

Criteria	Requirement	Project Spear Compliance	
Climb to 35,000 ft in 1 minute	> 583 ft/s	**605 ft/s**	✓
1-g Specific Excess Power Military Thrust: Mach = 0.9 at Sea Level	> 200 ft/s	**315 ft/s**	✓
1-g Specific Excess Power Military Thrust: Mach = 0.9 at 15,000 ft	> 50 ft/s	**279 ft/s**	✓
1-g Specific Excess Power Max Thrust: Mach = 0.9 at Sea Level	> 700 ft/s	**818 ft/s**	✓
1-g Specific Excess Power Max Thrust: Mach = 0.9 at 15,000 ft	> 400 ft/s	**649 ft/s**	✓
5-g Specific Excess Power Max Thrust: Mach = 0.9 at Sea Level	> 300 ft/s	**659 ft/s**	✓
5-g Specific Excess Power Max Thrust: Mach = 0.9 at 15,000 ft	> 50 ft/s	**381 ft/s**	✓
Sustained Load Factor Max Thrust: Mach = 0.9 at 15,000 ft	> 5.0 g's	**5.07 g's**	✓
Maximum Instantaneous Turn Rate at 35,000 ft	> 18 deg/s	**17.8 deg/s**	✗

Payload vs Range

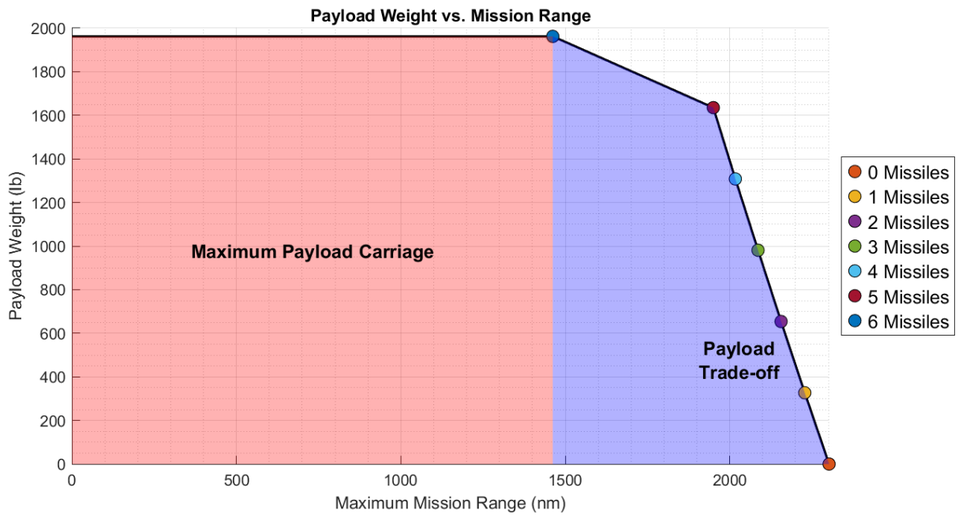

7 Stability and Control

Empennage design and sizing was performed based on traditional horizontal and vertical tail sizing. The empennage sizing parameters such as span, moment arm, and aspect ratio were iteratively calculated until they aligned with historical data for aircraft of this category. The empennage sizing for *SPEAR* is further discussed in 7.1. Additionally, the control surface sizing analysis is outlined in 7.2.

The RFP outlines a static stability margin for the aircraft to be $\pm 10\%$. A flight control system is required if the aircraft is statically unstable. Stability analysis was conducted using methods in Nicolai [2], Raymer [1], and Mason [10] to determine the longitudinal and lateral-directional static stability.

SPEAR is engineered to have a static margin within the RFP threshold, maintaining a slight instability for a few mission segments, requiring the use of a digital flight control system. To optimize *SPEAR's* dynamic stability performance, dynamic stability analysis was conducted in *DATCOM*. If the aircraft was determined to be dynamically unstable, the aircraft configuration was iteratively manipulated until its dynamic modes were dynamically stable. The static and dynamic stability analysis conducted on *SPEAR* is discussed in 7.3 and 7.4.

7.1 Empennage Design

A stability analysis was conducted on *SPEAR* to determine appropriate control surface sizing and evaluate overall controllability. This analysis included calculating the tail volume coefficients, which are critical in assessing the aircraft's static stability characteristics. The tail volume coefficients were computed using the following equations:

$$c_{HT} = \frac{L_{HT} S_{HT}}{MAC_{wing} S_{wing}} \tag{5}$$

$$c_{VT} = \frac{L_{VT} S_{VT}}{MAC_{wing} S_{wing}} \tag{6}$$

where L_{HT} is the moment arm from the Mean Aerodynamic Chord (MAC) of the wing to the MAC of the horizontal tail and L_{VT} is the moment arm from the MAC of the wing to the MAC of the vertical tail. S_{HT} and S_{VT} are the areas of the horizontal and vertical tails, respectively. These coefficients were calculated and are found in Table 16. These values align closely with typical design targets for fighter aircraft, 0.4 and 0.07, respectively, as cited in Nicolai [2].

Table 16: Empennage Tail Characteristics

Characteristic	Horizontal Tail	Vertical Tail
Root Airfoil	NACA 0006	NACA 0010
Tip Airfoil	NACA 0004	NACA 0006
b (ft)	13	7.25
λ	31.7	44.4
S (ft^2)	68.5	47.1
AR	2.47	1.12
$\Lambda_{\frac{c}{4}}$ **(deg)**	40	50
L_{HT} **(ft)**	19.3	-
L_{VT} **(ft)**	-	13.5
Volume Coefficients	0.42	0.07

The horizontal tail has a 0 ft offset with respect to the wing to prevent unwanted pitching moments. By having a 0 ft vertical offset, a neutral balance is maintained between the lift forces generated by the wing and the counteracting forces generated by the horizontal tail. When the horizontal tail and wing are aligned at the same height, there is no additional vertical force component being introduced that could cause an imbalance in the aircraft's pitch behavior. This ensures that the pitching moments from the wing and tail are more controlled and predictable. Additionally, the wing downwash can have an adverse effect on the horizontal tail. By placing the tail at the same height as the wing, the effects of downwash are less likely to cause unpredictable aerodynamic forces on the tail.

7.2 Control Surface Sizing

Control surface sizing was determined by historical aircraft data provided in Nicolai [2]. Table 17 provides the additional control surfaces used on *SPEAR* that are not highlighted in Table 16.

Table 17: Wing Control Surface Sizing

Characteristic	Flap	Aileron
Span (ft)	4.11	10.26
Chord (ft)	3.71	2.33
Area (ft^2)	16.07	23.91
Deflection (deg)	± 25	± 25

The trailing edge flaps span from 0.2 ft outboard of the strake root to 90% of the distance between the strake root and

strake tip. The overall flap area is 16.07 sq. ft. The ailerons initially were sized to span from where the wing's trailing edge transitions from its LEX to 90% of the wingspan. However, after refined structural analysis was conducted that analyzed the implications of wingtip-mounted missiles, the aileron's starting location was shifted 4 in. outboard of the break point between the strake and wing. The overall aileron area is 23.91 sq. ft. The dimensioned control surfaces are shown in Figure 38.

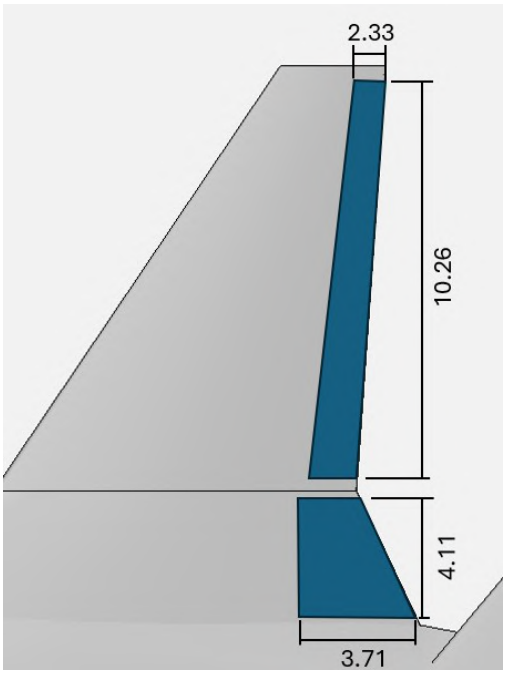

Figure 38: Wing Control Surface Sizing

The rudder was sized using rules from Raymer [1]. It spans from the fuselage to 90% of the vertical tail length and is 30% of the vertical tail chord. The overall rudder area is 19.14 sq. ft. The dimensioned rudder control surface is shown in Figure 39.

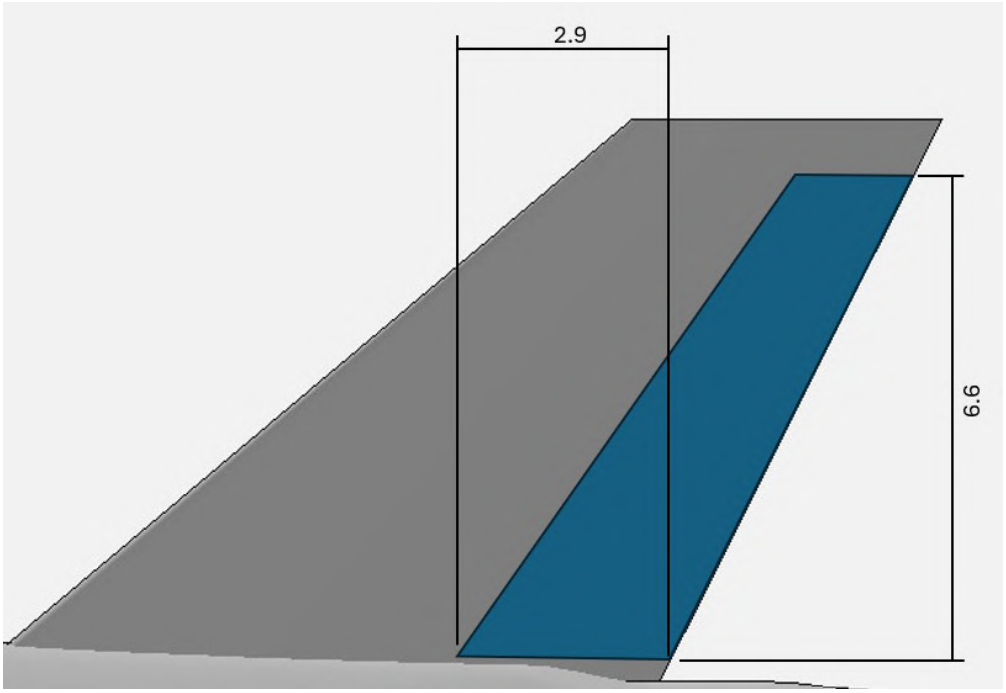

Figure 39: Vertical Tail Control Surface Sizing

7.3 Static Stability Analysis

The RFP requires the aircraft to maintain a longitudinal static margin within ±10%. Stability analyses were conducted using established methods from Roskam [14], Nicolai [2], and instructional materials from the late Dr. Bill Mason of Virginia Tech [10]. These analyses assessed both longitudinal and lateral-directional static stability for *SPEAR* across all mission flight segments defined by the RFP. *SPEAR* satisfies the static margin requirement for each mission phase; however, it exhibits a slight degree of aerodynamic instability. As such, compliance with the RFP necessitates the integration of a flight control system to ensure acceptable handling qualities. Dynamic stability derivatives were also computed using Digital Compendium (DATCOM) and legacy *FORTRAN* tools developed by Dr. Mason [10]. A detailed discussion of both the static and dynamic stability characteristics of *SPEAR* is provided in the following sections.

7.3.1 Longitudinal Static Stability

Following the sizing of the empennage and control surfaces, key longitudinal stability metrics—including center of gravity (Center of Gravity (CG)), neutral point (Neutral Point (NP)), and static margin (Static Margin (SM))—were calculated for takeoff and across all flight phases. These values are presented in Table 18.

Table 18: General Stability

Characteristic	Metric
Center of Gravity (ft)	24.74
Neutral Point (ft)	24.33
Static Margin	-0.04%

In addition, *SPEAR's* inertial properties were calculated using estimation methods described by Raymer [1]. The key components of the aircraft's inertial matrix are summarized in Table 19.

Table 19: *SPEAR's* inertial matrix

Characterist	Metric
I_{xx} ($\frac{slugs}{ft^2}$)	92868
I_{yy} ($\frac{slugs}{ft^2}$)	43320
I_{zz} ($\frac{slugs}{ft^2}$)	79049
I_{xz} ($\frac{slugs}{ft^2}$)	0

These inertial values were used to calculate the longitudinal aerodynamic stability derivatives, which are critical to assessing the effectiveness of the horizontal tail. The key derivatives are listed in Table 20.

Table 20: Longitudinal Static Stability Derivatives

Derivative	Value
C_{L_α}	3.56
C_{M_α}	-0.53
$C_{M_{\delta_e}}$	-0.64

The negative pitching moment slope, $C_{M_\alpha} = -0.53$, confirms that *SPEAR* exhibits positive static longitudinal stability by generating a restoring moment in response to pitch disturbances. Additionally, the elevator control derivative, $C_{M_{\delta_e}} = -0.64$, indicates effective pitch control authority, which is essential for agile response and maneuverability in high-performance flight regimes.

7.3.2 Lateral-Directional Static Stability

The United States Air Force Stability and Control Digital DATCOM tool was used to evaluate the lateral-directional static stability of *SPEAR*. The results of this analysis are summarized in Table 21.

Table 21: Lateral-Directional Static Stability Derivatives

Derivative	Value
C_{n_β}	0.18
C_{L_β}	-0.12
C_{n_p}	-0.01
C_{L_p}	-0.53
C_{Y_p}	0.01
C_{n_r}	0.36
C_{L_r}	0.34
C_{M_q}	-2.10
$C_{n_{\beta_{dyn}}}$	0.01
Lateral Control Spin Parameter	0.01

The derivatives in Table 21 exhibit correct signs consistent with established design criteria for fighter aircraft, as discussed in Nicolai [2]. In particular, $C_{n_\beta} = 0.18$ satisfies the requirement for static directional stability ($C_{n_\beta} > 0$) per MIL-HDBK-1797 [15]. A positive value aids in yaw damping and helps prevent divergent Dutch roll tendencies.

The negative roll damping derivative, $C_{L_p} = -0.53$, ensures compliance with roll-handling quality requirements defined in MIL-F-8785C [16] and MIL-HDBK-1797 [15]. Likewise, the slightly negative $C_{L_\beta} = -0.12$ meets the handbook's criterion that left aileron force is generated during left sideslip, which supports automatic roll correction and enhances lateral control stability. The pitching moment derivative, $C_{M_q} = -2.10$, contributes to damping in the short-period pitch mode and aligns with acceptable values reported in NASA-TN D-5361 [17] for high-performance aircraft. The dynamic directional stability derivative $C_{n_{\beta_{dyn}}} = 0.01$ indicates favorable spin resistance characteristics, particularly in high-angle-of-attack or sideslip conditions. Additionally, the positive lateral control spin parameter suggests that *SPEAR* is unlikely to experience roll reversal, which typically occurs near zero values of this parameter, as outlined by Nicolai [2].

7.4 Dynamic Stability Analysis

Dynamic stability was evaluated using a tool originally developed in *FORTRAN* by Mason [10], later translated into *MATLAB* for integration with the overall aircraft design optimization framework. This tool computed the aircraft controllability coefficients, generated transfer functions, and evaluated time-domain step responses for each dynamic

mode.

Initial simulations revealed excessive oscillatory behavior across several modes, indicating instability unsuitable for safe flight. To mitigate these effects, the aircraft configuration was iteratively refined. Key modifications included adjustments to wing placement, control surface dimensions, and tail sizing. Following these changes, updated stability analysis results indicate that *SPEAR* meets Level 1 and Level 2 handling quality standards as defined by MIL-F-8785C [16], across all evaluated dynamic modes.

8 Systems Architecture & Layout

8.1 Data Bus System

SPEAR's system architecture is built around modern components and configurations, with additional considerations for technological advancements. The FC-AE-1553 federated bus architecture has been chosen for *SPEAR*, a fiber-optic evolution of the MIL-STD-1553B standard. This modern variant supports significantly higher data rates and a greater number of nodes while maintaining compatibility with existing COTS line-replaceable units originally designed for the MIL-STD-1553B bus. The FC-AE-1553 bus retains the modularity of the MIL-STD-1553B bus, allowing expansion and reconfiguration in future revisions of *SPEAR*. The use of fiber optics provides near-total immunity to EMI, enhancing system resilience and offering inherent protection against certain types of cyberattacks. Pairing this architecture with a Real-Time Operating System (RTOS) improves system flexibility, simplifies software partitioning for enhanced security, and streamlines maintenance and future software updates.

8.2 Military Avionics, Electronic Warfare, and Armament

SPEAR is equipped with the Northrop Grumman APG-83 Scalable Agile Beam Radar (SABR), an Active Electronically Scanned Array (AESA) radar adapted from systems used on the F-22 and F-35 for integration onto legacy platforms such as the F/A-18. This electronically steered radar offers target detection ranges of up to 230 nautical miles and provides improved reliability and reduced acoustic and electromagnetic signatures due to its solid-state, non-mechanical design. In addition to the radar, *SPEAR* features comprehensive electronic warfare (EW) and Electronic Support Measures (ESM) capabilities. These systems provide radar warning, enhanced situational awareness, and jamming functionality using broadband periodic arrays and direction-finding localizers. *SPEAR*'s broadband periodic arrays covering bands 2, 3, and 4 (approximately 1–8 GHz), enable detection and classification of a wide range of radar emissions. These arrays are paired with high-precision direction-finding localizers, allowing for accurate and rapid geolocation of threats. Together, these systems provide *SPEAR* with broad-spectrum situational awareness and support the effective deployment of electronic countermeasures in contested electromagnetic environments. An integrated IRSTS supports passive detection, target tracking, and precision engagement of threats. The standard weapons

configuration includes four AIM-120D AMRAAM missiles mounted on two underwing pylons and two AIM-9X Sidewinders mounted on the wingtips, providing *SPEAR* with Beyond-Visual-Range (BVR) and short-range air-to-air combat capabilities. *SPEAR*'s standard armament configuration can be seen in Figure 40.

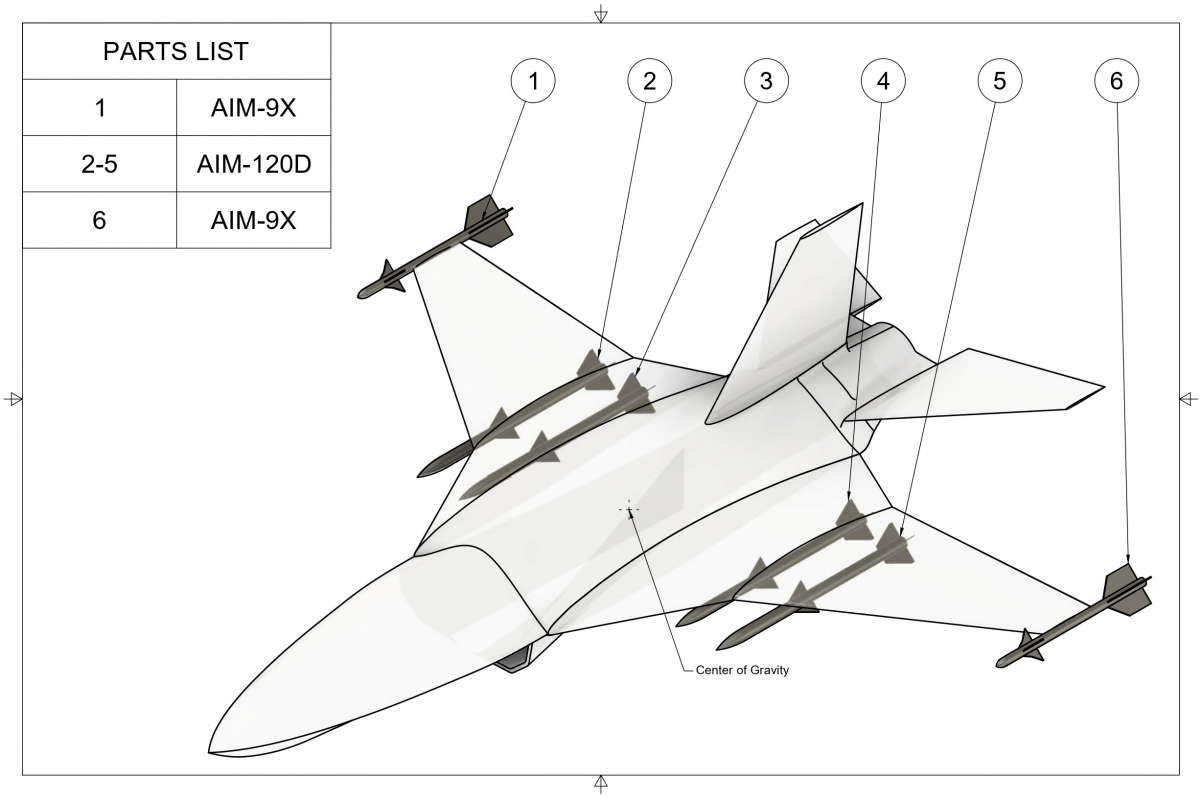

Figure 40: *SPEAR*'s Standard Armaments

8.3 Communication, Navigation, and Identification System

All *SPEAR*'s safety and critical flight systems are designed with triple redundancy. The aircraft features three air data probes located at the front of the fuselage—two on the left side of the nose and one on the right. These multi-port pitot-static probes provide measurements of airspeed, angle of attack, sideslip, vertical speed, and other essential air data parameters. For navigation, *SPEAR* is equipped with a Global Positioning System (GPS), Instrument Landing Conditions (ILS) and a Tactical Air Navigation System (TACAN). It also supports both Wide-Area Augmentation System (WAAS) and Local-Area Augmentation Systems (LAAS) capabilities to improve positional accuracy during critical phases of flight. Communication and identification systems include High Frequency (HF), Very High Frequency (VHF) and Ultra High Frequency (UHF) radios along with an Identification Friend or Foe (IFF) Interrogator and Transponder. Intra-flight Data Link (IFDL) enables encrypted communications and data sharing with advanced platforms such as the F-22, F-35, and future systems such as the F-47 in joint operations. IFDL also enables operation in GPS denied areas, feeding telemetry to GPS denied *SPEARs*. Furthermore, should *SPEAR* be operating alone in

GPS denied areas, it will utilize a back-up inertial navigation system. Satellite Communications (SATCOM) provides Beyond Line of Sight (BLOS) communications with ground controllers and other assets. The pilots will experience between 60-100 ms of communication delays utilizing satellite constellations, such as Starshield, depending on where *SPEAR* is operating. *SPEAR*'s communication strategies are built around making the kill chain robust. Utilizing Line of Sight (LOS) radio communications, IFDL communications, and SATCOM BLOS communications gives *SPEAR* many possible lines of communications. *SPEAR* can afford to lose multiple lines of communications and remain connected to the pilot in control. Should *SPEAR* lose all connection, back-up autonomy is discussed in 8.6 The OV-1 diagram depicting *SPEAR*'s communication strategies can be seen in Figure 6.

8.4 Electrical Systems

SPEAR is equipped with a PTMS, derived from the architecture used in the F-35, in place of a traditional Auxiliary Power Unit (APU). The PTMS is located in the aft fuselage and is responsible for generating all electrical power required by onboard systems. It outputs 115 Volts Alternating Current (VAC), which is distributed to AC to DC converters located at the root of each wing and in the forward fuselage. These converters supply localized 28V DC power to subsystems within their respective zones. The nose-mounted AC–DC converter powers the forward avionics bays, while the converters at the wing roots serve central and wing-mounted systems. This decentralized architecture simplifies wiring complexity and increases fault tolerance. In the event of an engine shutdown, the PTMS will provide power for an attempted engine restart, while a battery, placed in the aft fuselage, will provide power to the rest of the airplane. If the PTMS is inoperative, electrical power for essential systems is maintained by an aft-mounted battery. For extended power needs during total engine and PTMS failure, the battery works in conjunction with a deployable Ram Air Turbine (Ram Air Turbine (RAT)) to support avionics and flight controls during an engine-out landing. A large amount of cooling will be done by utilizing heat exchangers and chilled fuel. The acPTMS provides cooling to avionics bays and other components around the aircraft. A layout of *SPEAR*'s avionics can be seen in Figure 41.

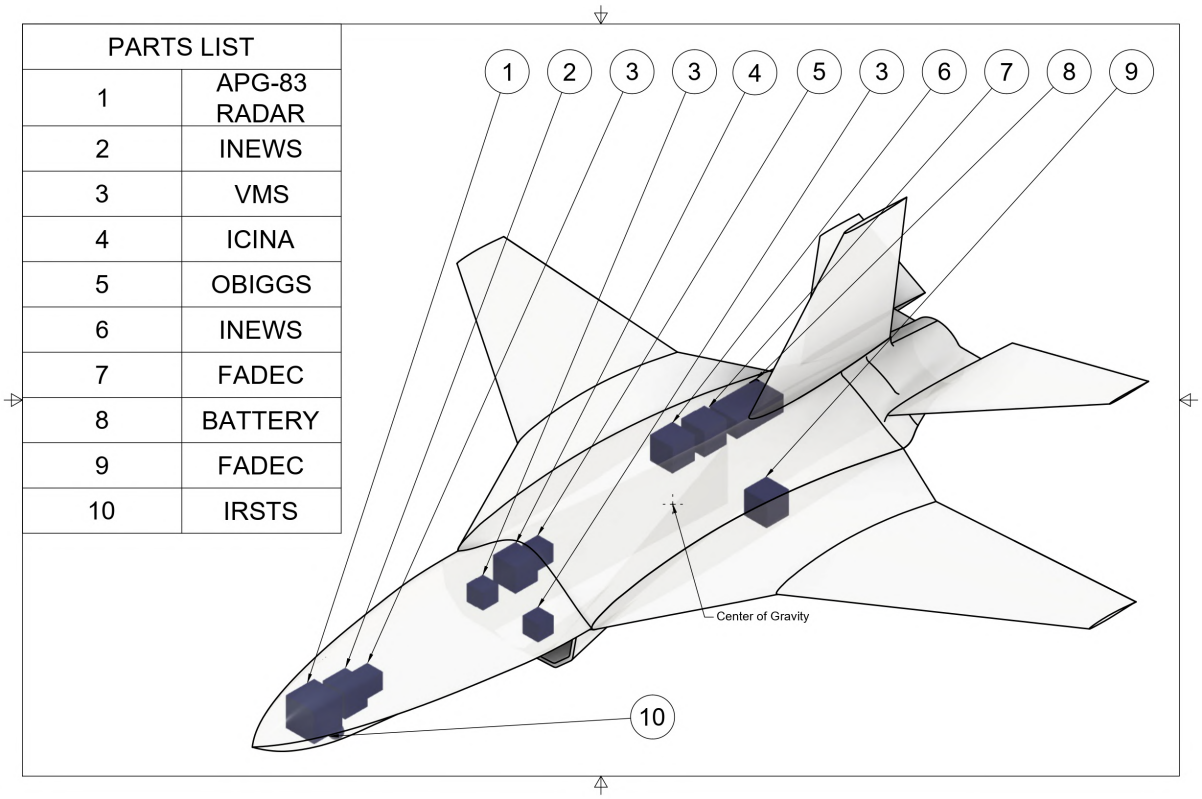

Figure 41: *SPEAR*'s Avionics

8.5 Environmental Control Systems

SPEAR is a remotely piloted, unmanned aircraft and therefore requires minimal onboard environmental control for crew comfort. However, remote operation increases the demand for onboard electronics, particularly in computing and communications systems. To accommodate this, the PTMS is sized not only to generate electrical power but also to provide active cooling for avionics and communication systems. Thermal management is achieved through dedicated cooling loops integrated into the PTMS, with excess heat exhausted adjacent to the engine exhaust plume. This design minimizes additional infrared (IR) signatures, enhancing the aircraft's survivability. By consolidating thermal and power management into a single system, the aircraft benefits from reduced weight, simplified architecture, lower maintenance requirements, and decreased operational costs. *SPEAR*'s propulsion configuration can be seen in Figure 42.

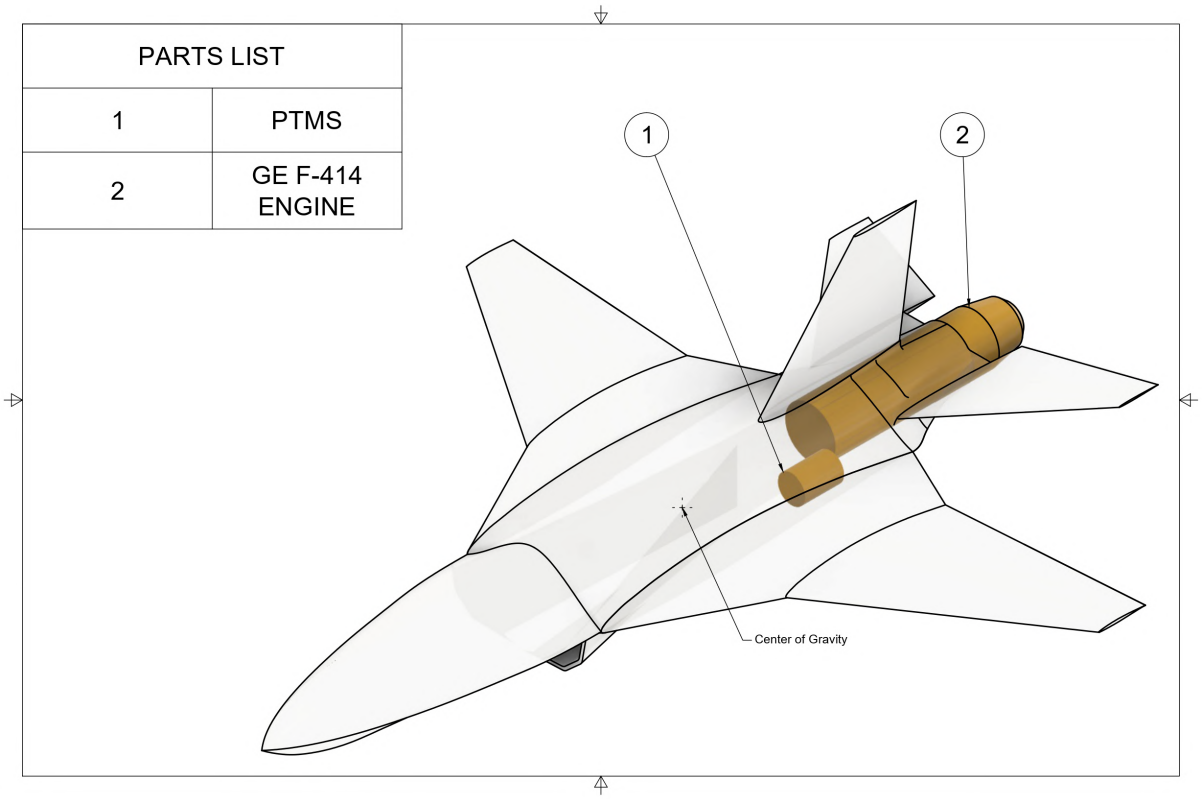

Figure 42: *SPEAR*'s Propulsion Configuration

8.6 Cockpit Systems

All cockpit systems for *SPEAR* are located in ground control stations operated by the remote pilot. The station includes a projected view of *SPEAR*'s surroundings, a primary panoramic display panel, which can be configured to show information in any desirable layout, and all necessary controls for manual flight. The interface allows flexible arrangement of flight data, sensor feeds, and mission information based on pilot preferences or mission requirements. The ground station's physical layout is designed to replicate conventional cockpit ergonomics. The left-side control panel contains the throttle, flight control switches, braking system, and landing gear controls. The right-side panel features the sidestick controller and electrical system interfaces. The center console houses the engine controls and primary aircraft system management interfaces. This setup enables the remote pilot to exercise full manual control of the aircraft when necessary, including during takeoff and landing. However, *SPEAR* will have autonomous capabilities. *SPEAR* will be able to perform flight paths, such as flying to a destination, tracking targets, escorting other aircraft, or loitering in certain areas, autonomously. The pilot will make high-level decisions, confirm the use of any weapon being deployed, and take manual control should the occasion require it. Notably, the station does not include backup displays and systems. Should a component of the station fail or should the pilot lose communication with *SPEAR*, the airplane will automatically Return to Base (RTB) and use systems such as Joint Precision Approach and Landing Systems (JPALS) to safely land.

8.7 Fuel System

SPEAR's propulsion system is supplied by five primary fuel tanks integrated throughout the airframe. These include two forward fuel tanks, a center fuel tank, and two wing tanks, one tank located in each wing. Together, these tanks can store up to 13,400 pounds, approximately 2,000 gallons, of JP-8 weighing 6.7 pounds per gallon specified by the RFP. The airplane is refueled via a single ground port located behind the engine intake on the side of the fuselage. A system of pumps and cross feeds will move fuel throughout the airplane during all phases of flight, allowing the remote pilot to trim the airplane with fuel. The center fuselage tank serves as the designated engine feed tank and is kept full in-flight to guarantee uninterrupted fuel delivery during high-g maneuvers or rapid attitude changes. Keeping the fuel in the center tank maintains the CG of the aircraft during flight. To enhance survivability in combat scenarios, all fuel tanks are self-sealing to minimize leakage in the event of structural damage. Additionally, the fuel system is equipped with an On-Board Inert Gas Generation System (OBIGGS) to pressurize and inert the tanks to reduce the risk of fire or explosion due to fuel vapor ignition. The airplane will be refueled from one port on the left wing, keeping equipment and personnel behind the inlet and not moving around the airplane during refueling. The layout of *SPEAR*'s fuel tank can be seen in Figure 43.

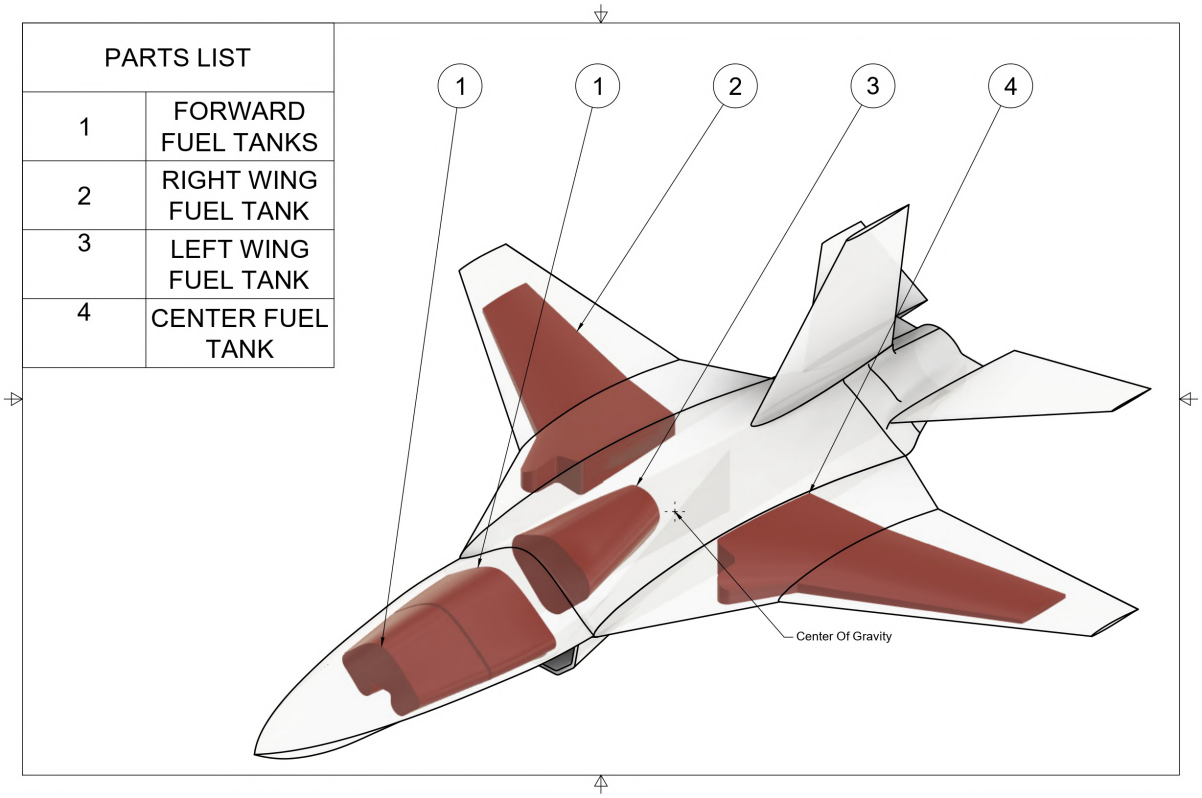

Figure 43: *SPEAR*'s Fuel Tank Layout

8.8 Landing Gear

The landing gear of this airplane will be sized to meet United States Air Force landing requirements, specifically a sink rate of 10 feet per second at touchdown. The airplane features a fully retractable tricycle landing gear configuration to reduce aerodynamic drag during supersonic flight. Although retractable gear introduces additional weight, mechanical complexity, and maintenance requirements, these tradeoffs are accepted to improve high-speed performance and fuel efficiency. A tricycle configuration was selected for its superior ground stability, ease of steering, and compatibility with delta-wing geometries. Since SPEAR does not require propeller clearance, tricycle gear offers simpler integration and more available internal volume for system packaging. A bicycle configuration was considered due to its potential weight savings and simplicity but was ultimately ruled out due to structural and packaging challenges in a single-engine airframe. The airplane's MTOW was increased by a factor of 1.26 from 27,000 lbs to 34,000 lbs for the purpose of landing gear design to account for future system and airplane weight growth and slight variations in ramp weight. A 90:10 static weight distribution was chosen to balance ground maneuverability, nose wheel steering authority, and takeoff performance. This results in approximately 3,400 lbs supported by the nose gear and 15,300 lbs on each main gear strut. Each gear strut supports a single wheel, as no individual location bears more than 25,000 lbs. This choice reduces weight, cost, and maintenance complexity while maximizing available space for internal systems. The main gear is equipped with Goodyear 34x11 Type VII tires, while the nose gear uses Goodyear 21x7.0 Three-Part tires. Braking is provided by electrically actuated carbon-on-carbon brakes, selected for their superior thermal performance during high-speed operations. Additionally, the main wheels are motorized to reduce fuel burn during taxi and improve ground scramble responsiveness. The Center of Gravity (CG) of the airplane is located 24.74 feet aft of the nose. The nose landing gear is 17.8 feet in front of the CG and the main landing gear is 1.9 feet behind the CG. This ensures 10% of the weight is borne by the nose gear and 90% of the weight is borne by the main gear. This geometry allows for a takeoff angle of attack of 15 ° which is 90% of the angle of attack of the maximum coefficient of lift. Additionally, the placement of the main gear yields a tip-over angle of 11.7 degrees and an overturn angle of 62.3 degrees ensuring the aircraft will not tip onto its side in crosswind and ground maneuvering. Additionally, the landing gear has been kept as short as possible, with the wing sitting just over six feet off the ground, to give aircraft maintenance program mechanics easy access to systems without the need for a ladder, removing the risk of elevated working. Locating all access panels on the bottom side and working from underneath the airplane reduces the chance of a tool being dropped on the composite structure of the aircraft. A diagram of the landing gear can be seen in Figure 44.

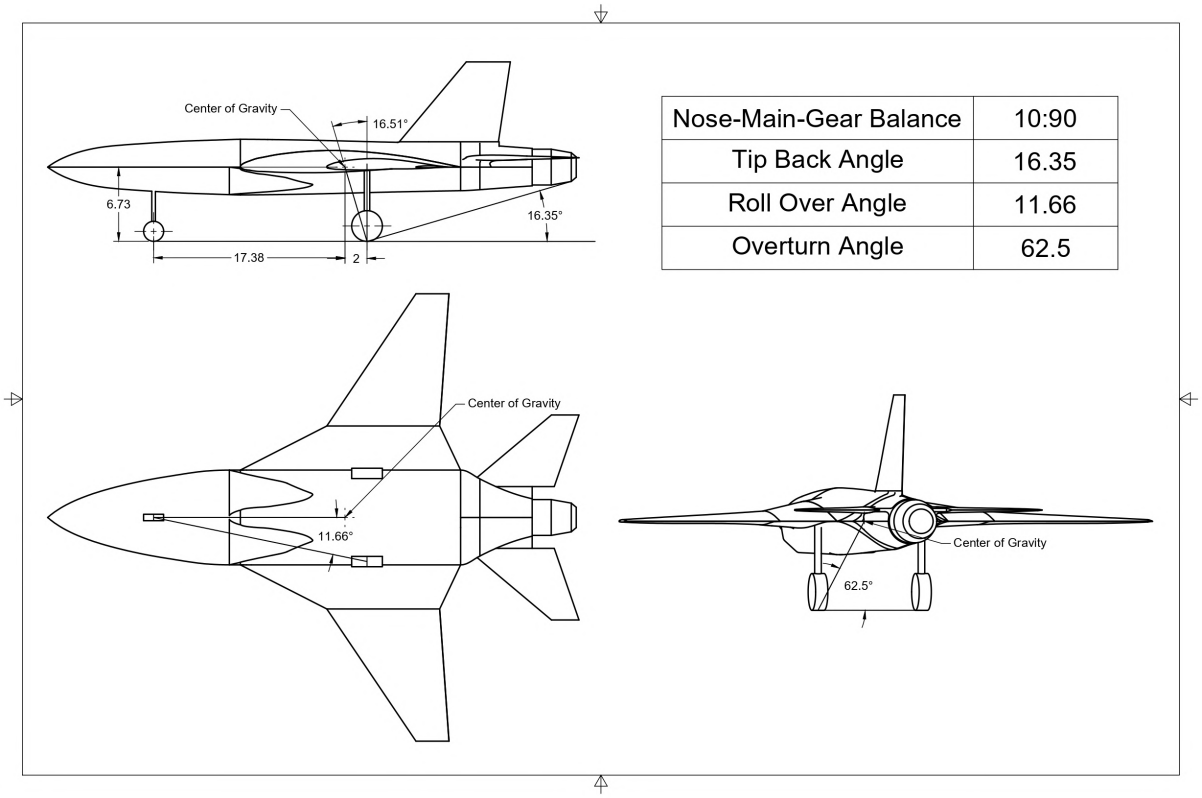

Nose-Main-Gear Balance	10:90
Tip Back Angle	16.35
Roll Over Angle	11.66
Overturn Angle	62.5

Figure 44: *SPEAR*'s Land Gear Layout

8.9 System Architecture

The *SPEAR* system architecture is built around three Vehicle Management System (VMS)s that coordinate navigation, flight control, mission systems, and utilities. Redundant inertial navigation and air data systems ensure robust guidance, while mission-specific payloads—including radar, electro-optics, and electronic warfare systems—are integrated via DASS buses. This triple redundant architecture allows one of the systems to fail or be damaged and still allow *SPEAR* to return safely and under control back to base for repair. The aircraft's power system, supplied by the PTMS and distributed through localized AC–DC converters, provides power to subsystems. Ground control is managed through dual mission CPUs interfacing with projected and panoramic flight displays, linking to a full suite of communication systems including SATCOM, IFDL, and legacy radios. This architecture supports high survivability, ease of maintenance, and adaptability to future mission requirements. The systems architecture can be seen in Figure 45.

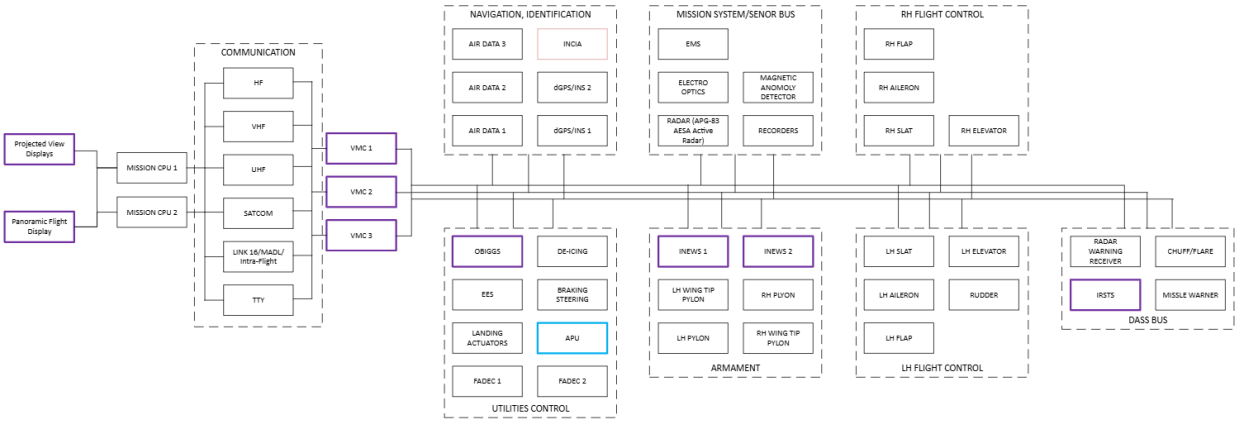

Figure 45: *SPEAR*'s Systems Architecture

Geometry

Wing Area	286 ft^2
Aspect Ratio	3.65
Takeoff Wing Loading	97 psf
Inner Sweep	63 °
Outer Sweep	34 °
Horizontal Area	68.5 ft^2
Vertical Area	47.1 ft^2

Weights

Wing Structure	2741 lbs
Fuselage Structure	3255 lbs
Skin	2179 lbs
Propulsion	3400 lbs
Subsystems	1100 lbs
Fuel	13400 lbs
Armaments	1680 lbs
Gross Takeoff Weight	27754 lbs

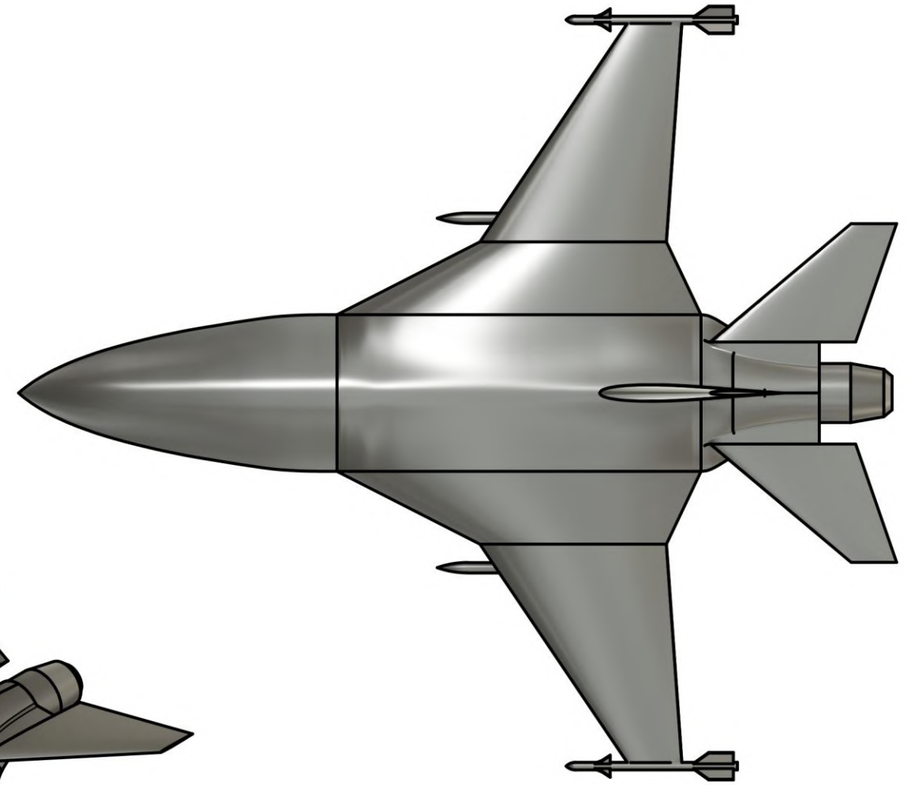

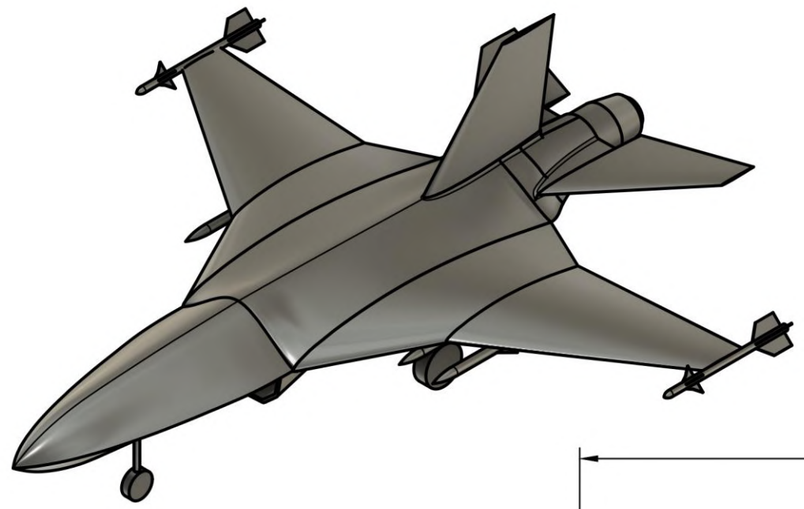

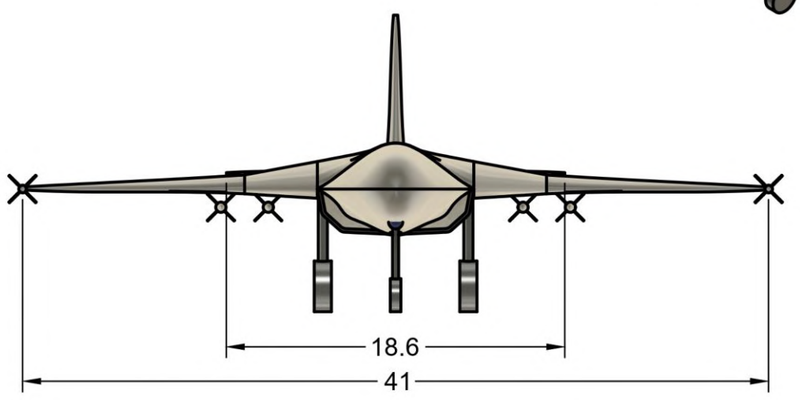

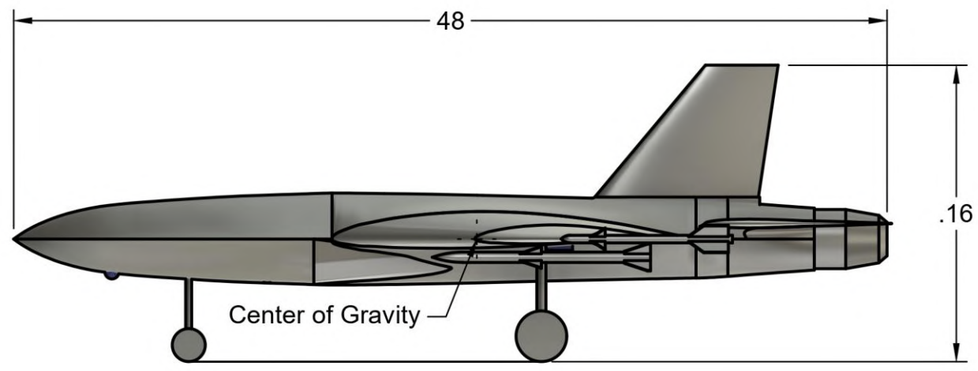

9 Structures and Materials

9.1 Velocity Loads Diagram

The V-n diagram in Figure 46 shows the loads *SPEAR* expects to experience during fight. The load limits are set according to the requirements stated in Section 2.3, which is +7g and -3g. The V-n diragram displays the limits *SPEAR*'s performance, defining a the highest load factor that it can achieve at different velocities.

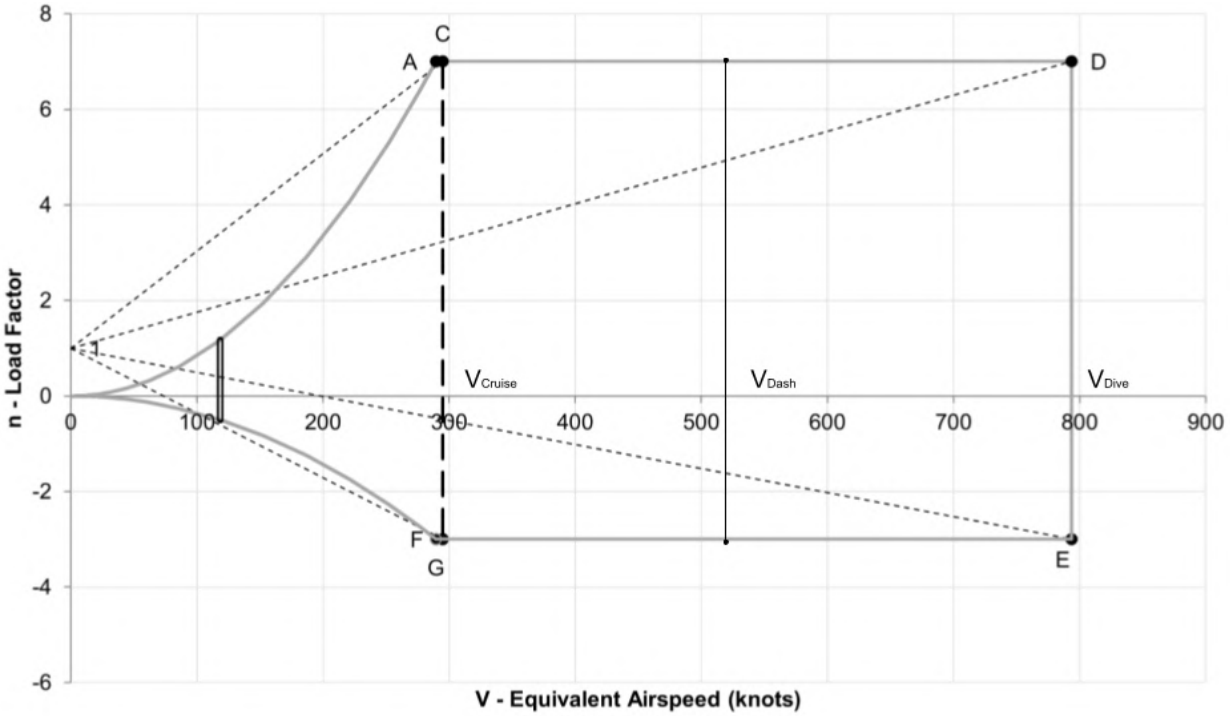

Figure 46: Velocity-load diagram

The dive speed, shown as D and E in 46 was set to be the maximum this aircraft is designed to handle, which is a dynamic pressure of 2133 psf, as stated in Section 2.3. This results in an equivalent airspeed of 194 knots. All velocities in Figure 46 are equivalent sea level velocities, which is defined according to Eq. 7.

$$V_{eq} = V\sqrt{\frac{\rho}{\rho_{SL}}} \tag{7}$$

The dash speed is 513.4 knots and the cruise speed, shown as points F and G, is 294.82 knots. Fig. 46 demonstrates that *SPEAR* can achieve all the airspeeds mentioned in the RFP and remain within the load limit.

9.2 Structural Layout

When planning a structural layout, it is crucial to evaluate the structure's metrics across a wide range of categories. The arrangement's load capacity, stiffness, buckling resistance, fatigue life, weight, manufacturability, and safety margins dictate where each structural element will be strategically placed. The following section provides a comprehensive guide to *SPEAR*'s structural layout.

9.2.1 Fuselage Structure Layout

SPEAR's fuselage layout's inspiration was drawn from other modern, high-performance fighters such as the F-35. The semi-monocoque design uses a system of closely spaced frames (ribs), longitudinal longerons, and stringers to form a stiff, load-bearing shell. This arrangement was selected to withstand the greatest anticipated load cases of –3g to +7g, and a safety factor of 1.5 without incurring high weight penalties. The final layout of the fuselage closely mirrored other performance aircraft to ensure the rest of the structure had a sound backbone.

The fuselage frames are cut from aluminum sheets and profiled to match the outer mold line of the skin. The frames carry hoop loads and transmit bending loads into the shell of the aircraft. Continuous longerons run forward and aft, tying all the frames together and resisting axial and bending stresses induced during high-g maneuvers. Additionally, stringers stitch between longerons, supporting the thin skin panels against local buckling and shear loads concentrated at locations with additional loads such as near the landing gear and wing roots. As shown in Figure 47 below, strategically placed cut-outs in the ribs reduce mass where stiffness demands are lower, saving weight to support the prolonged loiter missions necessary.

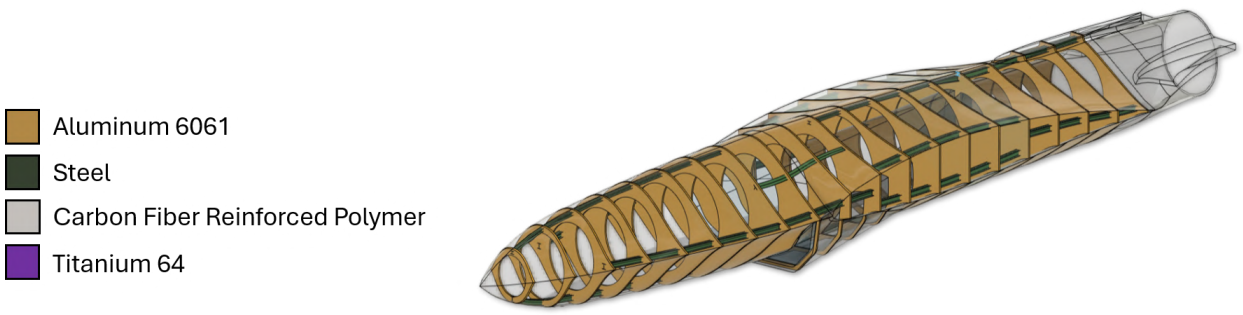

Figure 47: Fuselage Structural Configuration and Material Layout

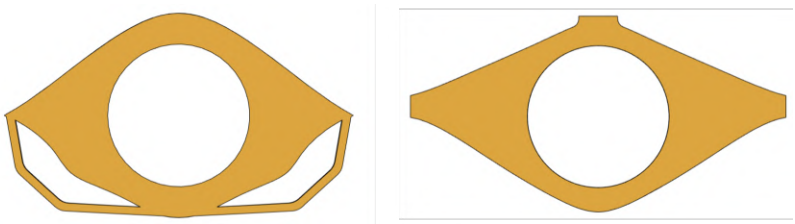

Figure 48: Typical Fuselage Structural Bulkhead

9.2.2 Wing Structure Layout

SPEAR's wing structure layout also draws inspiration modern high-performance aircraft adopting a semi-monocoque wing-box structure comprised of closely spaced ribs and seven main spars producing a rigid, load-bearing wing structure. This configuration was designed to resist the primary bending and torsional moments generated under the ranged flight envelope of –3 g to +7 g with a 1.5× safety factor while minimizing weight. The low profile outer mold line of *SPEAR* made it challenging to adequately size beams within the wing structure, making it necessary to utilize many closely spaced spars in the wing box. The spars have parts cut out near the neutral axis in order to save weight and allow fuel and bus line transfer throughout the structure. The forward and aft spars serve as the wing's backbone, shaping the overall structure and transmitting control surface loads directly into the fuselage attachments and distributing shear through the web panels. The ribs maintain the airfoil contour, carry local hoop loads at high-stress stations such as flap and aileron hinge points, and help prevent skin buckling.

Skin panels are profiled to match the desired airfoil and attach via flush fasteners to reduce drag; strategically located holes in the ribs and spars remove material where bending and shear demands are lower, especially near the neutral axis, which significantly reduces overall structural mass. This design mirrors the proven layouts of modern fighters, providing *SPEAR* with a stiff, durable wing that balances high-G maneuverability and low-weight efficiency necessary to support extended loiter missions.

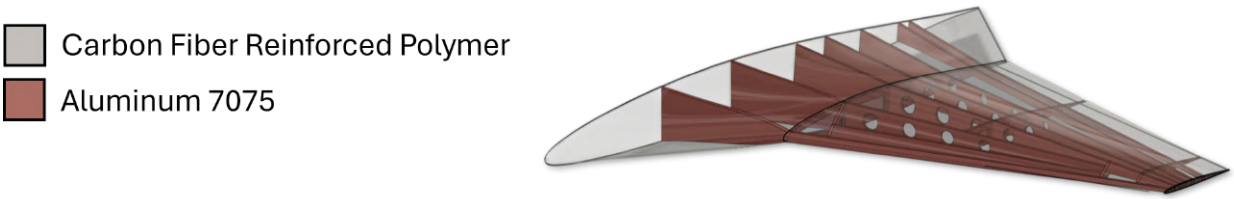

Figure 49: Wing Structural Configuration and Material Layout

9.3 Material Selection

When performing material selection for aircraft components and structure, it is imperative to evaluate the material's metrics in a wide range of categories. The material's strength, stiffness, fatigue resistance, cost, and other parameters

dictate where and how they should be used. The following section will provide a comprehensive guide to *SPEAR*'s material selection.

9.3.1 Fuselage Material Selection

The fuselage of *SPEAR* is mostly aluminum. The choice for an aluminum fuselage was driven primarily by the cost savings associated with aluminum versus composite material and manufacturing processes. Manufacturing with aluminum reduces the budget due to its low raw material cost in addition to its extensive historical use in manufacturing [18]. Complex geometries disproportionately affect the cost of manufacturing composites as an extensive manufacturing history does not yet exist for all parts. This means supporting manufacturing tooling must be developed to accommodate associated needs. On average, composite manufacturing processes can be 1.5x to 2x more expensive than aluminum processes.

With *SPEAR*'s design objectives focused on affordability and manufacturability, several aluminum alloys have been selected for different fuselage segments. Al-7075 has been chosen for the fuselage structure as it is a lightweight, commonly used aluminum alloy with excellent mechanical properties and high weld-ability. This makes it ideal for complex surfaces and geometry that must be welded in manufacturing. In an interceptor application, minimizing weight without sacrificing strength is the priority and Al-7075's reduced density compared to other aluminum alloys helps reduce weight which supports loiter missions [19].

Additionally, steel will be used in bulkheads since they require higher bearing strength and stiffness to handle concentrated loads structural attachments.

9.3.2 Wing Material Selection

The skin and wing structure will be composed of composite materials. Composite materials are used in this application due to their superior strength-to-weight ratios, enabling a lighter, more fuel-efficient aircraft. Less material in the wing structure also improves maneuverability and offers more volume to internal systems and fuel. Although higher manufacturing costs may be incurred when using composite materials, the performance gains in terms of reduced weight and enhanced aerodynamic efficiency are crucial in interceptor design where agility and speed are critical.

Additionally, CFRP wing skin is significantly less complex to manufacture than other structural components. Modern advancements have greatly improved automated fiber placement processes increasing speed and reliability while reducing cost and errors.

For the wing's primary structure, Al-6061 was selected for its high specific strength and better fatigue resistance when compared to other aluminum alloys [20]. The wing structure must handle distributed and concentrated loads while being subjected to intense vibrations and dynamic loading. Al-6061 offers a balance between stiffness, durability, and

cost-efficiency. While it is slightly more challenging to manufacture, it is commonly used in industry so tooling and processes are already in place to enhance efficiency and reduce cost.

9.3.3 Engine Mounts and Heat Sensitive Areas

In the landing gear, engine bay, and mounts, Grade V titanium (commonly referred to as Ti-6Al-4V) is used due to its excellent strength-to-weight ratio and superior temperature resistance. These properties are necessary in areas subject to high stress and thermal loads from the heat sources such as the brakes, engine and exhaust system. Titanium maintains structural integrity under elevated temperatures better than most aluminum alloys and composites, ensuring struts, engine mounts, and shrouding remain reliable throughout the aircraft's operation.

9.3.4 Landing Gear and High-Load Components

In other regions with demanding load requirements, such as the bulkheads, fasteners, and other components of the landing gear, reinforced steel is used sparingly to provide the requisite toughness and fatigue life. Steel's higher density becomes a trade-off in these areas because the landing gear and structural components must withstand repeated impact and point loads during takeoff and landing cycles. While it increases overall weight significantly, the added durability and extremely long fatigue life, so long as the fatigue limit is not exceeded, makes steel a necessary material.

9.4 Structural Weight Breakdown

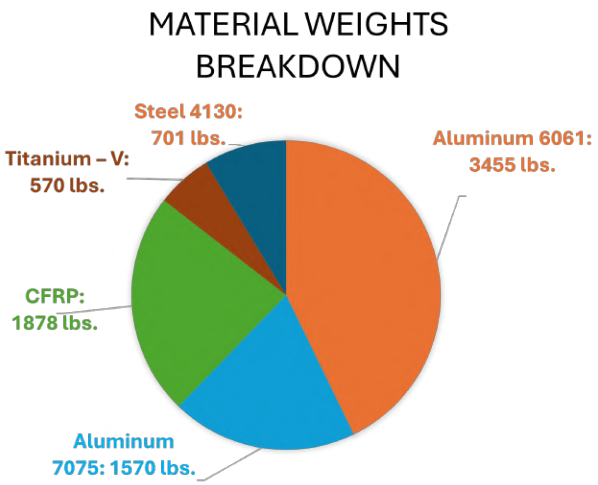

Figure 50: Material Structural Weight Breakdown

The chart above shows that the structure is dominated by aluminum, with 6061-T6 making up the largest portion of about 3,455 lb or (42% of the total 8,174 lb structural weight) and 7075-T6 contributing another 1,570 lb or (19%). Carbon fiber (CFRP) comes in next at 1,878 lb which is (23%), while the "hard metals" account for the remaining

structure: 4130 steel at 701 lb (9%) and Ti-6Al-4V at 570 lb (7 %).

9.5 Finite Element Analysis

In order to validate the initial structural sizing and layout of the internal wing structure, an FEA *Mathematica* code was developed. The wing developed for validation contains three ribs and four spars. The element-based representation of the structure contains 80 nodes, 174 elements, and 480 degrees of freedom. The structure was originally modeled with I-beam based structures before converting to solid circular cross section beams with equivalent second area moment and section modulus. The radius of the solid circular cross section was controlled such that no element in the internal structure would yield with six on-board missiles. Aerodynamic loads, gravity loads, and armament loads were applied between -4.5 G and 10.5 G. Loading was evaluated at critical conditions of -4.5 G, -3 G, 1 G, 5 G, 7 G, and 10.5 G. Missiles apply additional gravity and drag loads to the internal structure at the connection joints with the ribs inside the wing. FEA was conducted at the six different G loads in a clean configuration and with the wing-mounted missiles. It was crucial to evaluate how the structure would perform at the maximum anticipated load factor with missiles and a safety factor of 1.5x as the aircraft would likely encounter these load cases in combat and it could still be furnishing armament.

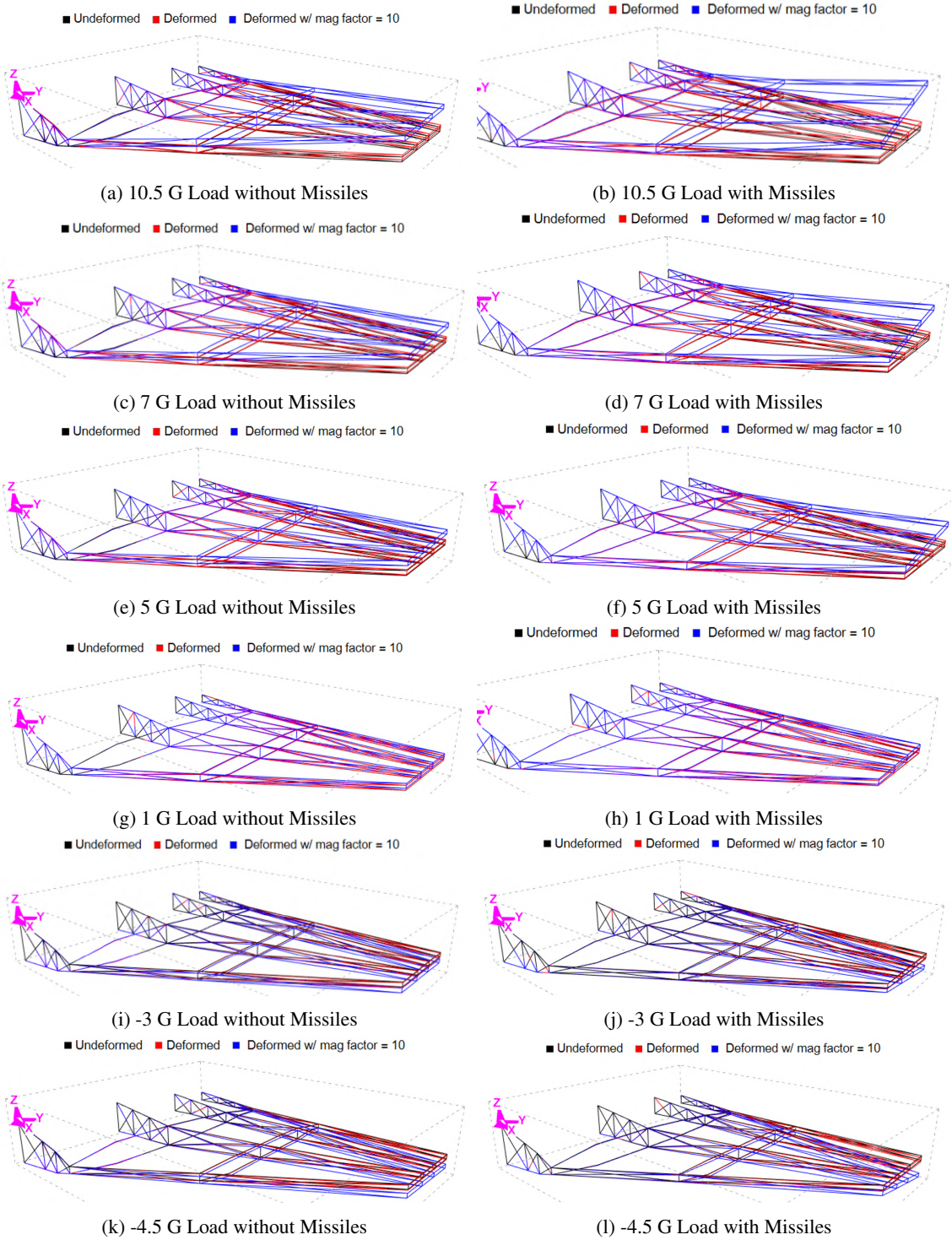

(a) 10.5 G Load without Missiles

(b) 10.5 G Load with Missiles

(c) 7 G Load without Missiles

(d) 7 G Load with Missiles

(e) 5 G Load without Missiles

(f) 5 G Load with Missiles

(g) 1 G Load without Missiles

(h) 1 G Load with Missiles

(i) -3 G Load without Missiles

(j) -3 G Load with Missiles

(k) -4.5 G Load without Missiles

(l) -4.5 G Load with Missiles

Figure 51: FEA - G Loading Deformation Analysis/Verification

When analyzing the results from the finite element analysis, there are key differences in the deformation behavior between identical load cases with and without armament. Comparing 51b and 51a, it is apparent that the addition of missiles under the extreme load case of 10.5 G induces an extreme chord-wise bending moment. The wing is rotated

counter-clockwise towards the nose due to the forces created by the leading-edge mounted armament. In 51a, the positive vertical wing tip deformation is symmetric about the spanwise axis as there is no additional load near the leading edge.

In all load cases, all four wing spar roots are constrained in all axes where they meet the fuselage. Under the most extreme load case, 10.5 G with armament, no structural elements yielded or buckled. When analyzing the individual load cases, there are key differences from iteration to iteration. In order to better visualize the unique deformations present in each load case, a 10x deformation plot is generated in blue, as seen in all figures above. This blue deformation plot represents the actual deformation values for each node multiplied by a scaling value of 10.

In 51g , there are no visible deformations. The three colored models all overlap with one another demonstrating the rigidity of the structure under its own weight. in 51h , there is a slight positive deformation apparent at the trailing edge wing tip under 10x magnification. This is because the added armament weight near the leading edge provides inertial relief, inducing a torsion about the chord-wise axis which rotates the wing forward. This is significantly more apparent in 51f and 51d. When comparing those two figures to 51e and51c , a similar trend is seen. There is a rotation towards the leading edge caused by the additional loads from the armament. The armament also provides inertial relief. In all figures with positive load factors and missiles, the leading edge vertical deflection is reduced as the weight of the armament counteracts the lift forces on the wing. The same physics work against the wing under negative load cases. In 51i and 51j , there is a visible larger negative deformation in the load case with missiles. This is because the inertial load and the negative lift are now working in the same direction. This increased deflection at a smaller magnitude of load is why negative load cases are more strenuous on the structure. Our structure is capable of withstanding -4.5G with missiles without any members of the structure failing.

Therefore *SPEAR* is confident in the structural integrity of the selected.

10 Cost Evaluation

The final purchase cost and operating cost were considered to be of utmost importance when designing *SPEAR*. It is essential that *SPEAR* maintains as low a cost throughout the entire lifespan of the contract to ensure continued use and competitiveness against other platforms. The flyaway unit cost target for a purchase order of 1,000 aircraft was set at $25 billion dollars in 2025 dollars, or $25 million per aircraft.

To estimate all associated costs in the research, development, production, and miscellaneous costs, Roskam's 2018 cost estimation method for fighter aircraft was used [21]. United States Air Force (USAF) research shows that cost estimation methods for fighters, such as Roskam's, translate well to the predicted cost of UCAVs, with advantages in costs coming from the lower empty weight [22]. Methods such as Roskam's use historical trends to predict the cost of different classes of aircraft while providing recommendations leading to conservative (high) and aggressive (low)

cost estimates. Roskam's method accounts for the use of advanced materials, operational costs, and many different research and development costs not commonly integrated in other estimation methods. The method primarily relies on assumptions on complexity, customer desires, and certain aircraft characteristics to account for variations in cost within an aircraft class. Roskam's method utilizes the takeoff weight, fuel weight, empty weight, engine weight, and wing area. Additional cost escalation to account for price change over the lifetime of a contract is applied both to previous costs, such as the 2005 costs from the RFP, as well as lifetime costs over the entire service life. The average service life for *SPEAR* was set at 20 years with 200 flight hours per year and a mission time of 5.5 hours with an average expected loss rate associated with traditional fighters.

Roskam's 2018 method neglects the cost of software development costs which, for recently developed aircraft, has lead to much higher research and development costs. To add in software development cost, a modified intermediate COCOMO model was developed with 16 multiplicative complexity factors. COCOMO models are frequently used for cost estimation in the software development industry and are primarily affected by Kilo-Lines of Code (KLOC) count [23]. Based on the research and development software, KLOC, used in advanced fighters, such as the F-22 and F-35, the initial development lines of code was set to 20 million and escalated over the service life of the aircraft. Additional efficiency improvements were applied based on software development and certification timelines in traditional fighters over the last-decade. All initial costs were applied to the Research, Development, Testing, and Evaluation (RDTE) cost inside the unit flyaway costs and future development cost was applied to life cycle cost.

The acquisition cost and manufacturing cost are added together to get the procurement unit cost. Procurement costs are multiplied by 1.1 to account for a 10% manufacturer profit margin before being added to RDTE costs to find a final Aircraft Estimated Price (AEP), which is taken as the unit flyaway cost. The unit costs associated with the acquisition, manufacturing, procurement, AEP, and lifecycle of the program are shown in Figure 52.

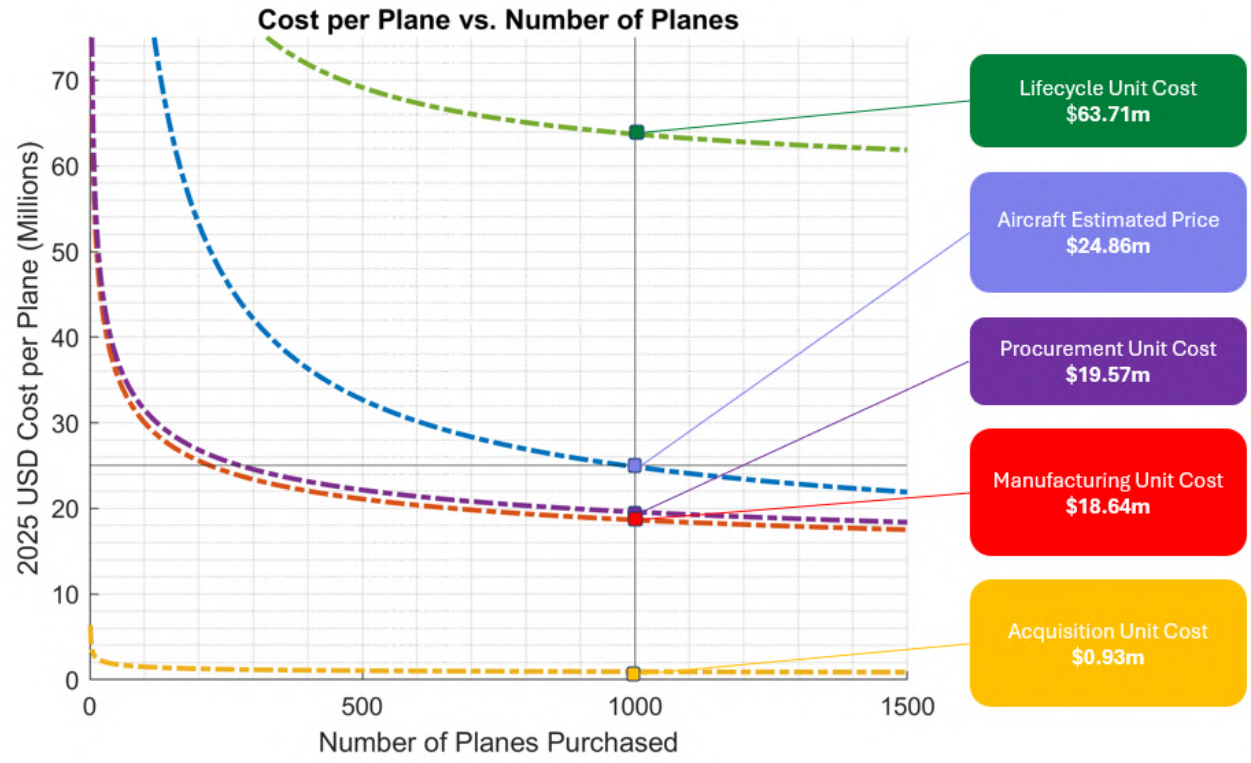

Figure 52: Unit Cost Breakdown (1000 aircraft)

The RDTE costs are broken down in Figure 53.

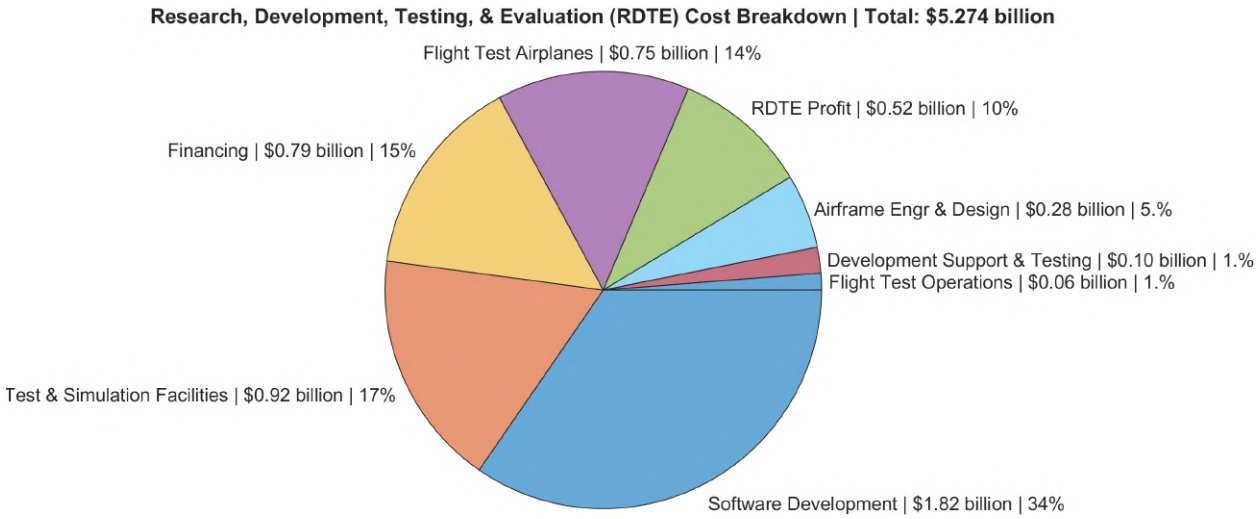

Figure 53: Research, Development, Testing, and Evaluation Cost Breakdown (1000 aircraft)

The program operating cost for 1000 aircraft is shown in Figure 54.

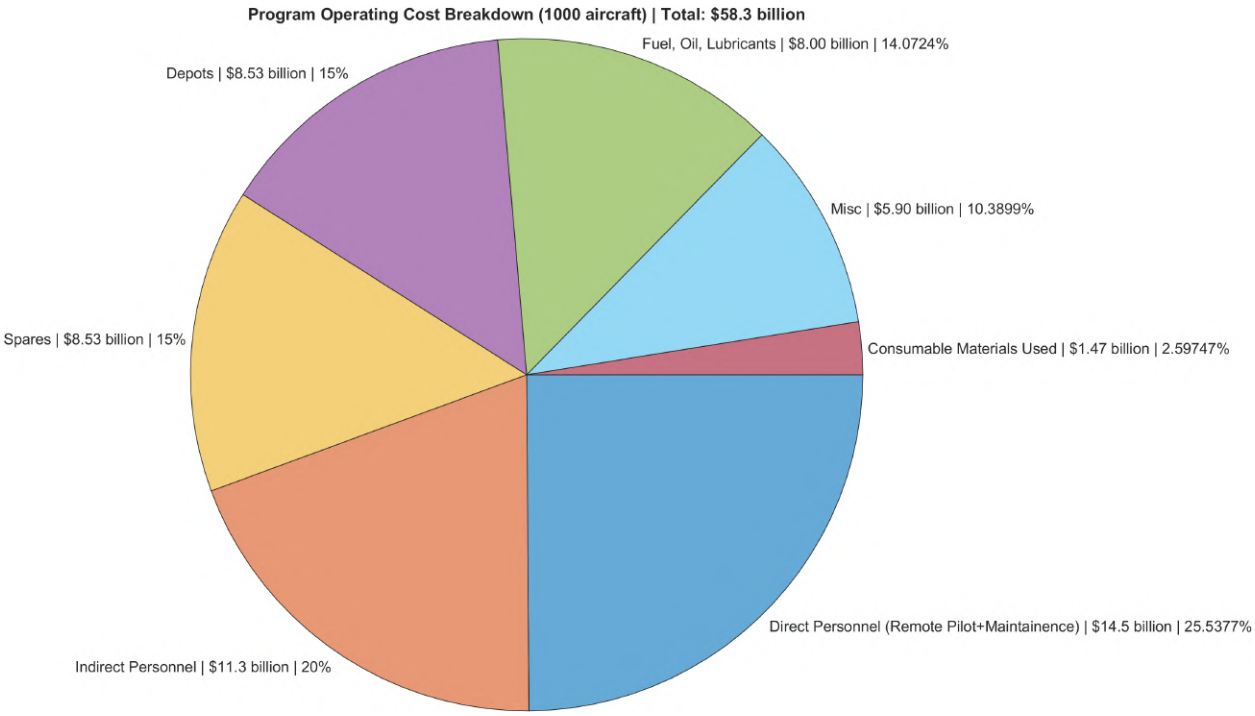

Figure 54: Program Operational Cost Breakdown (1000 aircraft)

Figures 52, 53, and 54 show that for a 1,000 aircraft contract, *SPEAR* is capable of meeting the RFP requirement of an AEP/flyaway unit cost of $25 million dollars per aircraft. The lifecycle associated costs with the aircraft approach $64 million dollars per aircraft, showing that the majority of the costs per aircraft is not from the initial purchase price, but the continued financial support throughout the service life of the entire program. Since it is possible that a different number of aircraft may be manufactured, Table 22 shows the AEP and operational costs for different purchase order sizes.

Table 22: Cost Escalation with Production Count

# of Aircraft Produced	Aircraft Estimated Price ($ million)	Program Lifetime Operational Cost ($ billion)
100	84.3	5.7
500	32.7	28.4
600	30.2	34.1
700	28.3	39.8
800	26.9	45.5
900	25.8	51.2
1000	24.9	56.9
1100	24.1	62.6
1200	23.4	68.2
1300	22.8	73.9
1400	22.3	79.6
1500	21.9	85.3

Table 22 shows that for a production contract of 500 aircraft, each aircraft would only cost $32.7 million dollars. Over 1,100 F-15s and over 2,000 F-16s have been produced. If full replacement occurred of various fourth generation fighter aircraft, such as the F-15 and F-16, additional production above 1,000 aircraft would be expected for homeland defense. For the cost of only $21.9 million per aircraft at a purchase order of 1,500 aircraft, *SPEAR* would be the world's lowest-cost next-generation homeland defense solution by a significant margin.

11 Project Management

11.1 Risks and Mitigations

The technological advancements made through *SPEAR*'s design equivalently introduced a series of risks. To develop a full profile of the risks associated with this design, three different categories were investigated: Technical, Program, and Operational risks.

11.1.1 Technical Risks

The main technical risks that pose the greatest concern are those associated with *SPEAR's* fully remote operability and supersonic aerodynamic parameters. The matrix below displays the initial scores for each risk, as well as their final placement following the incorporation of their respective mitigation strategies. A table displaying each evaluated risk and its respective mitigation follows the matrix.

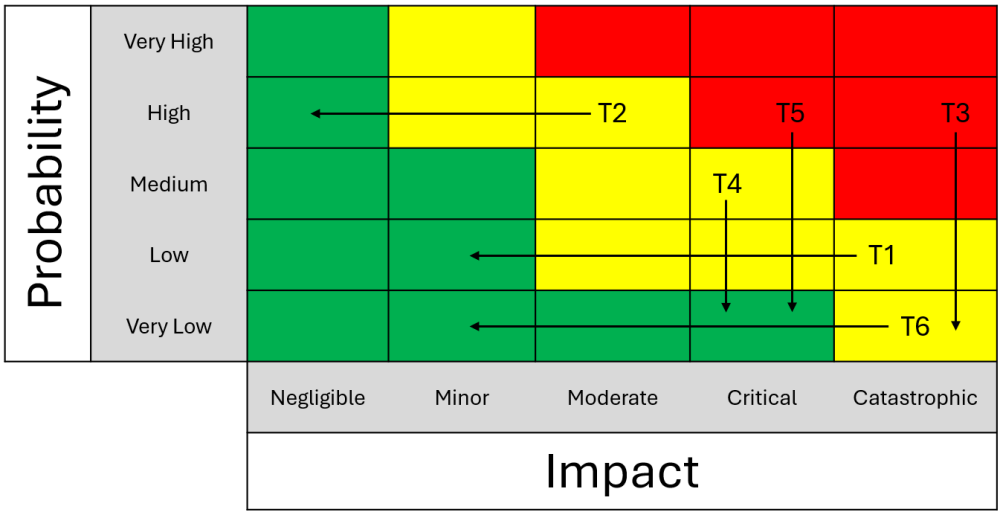

Figure 55: Technical Risk Matrix

Table 23: Technical Risks and Mitigation Strategies

No.	Risks	Mitigation Strategy
T1	Failure to withstand load of +7/-3g	Advanced FEA, high strength and lightweight materials
T2	Unable to operate with expected payload	Optimization of payload configurations, mass budgeting
T3	Software bug present	Periodic ground testing, validation procedures
T4	Unable to operate in IMC	Synthetic vision, advanced instrumentation
T5	Uncertainties in supersonic wave drag prediction	High-fidelity CFD analysis, wind tunnel testing campaigns
T6	Inlet design leads to thermal management failure	Bleed systems, integrated propulsion-inlet testing

SPEAR's fully-remote operability opens the doors to dangerous levels of uncontrollability if the aircraft were to be compromised. The introduction of any kind of software bug or malware into its advanced software easily has the potential to endanger innocent civilians and more. To mitigate this risk, a series of ground test verification procedures and audits need to be instituted and executed throughout *SPEAR's* developmental stage. Aside from in-house strategies, *SPEAR's* operating systems includes triple redundancy and fail-safes, giving pilots the ability to counteract any unsolicited use of force or endangering maneuvers.

Aside from considerations in software redundancy and safety, the uncertainties present in the aerodynamic analysis behind *SPEAR's* supersonic performance poses a risk to jeopardizing the aircraft's ability to execute the dash segment of its mission. As a homeland interceptor, reaching high speeds in as little time as possible can make or break the

safety of our shores. To face situations that require rapid response, *SPEAR* is able to reach a maximum Mach number of 1.83. However, if the supersonic wave drag calculations of this aircraft are inaccurate, this critical mission segment of *SPEAR* can be compromised. Throughout the development cycle of this aircraft, utilizing high-fidelity CFD tools and simulations can validate whether these performance requirements are met. Wind tunnel campaigns can also be conducted to collect data and cross-validate any findings from the aforementioned CFD simulations.

11.1.2 Program Risks

While technical risks account for hazards throughout the development cycle of this aircraft, program risks assist with understanding what may jeopardize the development of a fully-remote, autonomous fighter jet with a business focus. A program risk matrix and table listing all evaluated risks and their respective mitigations can be seen below.

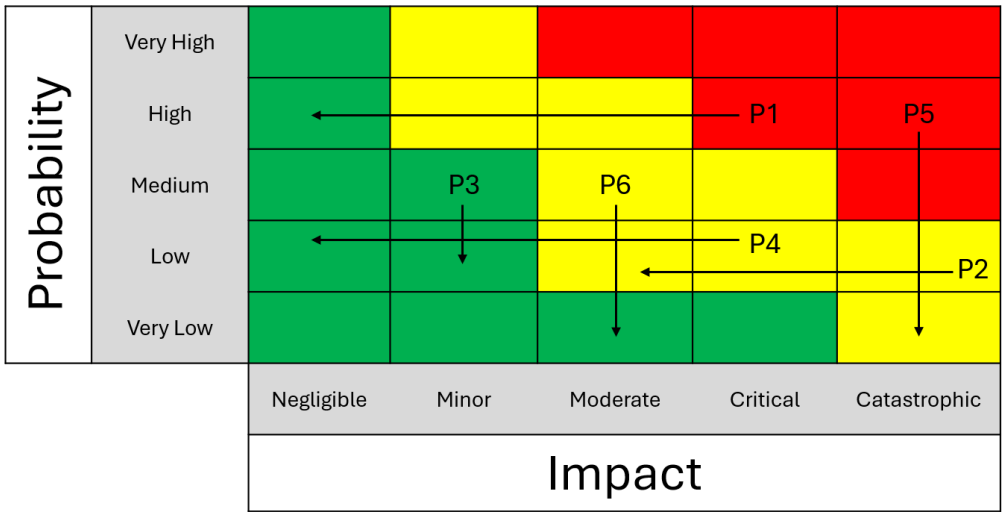

Figure 56: Program Risk Matrix

Table 24: Program Risks and Mitigation Strategies

No.	Risks	Mitigation Strategy
P1	Failure to meet deadlines causing large-scale delay	Build contingency plans into the timeline
P2	Funding uncertainty	Progress updates and focus on high public perception of program
P3	Resource limitations and supply chain inefficiency	Diversify suppliers and maintain high communication between all parties
P4	Lack of talent in workforce pipeline	Rigorous company selection process
P5	Program runs over budget	Regular cost monitoring and realistic budgeting
P6	Certification Issues	Use COTS parts and technologies

The current RFP requires the aircraft to be low cost. The challenge of producing a fighter jet interceptor for under $25 million US dollars per unit introduces a risk of running the program over budget. A budget overrun for this program would invalidate its entire purpose. With the goal of producing 1,000 aircraft, any violation of a budget requirement would lead to an immediate shutdown, or severely impact how well *SPEAR* can be marketed. To address this risk, regular cost monitoring and realistic budgeting can be implemented. Budgeting software can establish several accounts for different avenues of funding. Keeping a close watch on where funding is being spent can bulletproof any misuse or careless spending. Preliminary cost breakdowns to forecast funding allocation can also provide officials with a solid scope of the project to follow.

Aside from financial constraints, time constraints also facilitate the risk of failing to meet deadlines and causing a large-scale program delay. Delays can result from unexpected technical challenges, inefficient management, compliance issues, and more. When examining timelines of recent industry aircraft development, it is evident that obtaining type certification from the Federal Aviation Administration almost always exceeds the expected timeline. Not only does this accrue an additional time cost for the program, it can also lead to an additional financial commitment. To mitigate this, contingency plans can be built into the timeline along with incremental development. Incorporating buffer periods into the timeline of this program can prevent additional delays of any kind. Regular status reviews and proactive problem solving can prevent jeopardizing tardiness.

11.1.3 Operational Risks

To bridge the gap between technical and program risks, operational risks serve to analyze the potential hazards that could occur during *SPEAR* physical use. Operational risks force engineers to consider "what if" situations and work

backwards to ensure that an aircraft can effectively complete its mission. The risk matrix below illustrates the initial placement of each operational risk, along with arrows to indicate their final rank following mitigation implementation. An accompanying table displays each risk and the mitigation that was selected.

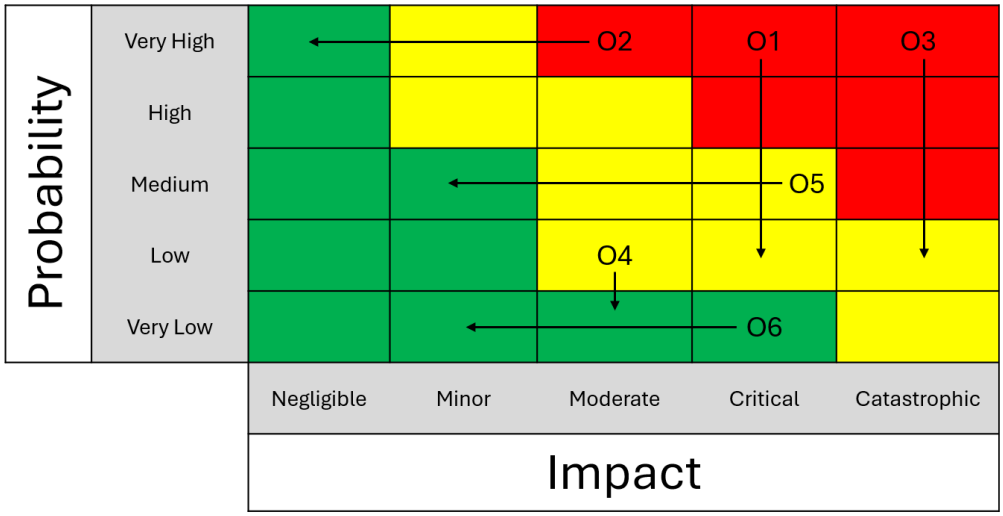

Figure 57: Operational Risk Matrix

Table 25: Operational Risks and Mitigation Strategies

No.	Risks	Mitigation Strategy
O1	Cyber-attack on aircraft	Fly-by-light technology
O2	Damage to engine (FOD ingestion or weapon induced damage)	Optimization of flight path and development of dead stick procedures
O3	Shot by enemy missile	Chaff and flare and various countermeasures
O4	Subsystem Integration Issues	Modular system design
O5	High speed airflow skips	Real-time engine monitoring
O6	Failure to deploy payload successfully	Redundant release mechanisms, pyrotechnic actuators, and mechanical fail safes

With *SPEAR* serving as a homeland defense interceptor, there is a very high probability that an attempt will be made by enemy forces to jam the aircraft and prevent the deployment of *SPEAR's* armament. With modern military aircraft heavily relying on digital communication and data sharing, cyber attacks hold the potential to compromise an intercept aircraft's entire purpose. Jamming technology can be used to manipulate data and damage critical systems. To combat this, *SPEAR* is equipped with fly-by-light technology. This reduces the reliance on electronic signals for control

systems and therefore minimizes the possibility of electromagnetic interference. In additional partitioning software applications enforces that a corrupted subsystem will not directly impact another.

As expected, *SPEAR* will engage in combat scenarios. Upon doing so, a reasonable risk to investigate is the use of kinetic weapons against the aircraft. The aircraft is highly likely to be targeted by infrared, radar, and laser-guided weaponry. Weapons of this caliber can reduce mission effectiveness to zero. To avoid entirely losing the asset, a series of countermeasures will be onboard the aircraft. Deploying chaff and flare is a traditional countermeasure that is tried and true. This serves as just one line of defense against threatening weaponry. Other countermeasures such as threat detection and evasive maneuvering algorithms can be implemented to reduce the workload of the remote pilot in such situations. These detection systems will be directly linked to the pilot's operating station, promoting minimal reaction time and ease of use.

11.2 Entry-into-Service Timeline

The RFP states that 1,000 units must be ready by 2045. To meet this requirement, *SPEAR* is to end the phase of preliminary design and enter advanced design in the first quarter of 2026, which will last through the third quarter of the same year.

Testing is set to start with avionics testing in the third quarter of 2025. Upon completion of the avionics tests in the third quarter of 2026, ground testing will begin. It will run through the second quarter of 2028, and overlap slightly with flight testing, which is to go from the fourth quarter of 2027 through the fourth quarter of 2031. The design and testing timelines are shown in Figure 58.

Manufacturing is set to start in the second quarter of 2026, starting with converting manufacturing capabilities and technicians trainings to ensure two test aircraft can be built by the end of 2026. The manufacturing plan for the airplanes is to start by manufacturing three aircraft per month in 2032 while building manufacturing floors. The production is set to ramp up to 12 aircraft per month by the fourth quarter of 2042. This ensures 1,000 aircraft built by 2045. The manufacturing plan is highlighted in more detail in Figure 59, some time periods during which the plan does not evolve are hidden to show everything on the figure.

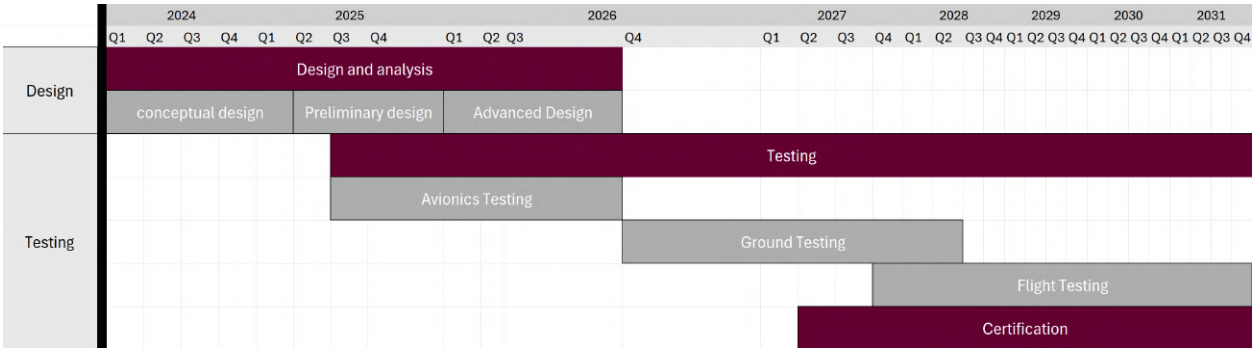

Figure 58: Design and testing timeline

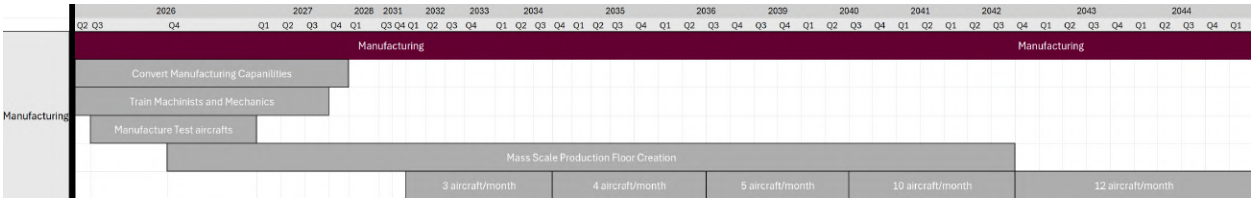

Figure 59: Manufacturing timeline

12 Competitors & Comparators

To assess legacy platform benchmarks relevant to *SPEAR*'s role, Table 26 was created for performance comparison.

Table 26: Aircraft Characteristics Comparison

Condition	SPEAR	F-16D [24]	F-15D [25]
Empty Weight (lbs)	12,674	19,700	29,000
Maximum Takeoff Weight (lbs)	27,754	37,500	68,000
Ferry Range (nm)	2,378	1,740*	3,000*
Endurance (hrs)	5.50	3.12	4.11
Max Mach	1.83	2.0	2.45
Armament	4x AIM-120D + 2x AIM-9X OR 6x AIM-120D	1x M61A1 w/ 500 rounds 6x air-to-air/air-to-surface/ electronic countermeasure pods	1x M61A1 w/ 940 rounds 4x AIM-9 + 4x AIM-120 OR 8x AIM-120
Unit Cost	$24.9 m	$36.9 m**	$58.6 m**
Aircraft in Service Worldwide	-	2,084	919

*With Conformal + External Fuel Tanks
**FY1998 Data Inflation Adjusted to FY2025

Two of the United States Air Force 4th-generation fighters compared are the F-15D and F-16D. *SPEAR* aims to fill a rapid-response homeland air defense role, offering competitive performance at a reduced cost with greater operational simplicity. *SPEAR* features a significantly lighter airframe allowing for longer ferry range in comparison to the F-16D. The F-15D is a much larger aircraft, carrying significantly more fuel than *SPEAR*. *SPEAR* features an incredible endurance of 5.5 hours, much longer than both comparator aircraft. This is made possible through *SPEAR*'s incredibly efficient engine, high fuel load, and efficient aerodynamics. *SPEAR* was designed to the RFP's maximum Mach number requirement of 1.6, which is slower than both the F-15 and F-16. *SPEAR* is equipped with armament equivalent to the F-16, minus the M61A1 cannon. The flyaway unit cost of *SPEAR* comes in at $24.9 million; $12 million and $33 million cheaper than the F-16D and the F-15D, price adjusted to 2025 USD. There are a large number of 4th-generation fighters currently in service, 2,084 F-16s (all variants) and 919 F-15s [26]. Though these 4th-generation platforms do not feature stealth, there is a clear emphasis on their worldwide mission potential.

Another important metric of comparison is the operational cost of the aircraft. Maintenance, inspection, and fuel cost are the majority of cost for most airframes 10. Although *SPEAR* is not positioned as a 5th-generation peer, a comparison with both fourth and fifth generation Air Force platforms of cost was made in a bar graph in Figure 60.

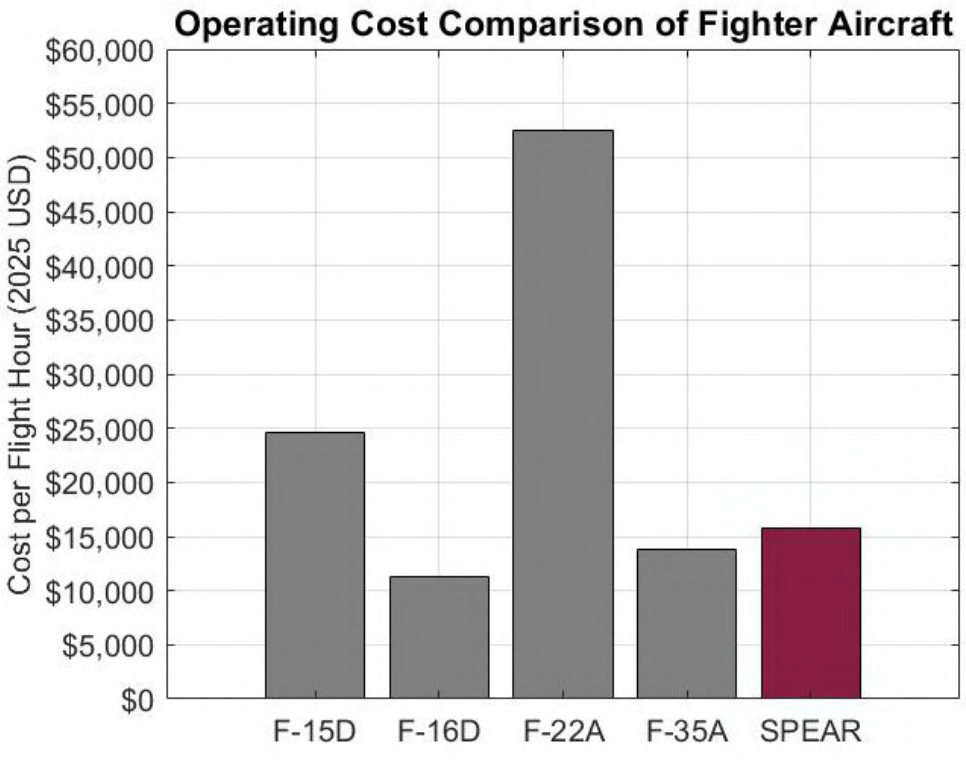

Figure 60: Operating Cost Comparison of Fighter Aircraft

SPEAR has a total hourly operation cost of $15,822. The F-15D has a much larger hourly operating cost of $24,598. The lowest hourly operating cost is the F-16D with $11,312. The operating cost available for the fighter aircraft comes from a memorandum published by the Secretary of Defense on external reimbursement rates [27]. The trend of current aircraft lowering operating cost indicates NATO's priority on lowering operating cost at the expense of acquisition cost.

Modern fighter platforms feature significant improvements to systems, radar, and interoperability. A comparison of the integration of *SPEAR*, the F-15, and the F-16 is shown in Table 27. Unlike the F-15 and F-16's, *SPEAR* is built to integrate seamlessly with all modern and future assets. Features like IFDL, remote pilot, short burst autonomy, and swarm capability gives *SPEAR* next generation compatibility. The Air Force is developing short burst autonomy for the F-16 through its Venom program [28]. Enhanced radar range and integration with modern systems grants a field advantage with which the F-15 and F-16 platforms cannot compete.

Table 27: Next-Generation Fleet Integration

Condition	SPEAR	F-16D [24]	F-15D [25]
Intra-Flight Data Link	✓	✗	✗
Remotely-Piloted	✓	✗	✗
Short Burst Autonomy	✓	✗	✗
Radar Range >200 nm	✓	✓	✗
Swarm Capability	✓	✗	✗
Built to Integrate with Modern Systems	✓	✗	✗

SPEAR is equipped to handle NATO's homeland defense requirements at a fraction of the cost, with competitive performance against the current arsenal. As the United States looks to phase out the F-16 and develop variants of previous and current generation platforms, *SPEAR* is ready to join the arsenal.

The current 4th-generation platforms are currently undergoing replacement programs. The F-15C/D are being replaced by the F-15EX. This new variant of the F-15 features significant performance boost, though at an acquisition cost rivaling the F-35 at $90 million. The F-16C/D are undergoing a gradual replacement by the F-35 for some missions. The F-16's long service life and low cost have prolonged its program life cycle. *SPEAR* is designed to supplement or replace legacy F-15 and F-16 fleets where stealth is not a requirement —such as rapid intercept, combat air patrol, or escort missions.

13 Conclusion

This report showcases why Project *SPEAR* is the most advanced solution to the current RFP. With an expected 1000 units produced by 2042, *SPEAR* bridges the gap into tomorrow's homeland defense needs. Boasting a max Mach of 1.83, 230nm radar range, and GE F414-400 afterburning engine, this aircraft successfully meets all but one of the RFP's requirements. *SPEAR* exceeds expectations with a 5.5 hour loiter and fully remote operating procedure. All internal systems excluding the APU are commercial-off-the-shelf items, which give the aircraft modularity and reduce cost. Whether our shores require rapid response, patrol and protection, or support to our forces, SPEAR is here to serve. Its compatibility with existing and future assets, optimized flight envelope, and ease of maintenance ensure that SPEAR will get the job done. All of this, for under 25 million USD per unit and life-cycle cost of 64 million USD. SPEAR isn't ready for the future- it's built for it.

Table 28: Project Spear Performance Compliance Summary

Criteria	Requirement	Project Spear Compliance
Dash	Mach 1.6	**Mach 1.83 ✓**
Loiter	4 hours	**5.5 hours ✓**
Climb to 35k ft in 1 minute	>583 ft/s	**605 ft/s ✓**
1-g Specific Excess Power Military Thrust: Mach = 0.9 @ Sea Level	>200 ft/s	**315 ft/s ✓**
1-g Specific Excess Power Military Thrust: Mach = 0.9 @ 15k	>50 ft/s	**279 ft/s ✓**
1-g Specific Excess Power Max Thrust: Mach = 0.9 @ Sea Level	>700 ft/s	**818 ft/s ✓**
1-g Specific Excess Power Max Thrust: Mach = 0.9 @ 15k	>400 ft/s	**649 ft/s ✓**
5-g Specific Excess Power Max Thrust: Mach = 0.9 @ Sea Level	>300 ft/s	**659 ft/s ✓**
5-g Specific Excess Power Max Thrust: Mach = 0.9 @ 15k	>50 ft/s	**381 ft/s ✓**
Sustained Load Factor Max Thrust: Mach = 0.9 @ 15k	>5.0 g's	**5.07 ✓**
Maximum Instantaneous Turn Rate @ 35k	>18 deg/s	**17.8 deg/s ✗**
Flyaway Cost Per Unit	<$25 million	**$24.86 million ✓**

References

[1] Raymer, D. P., *Aircraft Design: A Conceptual Approach*, American Institute of Aeronautics and Astronautics, Reston, VA, 5th ed., 2012.

[2] Nicolai, L. M., *Fundamentals of Aircraft and Airship Design, Volume 1 - Aircraft Design*, American Institute of Aeronautics and Astronautics, Reston, VA, 2010.

[3] Scott, J., "Axisymmetric & Thrust Vectoring Nozzles," https://aerospaceweb.org/question/propulsion/q0095.shtml, 2002, retrieved 13 May 2025.

[4] Garamone, J., "NORAD intercepts Russian and Chinese bombers operating together near Alaska in first such flight," https://edition.cnn.com/2024/07/24/politics/norad-russian-chinese-bombers-alaska/index.html, 2023, retrieved 12 April 2025.

[5] Liebermann, O. and Bertrand, N., "F-22 Safely Shoots Down Chinese Spy Balloon Off South Carolina Coast," https://www.defense.gov/News/News-Stories/Article/Article/3288543/f-22-safely-shoots-down-chinese-spy-balloon-off-south-carolina-coast/, 2024, retrieved 12 April 2025.

[6] Ellis, T., "Russian aircraft again intercepted in international airspace off Alaska," https://alaskapublic.org/news/2024-09-26/russian-aircraft-again-intercepted-in-international-airspace-off-alaska, 2024, retrieved 12 April 2025.

[7] Rhea, J., "Fly by Light," https://www.airandspaceforces.com/article/0388light/, 1988, retrieved 10 April 2025.

[8] Lednicer, D., "The Incomplete Guide to Airfoil Usage," https://m-selig.ae.illinois.edu/ads/aircraft.html, 2025, retrieved 13 May 2025.

[9] Tyrell, T., Funk, C., and Marton, N., "AIM-120C-5 Performance Assessment (Revision 2)," http://www.zaretto.com/sites/zaretto.com/files/missile-aerodynamic-data/AIM120C5-Performance-Assessment-rev2.pdf, 2014.

[10] Dr. William Mason, "Virginia Tech Aircraft Design Software," https://archive.aoe.vt.edu/mason/Mason_f/ACDesSR/review.html, retrieved 10 April 2025.

[11] RTX, "RTX's Pratt & Whitney awarded $1.5 billion F119 engine sustainment contract for U.S. Air Force's F-22 fleet," https://www.rtx.com/news/news-center/2025/02/20/rtxs-pratt-whitney-awarded-1-5-billion-f119-engine-sustainment-contract-for-u#:~:text=EAST%20HARTFORD%2C%20Conn.%2C%20Feb,Force's%20F%2D22%20fighter%20jets., 2025, retrieved 13 May 2025.

[12] Kelly, F., "Pratt & Whitney awarded $6.7 billion contract for F-22 Raptor engine sustainment," https://thedefensepost.com/2017/12/15/f-22-raptor-engine-pratt-whitney-contract/, 2025, retrieved 13 May 2025.

[13] NASA, "F-18 High Alpha Research Vehicle (HARV)," https://www.nasa.gov/reference/f-18-harv/, 2025, retrieved 13 May 2025.

[14] Roskam, J., *Airplane Design Part II: Preliminary Configuration Design and Integration of the Propulsion System*, DARcorporation, 2012.

[15] EverySpec, "MIL-HDBK-1797," http://everyspec.com/MIL-HDBK/MIL-HDBK-0099-0199/MIL-HDBK-179_23582/, 2002, retrieved 10 April 2025.

[16] EverySpec, "MIL-F-8785C," http://everyspec.com/MIL-SPECS/MIL-SPECS-MIL-F/MIL-F-8785C_5295/, 1980, retrieved 10 April 2025.

[17] Anglin, E. L. and Chambers, J. R., "NASATND-5361," https://ntrs.nasa.gov/citations/19690022959, 1969, retrieved 10 April 2025.

[18] Resetar, S. A., Hess, R. W., and Rogers, J. C., *Advanced Airframe Structural Materials: A Primer and Cost Estimating Methodology*, RAND Corporation, Santa Monica, CA, 1991.

[19] MatWeb Material Property Data, "Aluminum 7075-T6," https://www.matweb.com/search/datasheetText.aspx?bassnum=MA7075T
2006, retrieved: 2025-05-04.

[20] MatWeb Material Property Data, "Aluminum 6061-T6," https://www.matweb.com/search/DataSheet.aspx?MatGUID=b8d536e0b9
2006, retrieved: 2025-05-04.

[21] Roskam, J., *Airplane Design Part VIII: Cost Estimation*, DARcorporation, 2018.

[22] Younossi, O., Kennedy, M., and Graser, J. C., *Military Airframe Costs*, RAND Corporation, Santa Monica, CA, 2001.

[23] GeeksforGeeks, "Cocomo Model - Software Engineering," https://www.geeksforgeeks.org/software-engineering-cocomo-model/, 2025, retrieved 10 April 2025.

[24] U.S. Air Force, "F-16 Fighting Falcon Fact Sheet," https://www.af.mil/About-Us/Fact-Sheets/Display/Article/104505/f-16-fighting-falcon/, 2023, retrieved: 2025-05-04.

[25] U.S. Air Force, "F-15 Eagle Fact Sheet," https://www.af.mil/About-Us/Fact-Sheets/Display/Article/104501/f-15-eagle/, 2023, retrieved: 2025-05-04.

[26] Spray, A., “The World’s Top 10 Most Active Military Aircraft By Type In 2025,” https://simpleflying.com/worlds-top-10-most-active-aircraft-by-type-2025/, 2025, retrieved: 2025-05-04.

[27] U.S. Department of Defense, Office of the Under Secretary of Defense, “Department of Defense Financial Management: FY 2022 Budget Rates,” 2022, retrieved on May 4, 2025.

[28] U.S. Air Force, “Autonomous F-16 program advances with modifications, simulations,” https://www.af.mil/News/Article-Display/Article/4145227/autonomous-f-16-program-advances-with-modifications-simulations/, 2025, retrieved: 2025-05-04.